Electronic Supporting Information for

Synthesis, optical, electronic and solid-state properties of carbonyl-functionalised diketopyrrolopyrroles

Joshua Humphreys,[a, ‡] Ferdinando Malagreca,[a ‡] Paul A. Hume,[b] Flavia Pop,[a §] E. Stephen Davies,[c] Stephen P. Argent,[c] Graham N. Newton[a] and David B. Amabilino[d]*

a GSK Carbon Neutral Laboratories for Sustainable Chemistry, School of Chemistry, University of Nottingham, Triumph Road, Nottingham, NG7 2TU, UK.

b MacDiarmid Institute for Advanced Materials and Nanotechnology and School of Chemical and Physical Sciences, Victoria University of Wellington, Wellington 6010, New Zealand.

c School of Chemistry, University of Nottingham, University Park, NG7 2RD, UK

d Institut de Ciència de Materials de Barcelona (ICMAB-CSIC), Consejo Superior de Investigaciones Científicas, Carrer dels Til.lers, 08193 Cerdanyola del Vallès, Spain

§ Current Address MOLTECH-Anjou, UMR 6200, CNRS, Univ. Angers, 2bd Lavoisier, 49045 Angers, France

‡ These authors contributed equally to the work presented here.

Experimental

2.1 Materials and instrumentation

All commercially available reagents were purchased from Sigma-Aldrich and used as received. Anhydrous solvents were fitted with an Aldrich Sure-Seal from purchase and used as received. Chromatography purifications were performed using Sigma-Aldrich Silica Gel (pore size 60Å, particle size 40- 63 µm) and thin-layer chromatography (TLC) was carried out on E. Merck silica gel plates, irradiated using UV light (365 nm). THF was distilled to remove BHT stabiliser prior to use for measurements. NMR spectra were acquired on a Bruker AV400, Bruker AV(III)500 or Bruker DPX300 spectrometers and NMR spectra were recorded at room temperature. All chemical shifts are reported in δ parts per million (ppm), using the residual solvent signal as an internal standard and the coupling constant values (*J*) are reported in hertz (Hz). The following

abbreviations are used for signal multiplicities: s, singlet; d, doublet; t, triplet; m, multiplet; and b, broad. ESI-MS were recorded using a Bruker micro-TOF II instrument. Infra-red spectra were recorded on a Bruker Tensor 27 instrument equipped with a Pike GladiATR attachment with a diamond crystal. Melting points were determined on a Stuart SMP20 Melting Point Apparatus.

UV/Vis absorption studies were performed using a Cary 5000 UV-Vis-NIR absorption spectrometer. Emission studies were performed using an Edinburgh Instruments FLS980 photoluminescence spectrometer. For quantum yield studies, fluorescence spectra were recorded as aerated solutions using a Jobin Yvon Horiba FluoroMax-3 spectrometer at ambient temperature in a 1 cm pathlength quartz cuvette. Quantum yields were calculated by comparison with the fluorescence observed for fluorescein (F = 91 in NaOH) under identical conditions of irradiation.[1] Cyclic voltammetric studies were carried out using an Autolab PGSTAT20 potentiostat and in some cases an EmStat3 potentiostat. Standard cyclic voltammetry was carried out under an atmosphere of argon using a three-electrode arrangement in a single compartment cell. A glassy carbon working electrode, a Pt wire secondary electrode and a saturated calomel reference electrode, chemically isolated from the test solution *via* a bridge tube containing electrolyte solution and fitted with a porous Vycor frit, were used in the cell when using the Autolab PGSTAT20 potentiostat. For the EmStat3 potentiostat a three-electrode set up consisting of a platinum wire counter electrode, a platinum disc working electrode and an Ag/AgCl wire quasi reference electrode was used. Redox potentials are quoted versus the ferrocinium-ferrocene couple, which was used as an internal reference.[2] DMF was utilised as solvent for **PhEsterDPP NH, PhEsterDPP N-Hex, PhEsterDPP N-TBA** and acetonitrile for **PhAldDPP N-EA**, with tetrabutylammonium hexafluorphosphate was employed as supporting electrolyte for both electrochemical experiments.

HOMO and LUMO levels were calculated using the equations.[3]

E_{HOMO} = - (E_{onset}(ox) + 4.8 [eV]) and E_{LUMO} = -(E_{onset}(red) + 4.8 [eV]).

The band gap is calculated using the equation

$E_g = E_{HOMO} - E_{LUMO}$ [eV].

Alternatively, the band gap can also be calculated from the onset of the optical absorption of the film using the equation:

$E_g = 1240 / \lambda_{onset}$ [eV].

Electronic structure calculations were performed using Gaussian 16 Rev. C01. All calculations used the B3LYP exchange-correlation functional equipped with the 6-311+G(d,p) basis set. Alkyl chains were replaced with ethyl groups to speed up the calculations. Energetic minima were confirmed by calculation and inspection of the vibrational modes, which showed zero imaginary frequencies in all cases. Optical gaps were calculated using linear response time dependent DFT at the geometry of the ground state. Solvent effects were treated with polarizable continuum model (integral equation formalism) with the default parameters for *N,N*'-dimethylformamide.

2.1.1 SCXRD Experimental Details

Single crystals were selected and mounted using Fomblin® (YR-1800 perfluoropolyether oil) on a polymer-tipped MiTeGen MicroMountTM and cooled rapidly to 120 K in a stream of cold N_2 using an Oxford Cryosystems open flow cryostat.[4] Single crystal X-ray diffraction data for **PhEsterDPP NH** were collected on an Oxford Diffraction GV1000 AtlasS2 CCD area detector, mirror-monochromated Cu-Kα radiation source; λ = 1.54184 Å, ω scans Single crystal X-ray diffraction data for **PhAldDPP N-EA** were collected on a Rigaku XtaLab Pro MM007 Dectris PILATUS3 R 200K Hybrid Pixel Array Detector with Cu-Kα radiation source; λ = 1.54184 Å. Cell parameters were refined from the observed positions of all strong reflections and absorption corrections were applied using a Gaussian numerical method with beam profile correction (CrysAlisPro).[5] The structure was solved within Olex2[6] by dual space iterative methods (SHELXT)[7] and all non-hydrogen atoms refined by full-matrix least-squares on all unique F2 values with anisotropic displacement parameters (SHELXL).[8] For **PhEsterDPP N-Hex**, PhEsterDPP N-TBE and PhAcetDPP-N-EA X-ray diffraction measurements were performed in Experiments Hutch 1 (EH1) of Beamline I19, at Diamond Light Source.[9]

The data was collected at a wavelength of 0.6889 Å on either a Fluid Film Devices 3-circle fixed-chi diffractometer using a Dectris Pilatus 2M detector (**PhEsterDPP N-TBE** and **PhAcetDPP N-EA**) or a CrystalLogic Kappa (4 circle) with Rigaku Saturn724+ detector (**PhEsterDPP N-Hex**). The structures were solved within Olex. by dual space iterative methods (SHELXT) and all non-hydrogen atoms refined by full-matrix least-squares on all unique F2 values with anisotropic displacement parameters (SHELXL). Hydrogen atoms were refined with constrained geometries and riding thermal parameters. The structures were checked with checkCIF.[10] CCDC 2079927-

2079928 and 2579064-2579066 contains the supplementary data for this compound. This data can be obtained free of charge from The Cambridge Crystallographic Data Centre via www.ccdc.cam.ac.uk/data_request/cif.

SCXRD Refinement details

PhEsterDPP N-Hex To support the refinement of the structure against weak data with a low data to parameter ratio, maximum use of geometric restraints was made to reflect the internal symmetry of the DPP molecule. Rigid bond restraints have been applied to the anisotropic displacement parameters of all atoms in the structure (RIGU).

PhEsterDPP NH Geometric similarity restraints have been applied to the 1,2 and 1,3 bond lengths to reflect the two-fold symmetry of the molecule and phenyl moieties (SAME, SADI). Rigid bond restraints have been applied to the anisotropic displacement parameters of all atoms in the structure (RIGU). All carbon bound hydrogen atoms were geometrically placed and refined with a riding model. The amide hydrogen atoms were observed in the electron density map and their positions refined with anisotropic displacement parameters fixed at 1.5 times Ueq of their parent atoms. The two amide hydrogen N-H bond lengths are restrained to be similar (SADI) and each be co-planar with the C-N-C system to which they are attached (FLAT).

PhEsterDPP N-TBE Disorder was modelled for the *tert*-butyl and *tert*-amyl moieties. For each disordered moiety the occupancies of the two components were refined and constrained to sum to unity, resulting in values of 0.54(1) and 0.60(1) for the respective major components. All chemically identical 1,2 and1,3 distances in the pairs of disorder components were restrained to be similar (SADI). Rigid bond and similarity restraints were applied to the anisotropic displacement parameters of all disordered atoms (RIGU, SIMU), furthermore the anisotropic displacement parameters of heavily overlapping disordered atoms (O23, C15, C18 and C19) were constrained to be identical (EADP).

PhAcetDPP N-EA The very small needle-like crystals diffracted weakly with a low resolution diffraction limit despite the use of synchrotron radiation. Data used in the refinement was truncated to the diffraction resolution limit of 1.05Å. To aid refinement of the structure against the consequent weak data rigid bond and similarity restraints were applied to the anisotropic displacement parameters of all atoms in the structure (RIGU, SIMU).

PhAldDPP N-EA The Flack parameter of 0.49(12) means that the absolute structure cannot be determined from this experiment. Refinement of the structure as an inversion twin gave a batch scale factor of 0.5(3) and no improvement in the value of R1.

2.1.2 Theoretical calculations

Electronic structure calculations were performed using Gaussian 09.[11] Electronic coupling calculations used molecular geometries taken from the crystal structures and used the B3LYP exchange-correlation functional and 6-311G(d,p) basis set with an ultrafine integration grid. Calculations of reorganisation energies used the larger 6-311+(d,p) basis set, with alkyl groups replaced with methyl to speed up geometry optimisation. Coupling values were calculated by three different methods (DIPRO,[12] monomer projection[13] and Fock matrix),[14] which all provided comparable values. Mobilities were calculated using a sum-over-neighbours approach using rate constants derived from Marcus theory.[15]

Separation distances and electronic coupling for unique neighbouring molecules

DFT details: CAM-B3LYP/6-31+G(d,p), Gaussian 16 defaults

Electronic structure calculations were performed using Gaussian 16 Rev. C01.[11] All calculations used the B3LYP exchange-correlation functional equipped with the 6-311+G(d,p) basis set.[16-18] Alkyl chains were replaced with ethyl groups to speed up the calculations. Energetic minima were confirmed by calculation and inspection of the vibrational modes, which showed zero imaginary frequencies in all cases. Optical gaps were calculated using linear response time dependent DFT at the geometry of the ground state. Solvent effects were treated with polarizable continuum model (integral equation formalism) with the default parameters for *N,N*'-dimethylformamide.

2.2. Synthesis of compounds

2.2.1. *3,6-Bis(4-[1,3]dioxolan-2-yl-phenyl)-2,5-dihydro-pyrrolo[3,4-c]pyrrole-1,4-dione* **(PhAcetDPP NH)**

Using a method described in the literature,[19] which we describe here for convenience; In *tert*-amyl alcohol (40 mL), sodium (1.47 g, 64 mmol) was dissolved at 100 °C in the presence of $FeCl_3$ (5 mol%) - the process takes about an hour. Then, 4-[1,3]dioxolan-2-yl-benzonitrile (7.00 g, 40 mmol) was added.

Subsequently, to the resulting solution over the course of an hour, di-*tert*-amyl succinate (3.23 g, 16 mmol) in *tert*-amyl alcohol (20 mL) was added. The resulting suspension was stirred strongly for 24 hours at 100 °C. The mixture was allowed to cool to room temperature, glacial acetic acid (16 mL) and methanol (200 mL) were added, and the mixture was stirred. After 4 hours, the suspension was filtered, and the solid was washed several times with methanol and cold water. The dark red solid was dried *in vacuo* and taken as the product (3.87 g, 56%) which is sparingly soluble in solvents used for NMR spectroscopy. The IR data is virtually identical to that reported[19]; ν_{max} (ATR-IR) 3139 (NH stretch), 2983 (CH stretch), 3036 (CH stretch), 2975 (CH stretch), 2882 (CH stretch), 2853 (CH stretch), 2762, 2867 (CH stretch), 1640 (C=O DPP), 1601(C=C stretch), 1565, 1515 1443, 1401, 1319, 1142, 1093, 1033, 939, 831, 804, 664 cm^{-1}.

*2.2.2. 2,2'Diethylacetate-3,6-Bis(4-[1,3]dioxolan-2-yl-phenyl)-2,5-dihydro-pyrrolo[3,4-c]pyrrole-1,4-dione (**PhAcetDPP N-EA**)*

Following an analogous procedure for a related compound,[20] **PhAcetDPP NH** (1.00 g, 2.31 mmol) was added to caesium carbonate (2.34 g, 7.2 mmol) and ethyl bromoacetate (2 ml, 18 mmol) in anhydrous acetonitrile (20 ml) and heated to 85 °C, whilst stirring under an inert atmosphere for 24 hours. After the time elapsed, the mixture was cooled to RT and solvent removed *in vacuo*. To the crude product, dichloromethane (100 ml) was added, and the remaining unreacted starting material filtered off using a glass sintered crucible. The solution was then washed with water (200 ml) and extracted with dichloromethane twice more (2 x100 ml). The organic extract was then dried ($MgSO_4$), filtered and concentrated under reduced pressure to give the crude product, which was purified by column chromatography using an eluent system of 95:5 DCM: ethyl acetate to yield the product as red solid (550mg, 0.94 mmol, 39%). Mp: 161 °C; ESI-MS found:$[M+H]^+$ 605.2208 and $C_{32}H_{32}N_2O_{10}$ requires M 605.2238; ν_{max} (ATR-IR) 2981 (CH stretch), 2892 (CH stretch), 1736 (C=O), 1679 (C=O DPP), 1603 (C=C stretch), 1562, 1512, 1427, 1382, 1280, 1221, 1136, 1077, 1019, 982, 943, 830, 744, 659, 580, 519, 472, 434, 408 cm^{-1}; ^{1}H NMR (400 MHz, $CDCl_3$) δ 7.81-7.79 (4H, d, *J* = 8.0 Hz, ArH), 7.66-7.64 (4H, d, *J* = 7.9 Hz ArH), 4.48 (4H, s, NCH_2), 4.24, 4.19 (4H, d, *J* = 7.1 Hz, OCH_2) 4.16, 4.06 (8H, m, CH_2) 1.27, 1.24 (6H, t *J* = 7.2 Hz, CH_3) ppm. ^{13}C NMR (75 MHz, $CDCl_3$) δ 168.0, 162.2, 147.7, 141.5, 128.5, 128.2, 127.2, 110.0, 102.9, 65.4, 61.9 ppm.

*2.2.3. 2,5- Diethylacetate -3,6-bis(4-formylphenyl)pyrrolo[3,4-c]pyrrole-1,4-dione (**PhAldDPP N-EA**)*

A mixture of **PhAcetDPP N-EA** (500 mg, 0.82 mmol), THF (15 mL) and HCl (2 M, 10 mL) was stirred for 2 hours at 60 °C. After being cooled to room temperature, 30 mL of ethyl acetate was added, washed with water and dried over $MgSO_4$ and filtered and the solvent removed *in vacuo*. The crude product was purified by recrystallization in dichloromethane and methanol to yield the product as red powder (370 mg, 87%); Mp: 161 °C; ESI-MS found:[M+H]+ 517.1608 and $C_{27}H_{25}N_2O_8$ requires M 517.1605; ν_{max} (ATR-IR) 2999 (CH stretch), 2939 (CH stretch), 2859 (CH stretch), 1731 (C=O), 1700 (C=O), 1666 (C=O DPP), 1581 (C=C stretch), 1554, 1506, 1471, 1425, 1394, 1375, 1315, 1282, 1213, 1172, 1128, 1110, 1076, 1020, 983, 941, 896, 836, 775, 740, 663, 621, 507, 478, 453, 414 cm^{-1}; ^1H NMR (400 MHz, $CDCl_3$) δ 10.11 (2H, s, CH) 8.07-8.06 (4H, d, *J* 8.5 Hz, ArH), 7.98-7.96 (4H, d, *J* 8.1 Hz, ArH), 4.53 (4H, s, *J* 7.9 Hz, NCH_2) 1.27, 1.25 (6H, t, *J* 7.4 Hz, CH_3) ppm. ^{13}C NMR (75 MHz, $CDCl_3$) δ 191.1, 168.3, 161.9, 147.3, 138.0, 132.6, 129.1, 111.1, 62.3, 43.6, 14.0 ppm.

*2.2.4 Di-tert-pentyl-4,4'-(3,6-dioxo-2,3,5,6-tetrahydropyrrolo[3,4-c]pyrrole-1,4-diyl)dibenzoate (**PhEsterDPP NH**)*

Sodium (1.2 g, 52 mmol) and a catalytic amount of iron (III) chloride were added to anhydrous *tert*-amyl alcohol (70 ml, 0.64 mol) and heated at 120 °C for 1 hour, whilst stirring under an argon atmosphere, whilst stirring, until all the sodium had dissolved. The mixture was then cooled to 80 °C and methyl-4-cyanobenzoate (3.9 g, 24 mmol) added in one portion. The reaction was then heated to 130 °C and then di-*tert*-amyl succinate (3.5 g, 14 mmol) diluted in *tert*-amyl alcohol (15 ml, 0.21 mol) was added via syringe pump over 3 hours. Upon complete addition, the reaction was heated at 130 °C for 48 hours. After this time had elapsed, the reaction mixture was cooled to 50 °C and toluene added (100 ml) and the solution refluxed at 120 °C for 1 hour. The mixture was then filtered over a glass sintered crucible (No. 4 porosity), washed with methanol and allowed to dry in a vacuum desiccator to afford the novel pure product as a red solid (1.6 g, 3.1 mmol, 25%). This compound is novel and has: Mp: 256 °C ; MALDI-TOF MS found M 516.143 and $C_{30}H_{32}N_2O_6$ requires M 516.226; ν_{max} (ATR-IR) 3139 (NH stretch), 3086 (CH stretch), 3036 (CH stretch), 2975 (CH stretch), 2882 (CH stretch), 2853 (CH stretch),

2762 (CH stretch), 1710 (C=O), 1640 (C=O DPP), 1601(C=C stretch), 1510, 1442, 1382, 1279, 1199, 1141, 1110, 1018, 927, 867, 814, 756, 690, 626, 575, 519, 439 cm^{-1}; ^{1}H NMR (300 MHz, DMSO-d_6) δ 11.51 (2H, s, NH), 8.60-8.50 (4H, m, ArH), 8.09-7.99 (4H, m, ArH), 1.90 (4H, m, CH), 1.54 (12H, s, Me), 0.93 (6H, s, R-CH_3) ppm; ^{13}C NMR (75 MHz, DMSO-d_6) δ 164.0, 162.3, 143.5, 133.5, 129.5, 127.8, 112.3, 83.6, 33.0, 25.3, 8.2 ppm.

2.2.5 *Di-tert-pentyl4,4'-(2,5-dihexyl-3,6-dioxo-2,3,5,6-tetrahydropyrrolo[3,4-c]pyrrole-1,4diyl)-dibenzoate (**PhEsterDPP N-Hex**)*

PhEsterDPP NH (260 mg, 0.504 mmol) was added to caesium carbonate (821 mg, 2.52 mmol) and hexyl iodide (0.4 ml, 2.52 mmol) in anhydrous acetonitrile (25 ml) and heated to 80 °C, whilst stirring under an inert atmosphere for 24 hours. The mixture cooled, water (200 ml) added and extracted with dichloromethane (3 × 100 ml). The organic extract was then dried ($MgSO_4$), filtered and concentrated under reduced pressure to give the crude product, which was purified by column chromatography using an eluent system of 98:2 DCM: ethyl acetate to yield the product as an orange solid (65 mg, 95 µmol, 19%). This compound is novel and has: Mp: 131 °C; ESI-MS found:$[M+H]^+$ 685.4194 and $C_{42}H_{57}N_2O_6$ requires M 685.4138; ν_{max} (ATR-IR) 2929 (CH stretch), 2859 (CH stretch), 1708 (C=O), 1671 (C=O DPP), 1594 (C=C stretch), 1506, 1456, 1411, 1368, 1277, 1207, 1160, 1112, 1018, 925, 869, 845, 791, 737, 678, 420 cm^{-1}; ^{1}H NMR (300 MHz, $CDCl_3$) δ 8.14 (4 H, d, *J* 8.5 Hz, ArH), 7.86 (4 H, d, *J* 8.4 Hz, ArH), 3.74 (4 H, t, *J* 7.5 Hz, NCH_2), 1.94 (4 H, q, *J* 7.3 Hz, CH_2), 1.66-1.50 (12 H, m, CH_2), 1.27-1.14 (12 H, m, CH_2), 0.99 (6 H, t, *J* 7.4 Hz, Me), 0.82 (6 H, t, *J* 6.9 Hz, R-CH_3) ppm; ^{13}C NMR (75 MHz, $CDCl_3$) δ 164.9, 162.6, 148.0, 134.3, 131.8, 130.0, 128.6, 110.8, 84.3, 42.1, 33.9, 31.3, 29.6, 26.5, 25.8, 22.6, 14.1, 8.5 ppm.

*2.2.6 Di-tert-pentyl4,4'-(2,5-dihexyl-3,6-dioxo-2,3,5,6-tetrahydropyrrolo[3,4-c]pyrrole-1,4-diyl)-dibenzoate (**PhEsterDPP N-TBA**)*

PhEsterDPP NH (1.00 g, 2.31 mmol) was added to caesium carbonate (2.34 g, 7.2 mmol) and ethyl bromoacetate (2 ml, 18 mmol) in anhydrous acetonitrile (20 ml) and heated to 85 °C, whilst stirring under an inert atmosphere for 24 hours. After the time elapsed, the mixture was cooled to RT and solvent removed in vacuo. To the crude product, dichloromethane (100 ml) was added, and the remaining

unreacted starting material filtered off using a glass sintered crucible. The solution was then washed with water (200 ml) and extracted with dichloromethane twice more (2 x100 ml). The organic extract was then dried ($MgSO_4$), filtered and concentrated under reduced pressure to give the crude product, which was purified by column chromatography using an eluent system of 95:5 DCM: ethyl acetate to yield the product as orange solid (850mg, 1.15 mmol, 59%). Mp: 143 °C; ESI-MS found: $[M+H]^+$ 745.3669 and $C_{42}H_{57}N_2O_6$ requires M 745.3695; ν_{max} (ATR-IR) 2977 (CH stretch), 2936 (CH stretch), 2886 (CH stretch), 1738 (C=O), 1712 (C=O), 1695 (C=O DPP), 1617 (C=C stretch), 1598 (C=C stretch), 1505, 1456, 1418, 1382, 1369, 1360, 1285, 1234, 1153, 1117, 1076, 1016, 983, 939, 926, 895, 867, 840, 789, 747, 714, 695, 673, 644, 574, 498, 464, 414 cm^{-1}; ^1H NMR (300 MHz, $CDCl_3$) δ 8.14 (4 H, d, *J* 8.5 Hz, ArH), 7.86 (4 H, d, *J* 8.4 Hz, ArH), 4.42 (4 H, s, *J* 7.5 Hz, NCH_2), 1.97 (4 H, q, *J* 7.3 Hz, CH_2), 1.60 (12 H, s, CH_2), 1.41 (18 H, s, CH_2), 1.00 (6 H, t, *J* 7.4 Hz, Me) ppm; ^{13}C NMR (75 MHz, $CDCl_3$) δ 167.2, 164.5, 162.0, 147.7, 134.3, 131.2, 130.0, 128.5, 110.8, 84.3, 82.9, 44.1, 33.6, 27.9, 25.6, 8.3, 1.0 ppm.

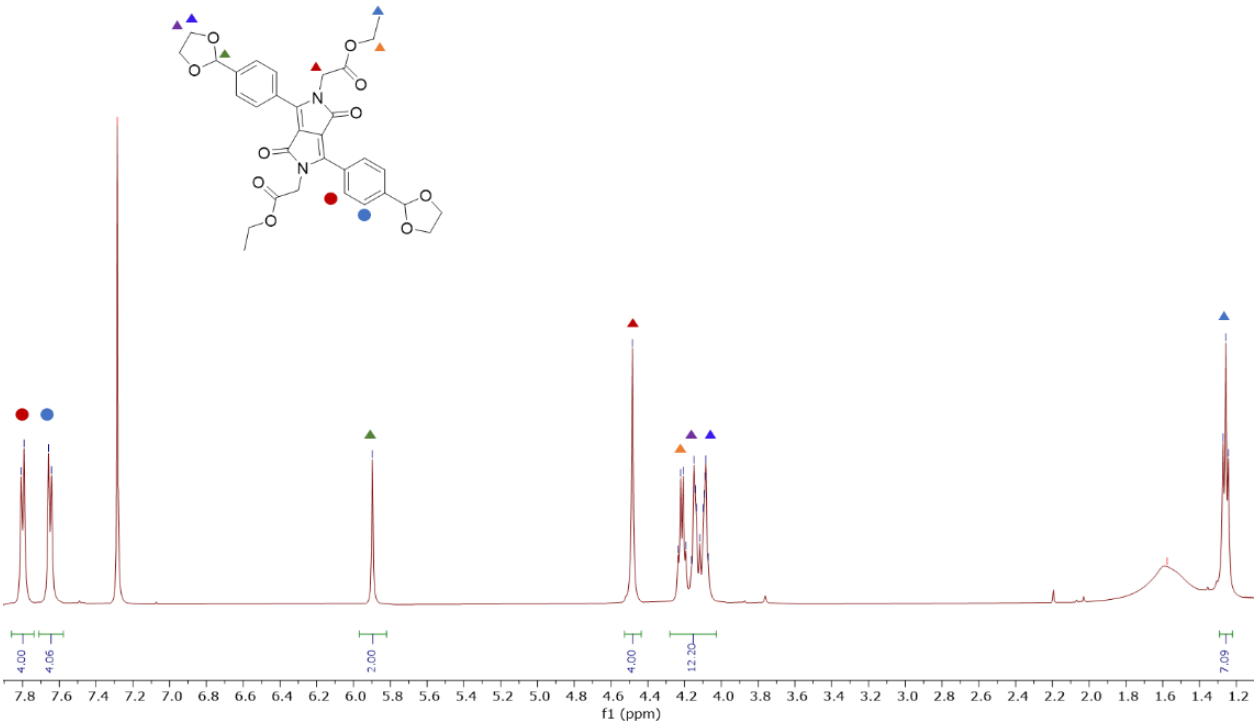

Figure S1. ^1H NMR **PhAcetDPP N-EA** in $CDCl_3$.

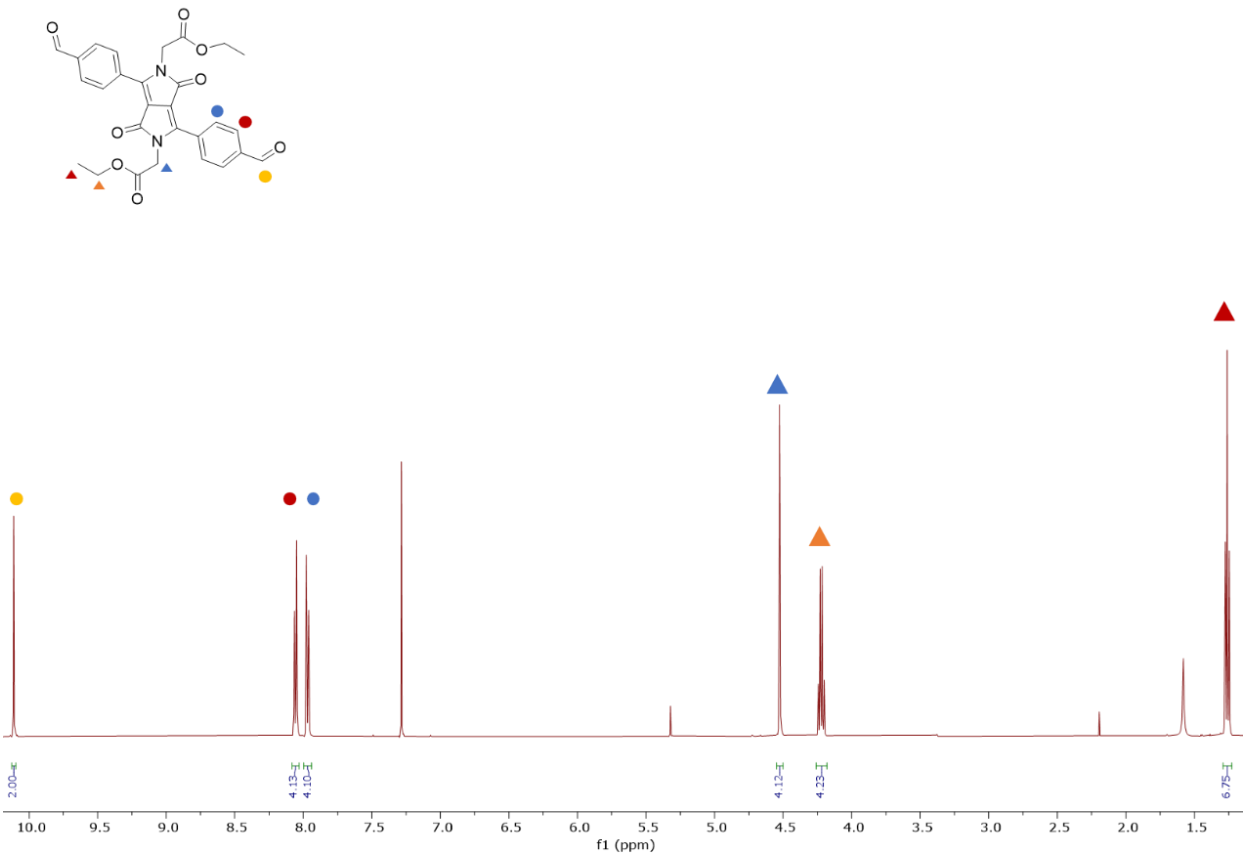

Figure S2. ^{1}H NMR **PhAldDPP N-EA** in $CDCl_3$.

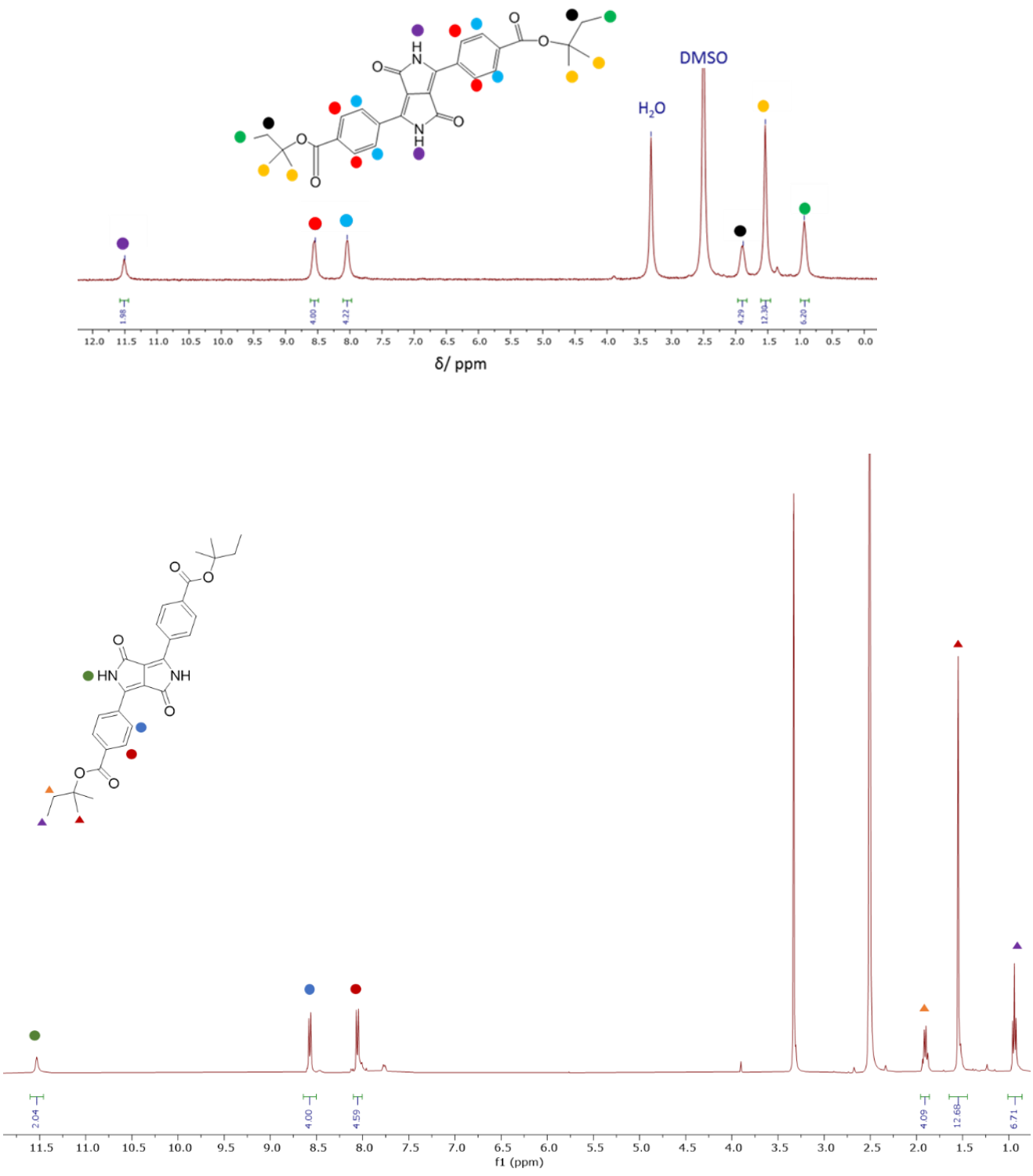

Figure S3. ^{1}H NMR **PhEsterDPP NH** in DMSO d_6.

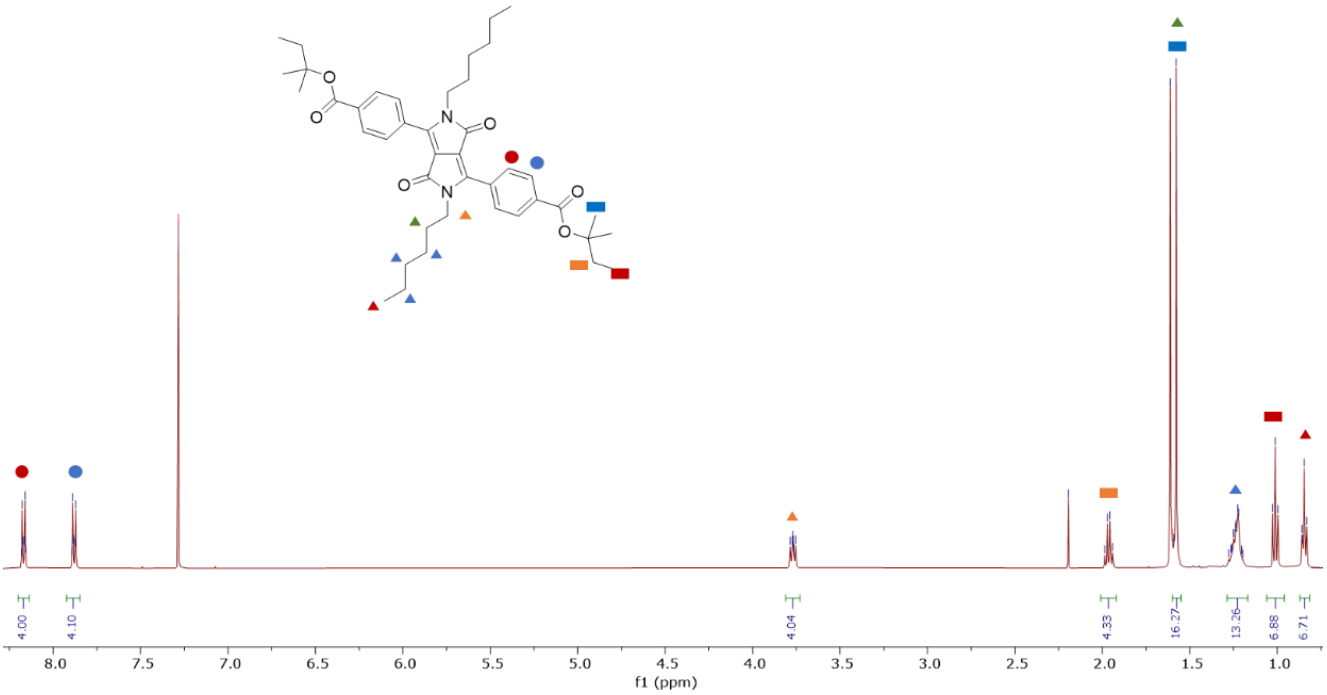

Figure S4. ^{1}H NMR **PhEsterDPP N-Hex** in $CDCl_3$.

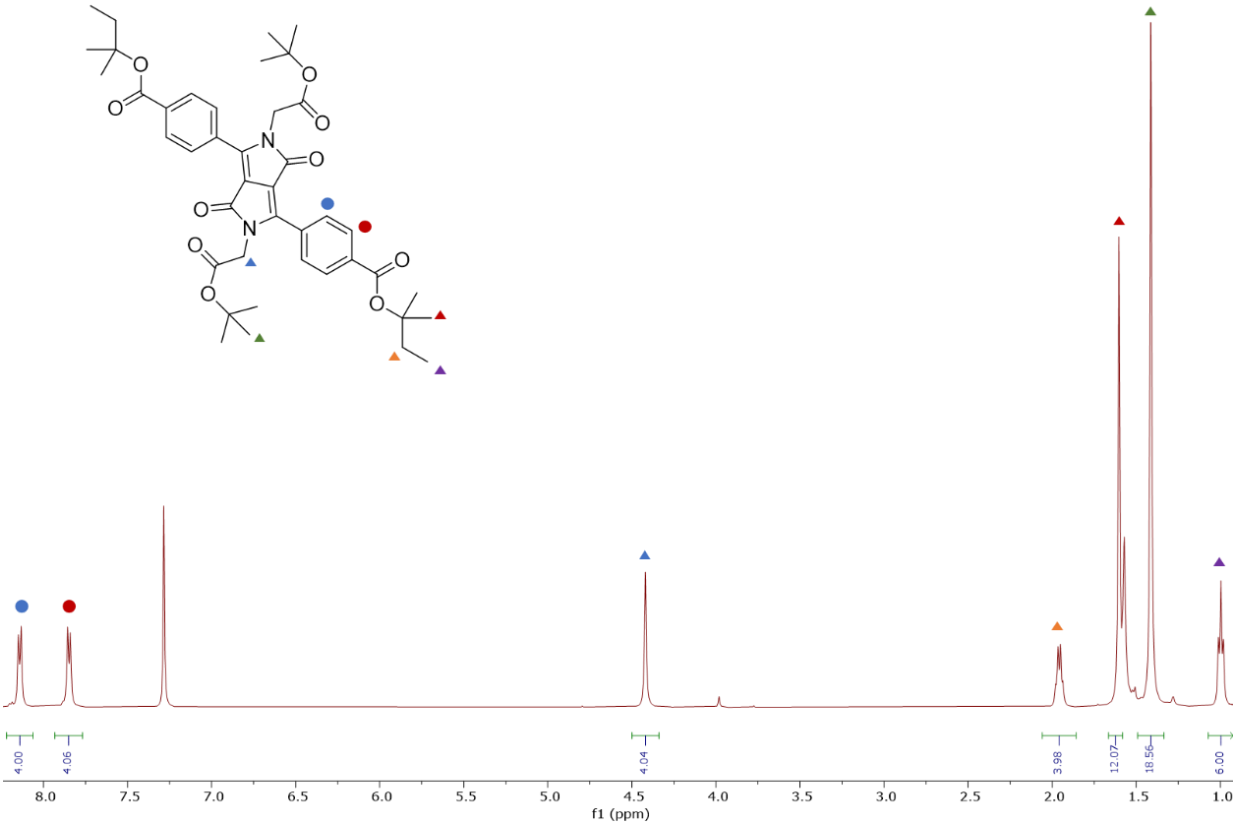

Figure S5. ^{1}H NMR **PhEsterDPP N-TBA** in $CDCl_3$.

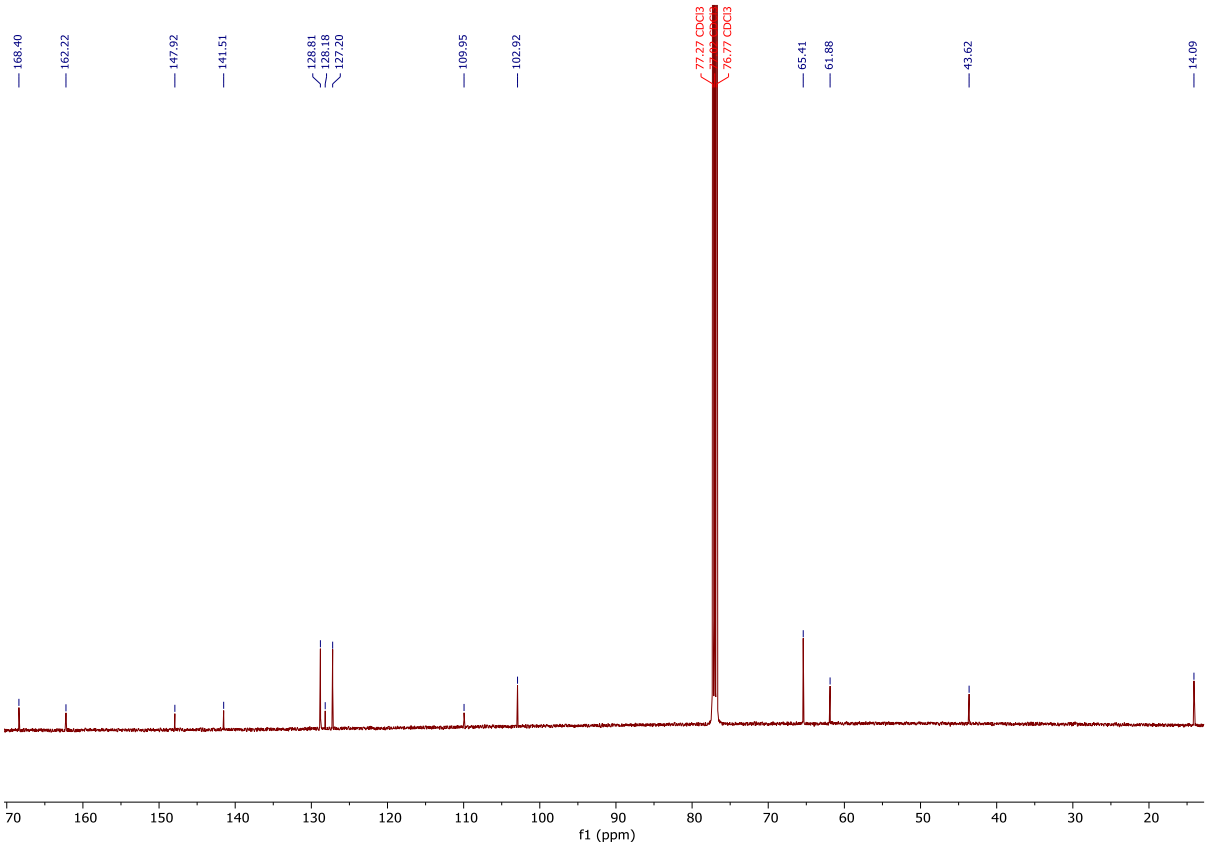

Figure S6. ^{13}C NMR **PhAcetDPP N-EA** in $CDCl_3$.

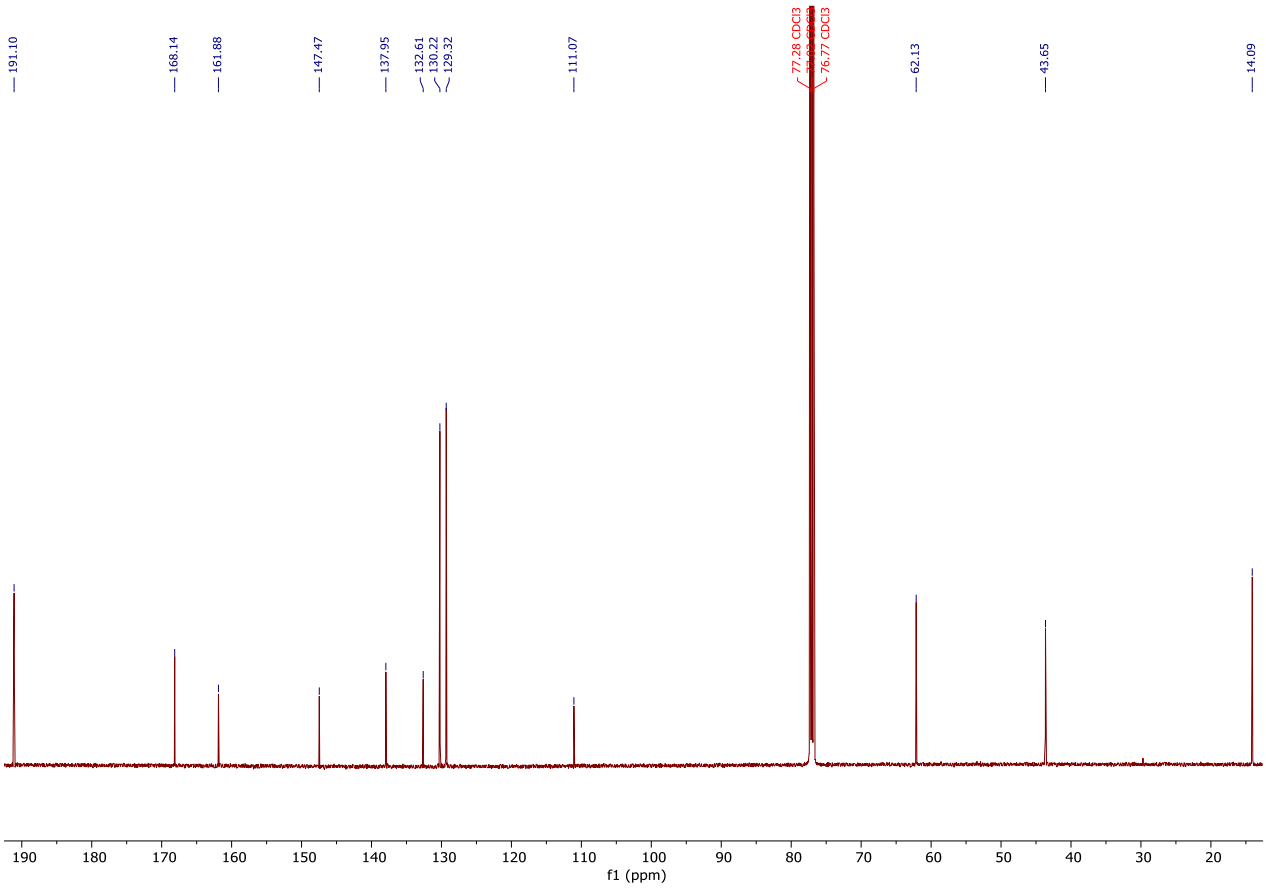

Figure S7. ^{13}C NMR of **PhAldDPP N-EA** in $CDCl_3$**.**

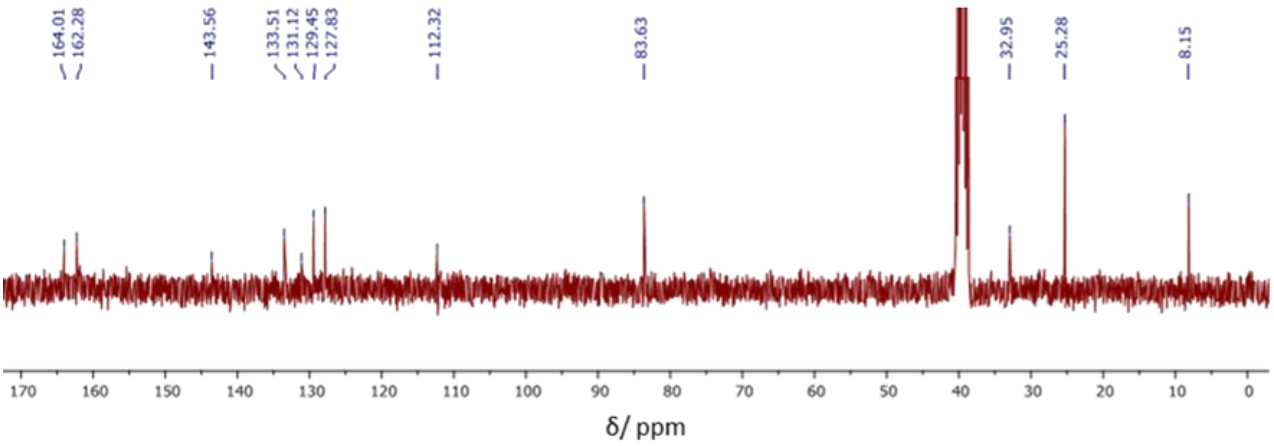

Figure S8. ^{13}C NMR **PhEsterDPP NH** in DMSO-d_6**.**

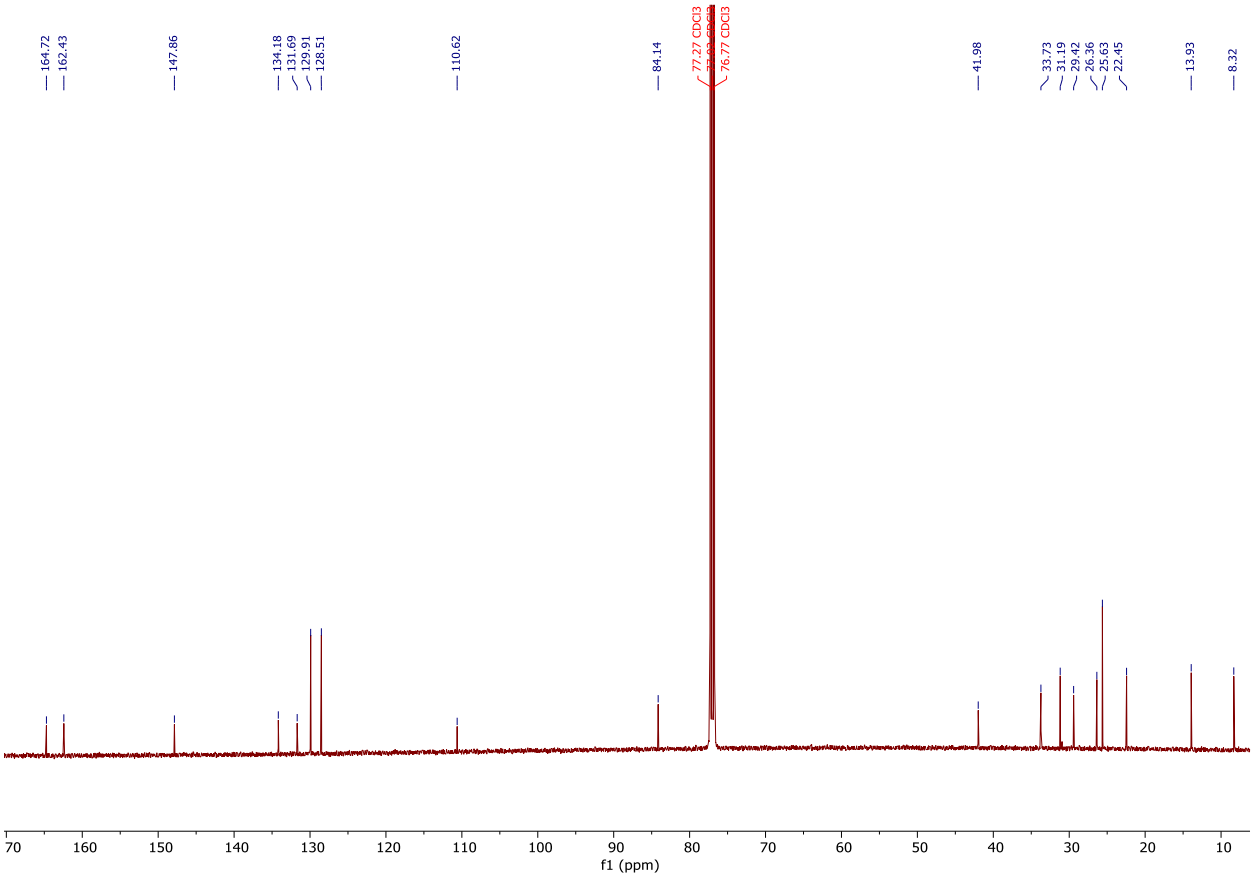

Figure S9. ^{13}C NMR **PhEsterDPP N-Hex** in $CDCl_3$.

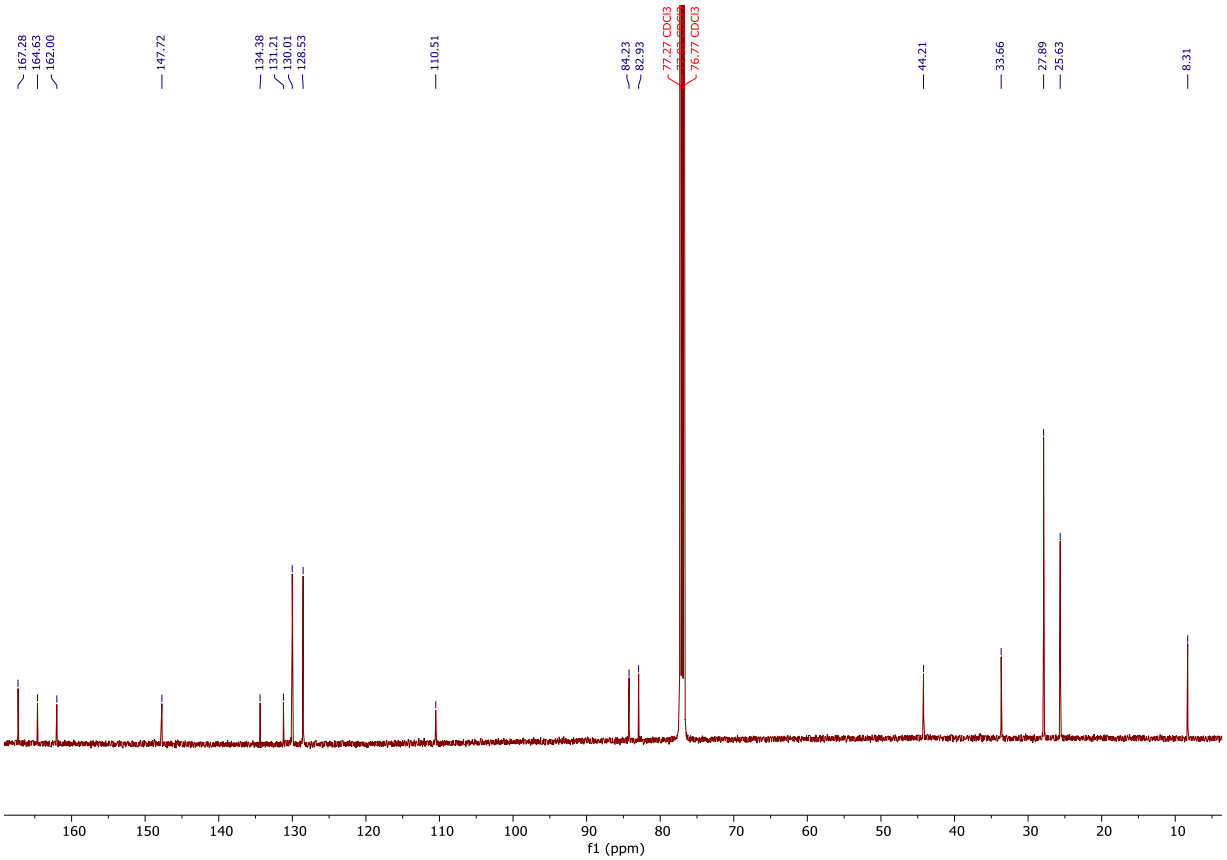

Figure S10. ^{13}C NMR **PhEsterDPP N-TBA** in $CDCl_3$.

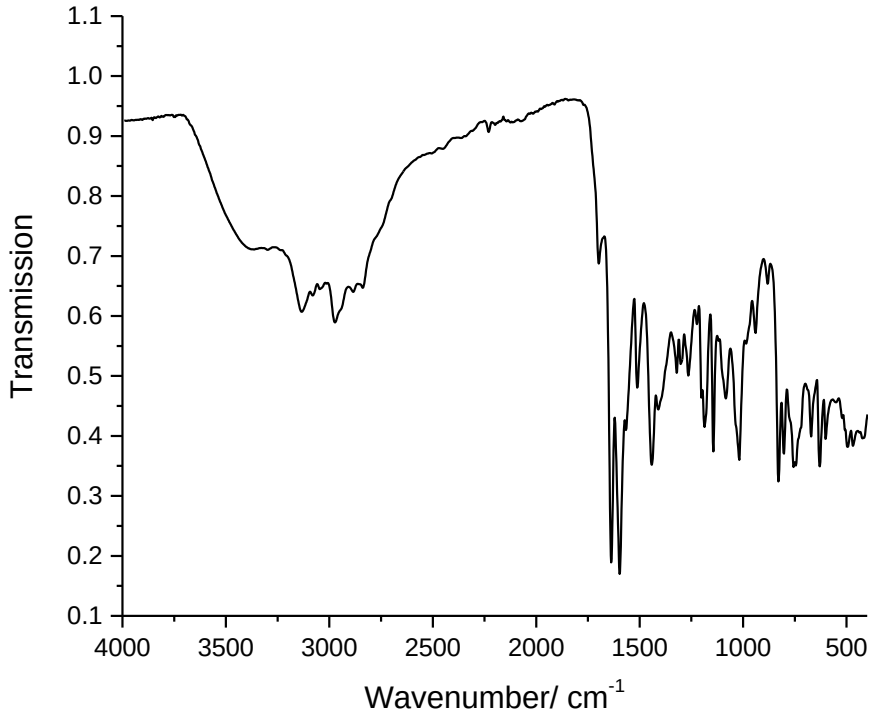

Figure S11. ATR-IR **PhAcetDPP NH**.

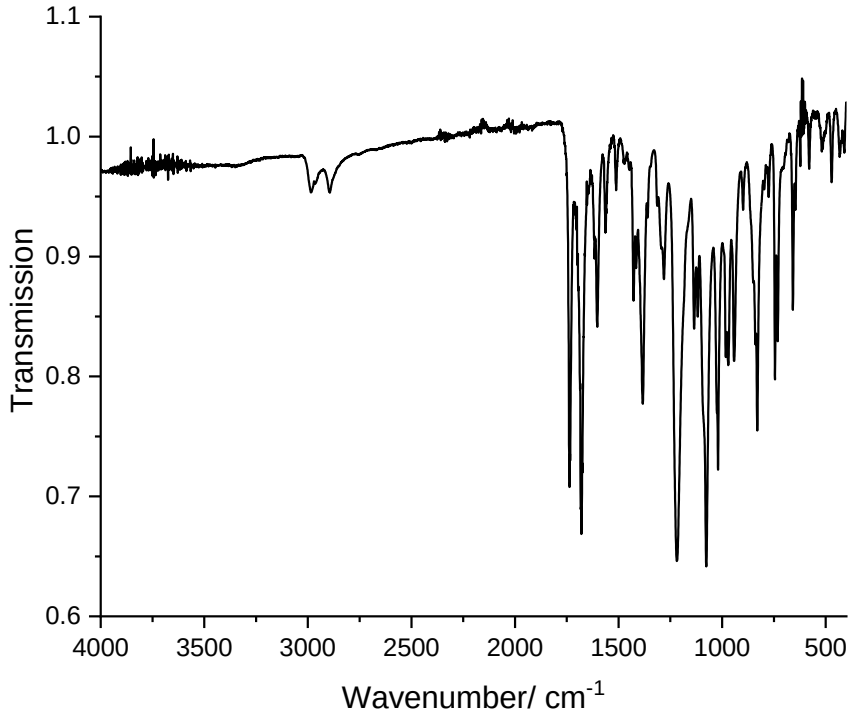

Figure S12. ATR-IR **PhAcetDPP N-EA**.

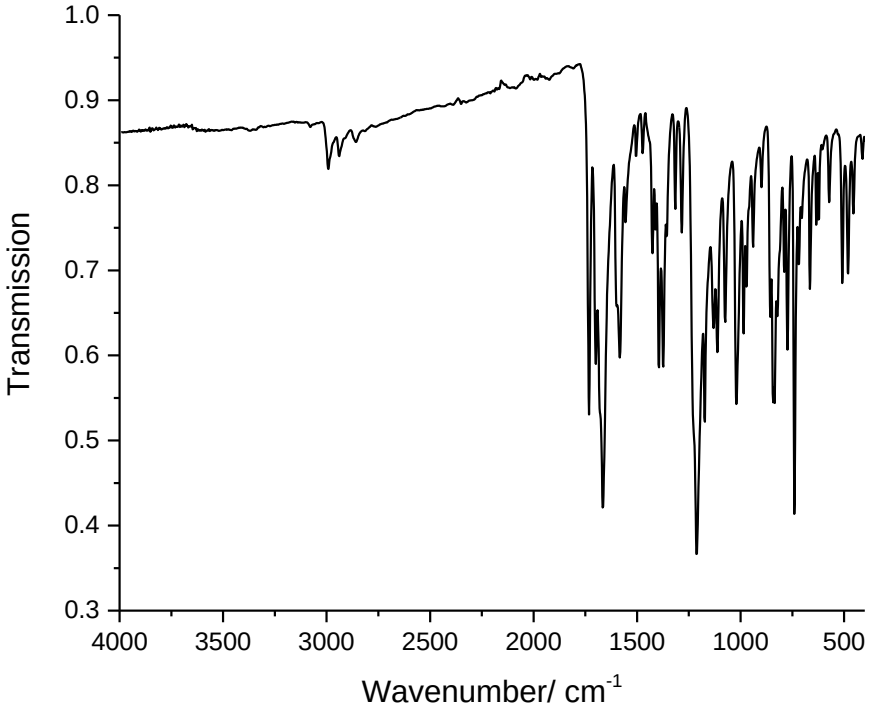

Figure S13. ATR-IR of **PhAldDPP N-EA.**

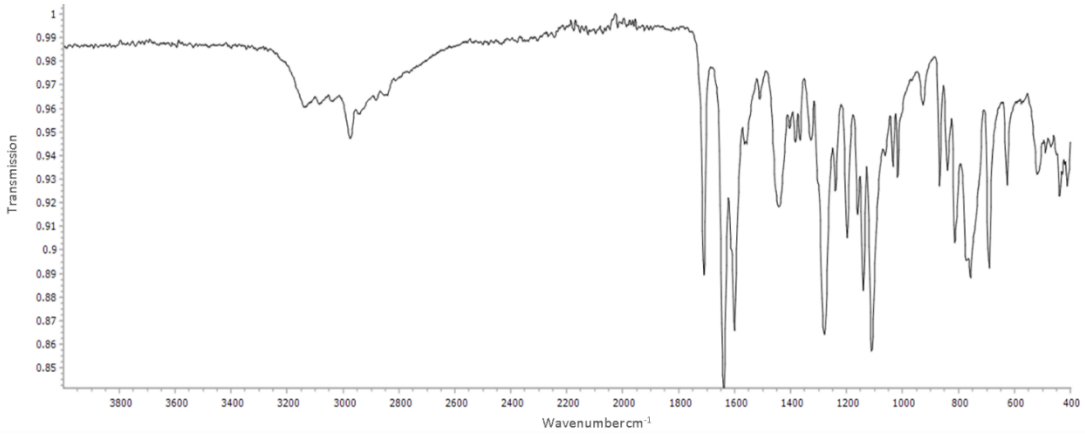

Figure S14. ATR-IR **PhEsterDPP NH.**

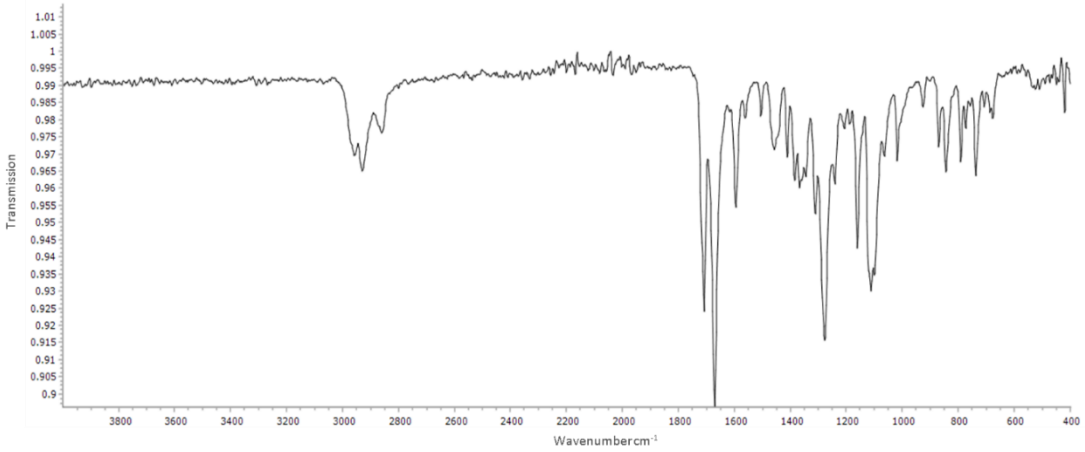

Figure S15. ATR-IR **PhEsterDPP N-Hex**.

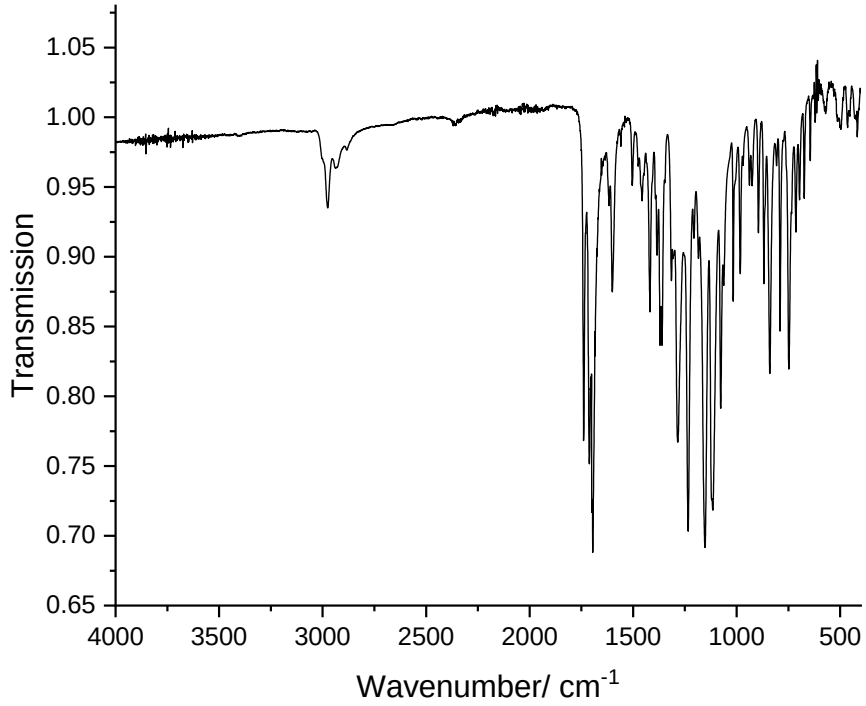

Figure S16. ATR-IR **PhEsterDPP N-TBA**.

Additional supporting figures and tables

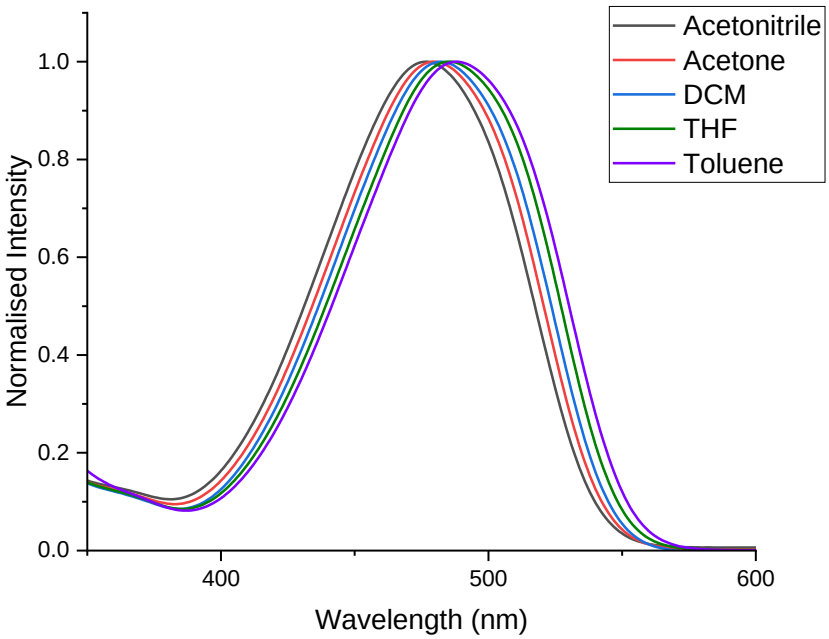

ESI 1.1 UV/vis absorption spectrum of **PhAldDPP N-EA** in various solvents indicating negative solvatochromism.

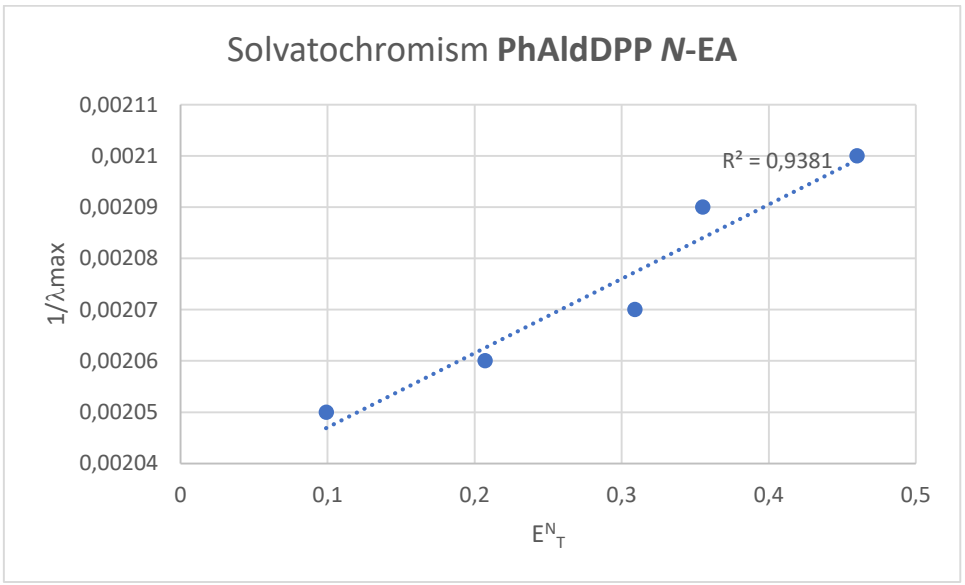

ESI 1.2 A plot of 1/ λ_{max} absorption vs. the Dimroth–Reichardt parameter for **PhAldDPP N-EA,** in various solvents, indicating negative solvatochromism.

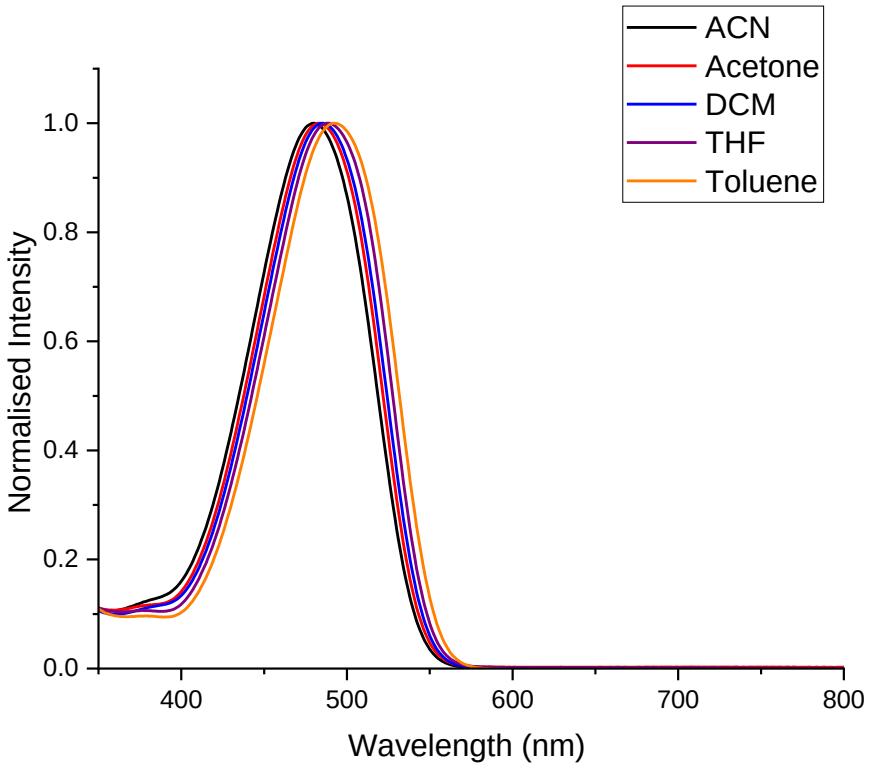

ESI 1.3 UV/vis absorption spectrum of **PhEsterDPP N-Hex** in various solvents indicating negative solvatochromism.

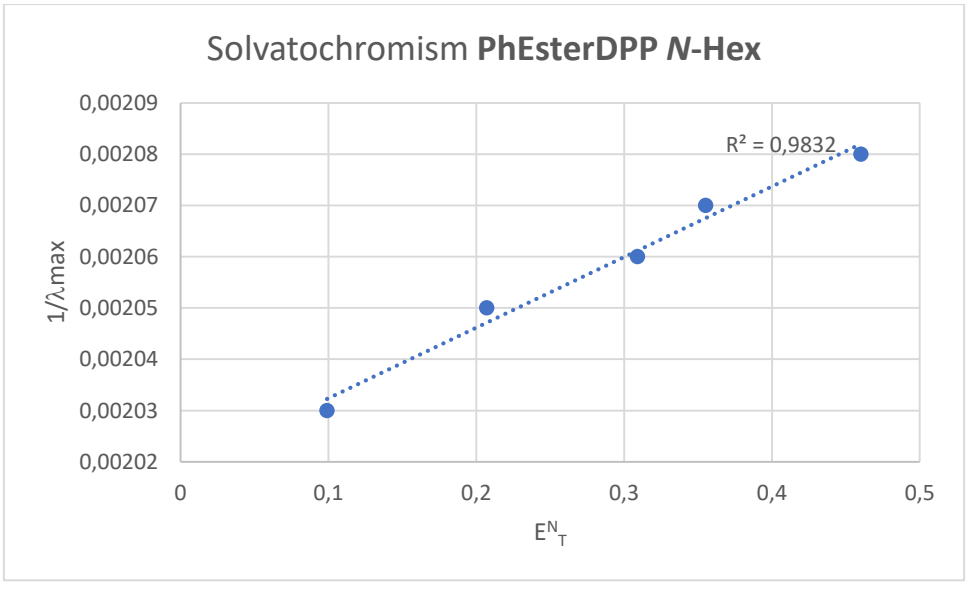

ESI 1.4 A plot of 1/ λ_{max} absorption vs. the Dimroth–Reichardt parameter for **PhEsterDPP N-Hex,** in various solvents, indicating negative solvatochromism.

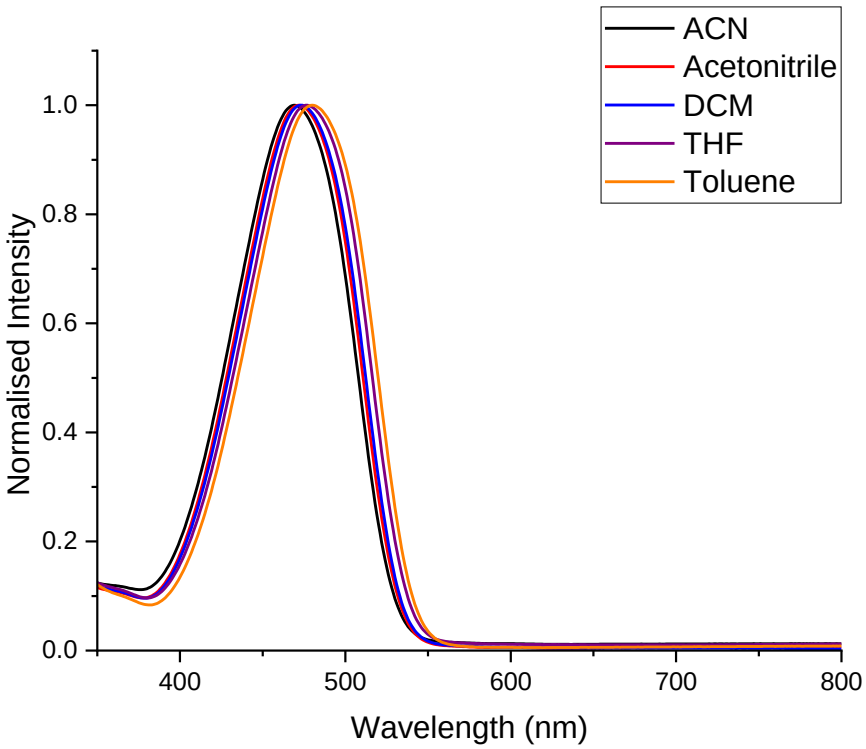

ESI 1.5 UV/vis absorption spectrum of **PhEsterDPP N-TBA** in various solvents indicating negative solvatochromism.

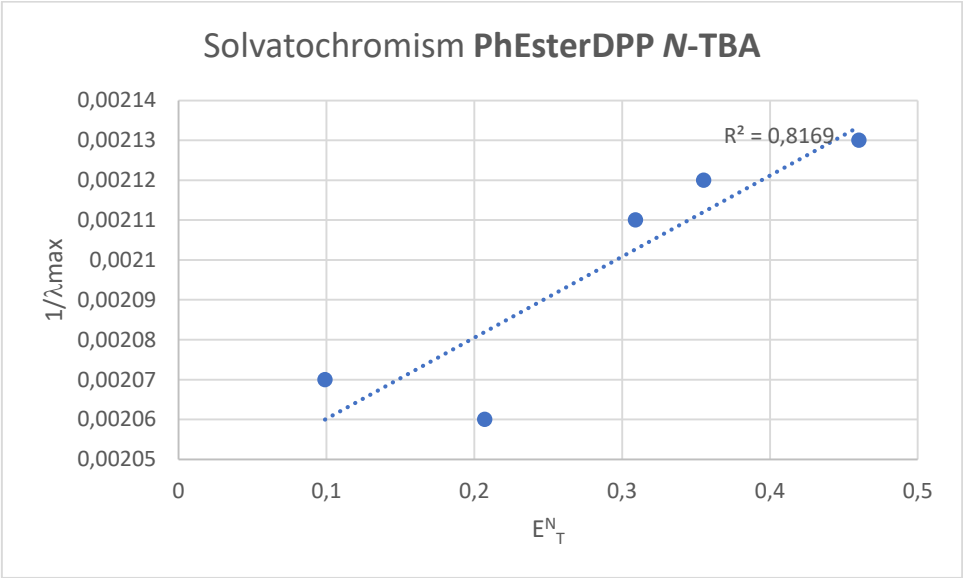

ESI 1.6 A plot of 1/ λ_{max} absorption vs. the Dimroth–Reichardt parameter for **PhEsterDPP N-TBA,** in various solvents, indicating negative solvatochromism.

ESI 1.7 Table of UV/vis absorption λ_{max} and ε for the **PhAldDPP N-EA, PhEsterDPP N-Hex** and **PhEsterDPP N-TBA** in various solvents

Compound	Solvent		Absorption λ_{max} [nm]	ε [dm^3mol^{-1} cm^{-1}]
PhAldDPP N-EA	Toluene		488	16,200
	THF		486	16,200
	DCM		482	16,000
	Acetone		479	14,600
	Acetonitrile		477	20,000
PhEsterDPP N-Hex	Toluene		493	17,000
	THF		488	23,100
	DCM		485	24,500
	Acetone		483	26,600
	Acetonitrile		480	24,900
PhEsterDPP N-TBA	Toluene		482	17,000
	THF		486	19,500
	DCM		473	19,500
	Acetone		472	21,000
	Acetonitrile		469	19,200

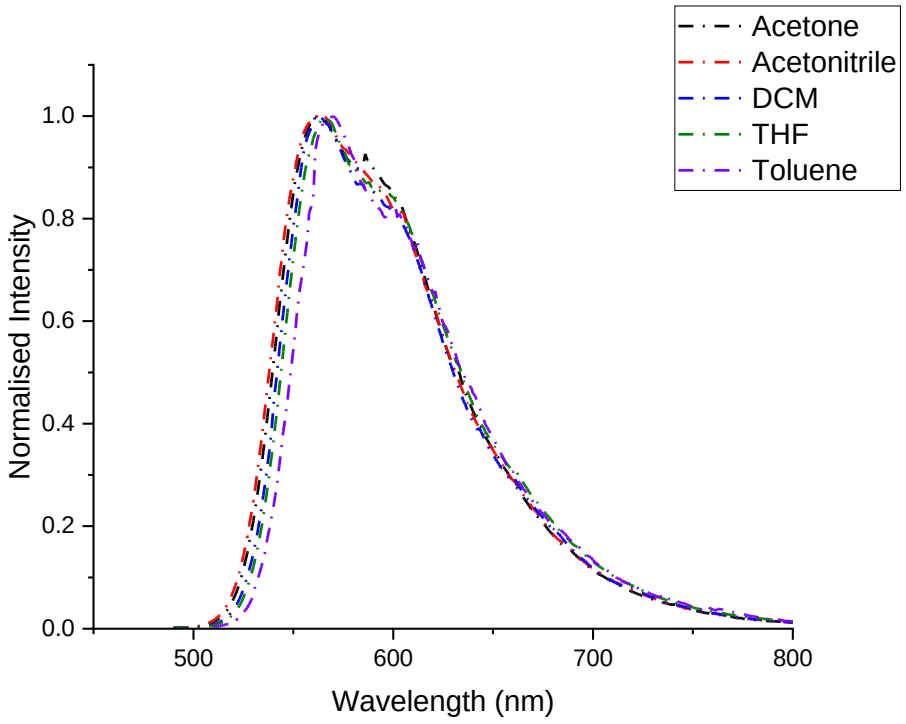

ESI 1.8 . Normalised Emission spectrum for **PhAldDPP N-EA** in various solvents

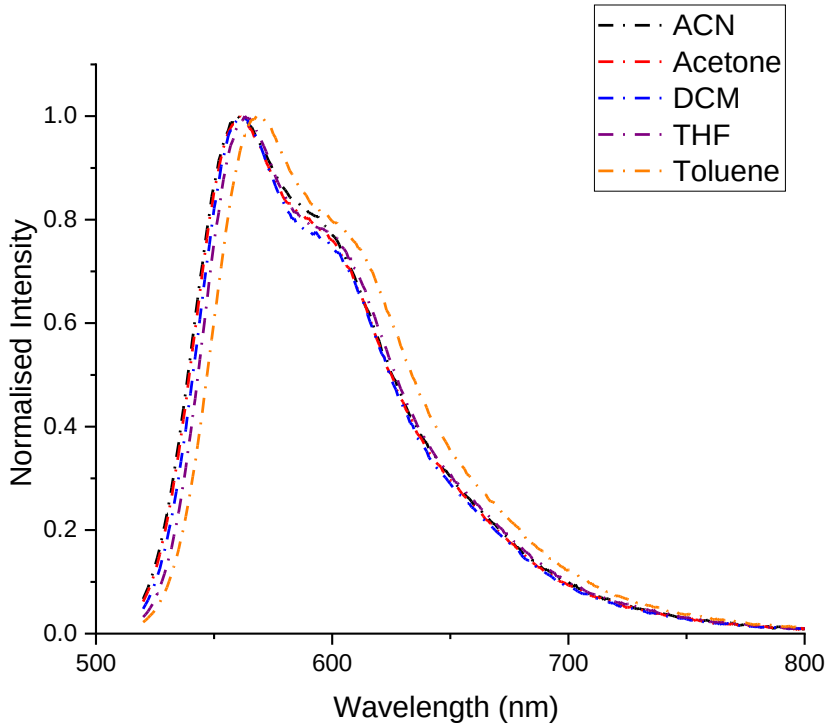

ESI 1.9 Normalised Emission spectrum for **PhEsterDPP N-Hex** in various solvents

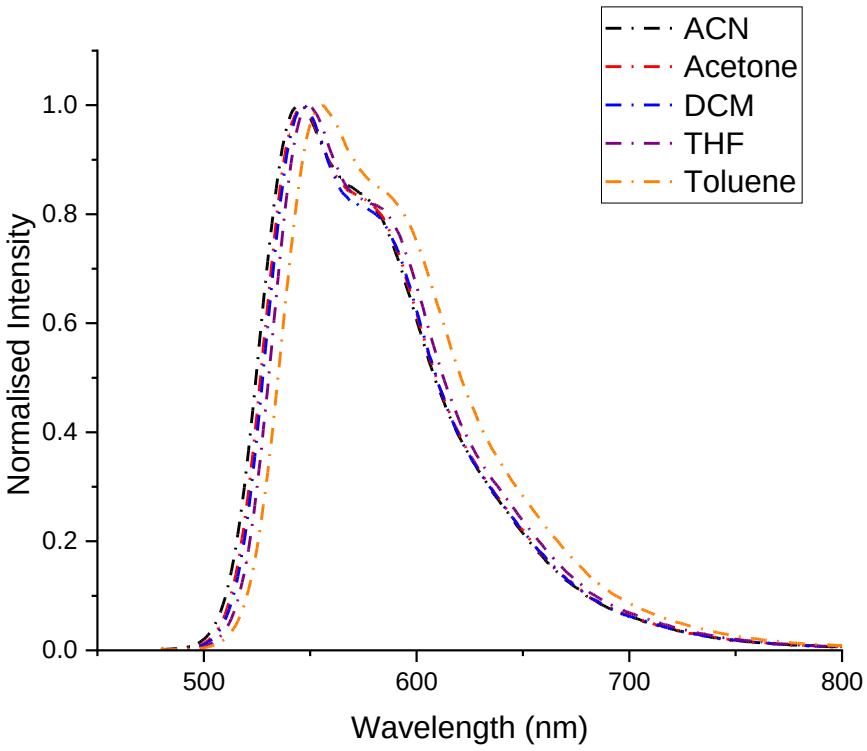

ESI 1.10 Normalised Emission spectrum for **PhEsterDPP N-TBA** in various solvents

ESI 1.11 Table of Solution UV/Vis absorption λ_{max}, fluorescence λ_{max} and Stokes shift of **PhAldDPP N-EA** , **PhEsterDPP N-TBA** and **PhEsterDPP N-Hex** in various solvents.

Compound	Solvent	Absorption λ_{max} [nm]	Emission λ_{max} [nm]	Stokes shift [nm]
PhAldDPP N-EA	Toluene	488	570	82
	THF	486	565	79
	DCM	482	563	81
	Acetone	479	561	81
	Acetonitrile	477	561	84
PhEsterDPP N-Hex	Toluene	493	568	75
	THF	488	563	75
	DCM	485	561	76
	Acetone	483	561	78
	Acetonitrile	480	560	80
PhEsterDPP N-TBA	Toluene	488	570	76
	THF	486	565	71
	DCM	473	547	74
	Acetone	472	547	75
	Acetonitrile	469	547	75

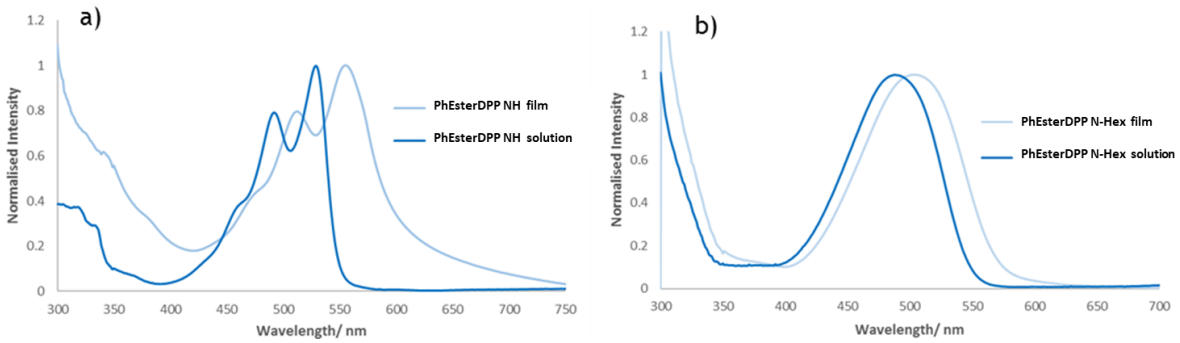

ESI 1.12 Solution and thin film UV/Vis absorption spectra of a) **PhEsterDPP NH** and B) **PhEsterDPP N-Hex** in THF

ESI 1.13 Table of Solution and solid state absorption properties of **PhEsterDPP NH** and **PhEsterDPP N-Hex**

Compound	Absorption λ_{max} solution [nm]	Absorption λ_{max} film [nm]	Absorption edge onset film [nm]	Optical Eg film [eV]
PhEsterDPP NH	529	555 [a]	613 [a]	2.03 [a]
PhEsterDPP N-Hex	488	504 [a]	577 [a]	2.15 [a]

. [a]Thin films were formed on glass slides by drop casting of a concentrated THF solution (0.5 mg ml^{-1})

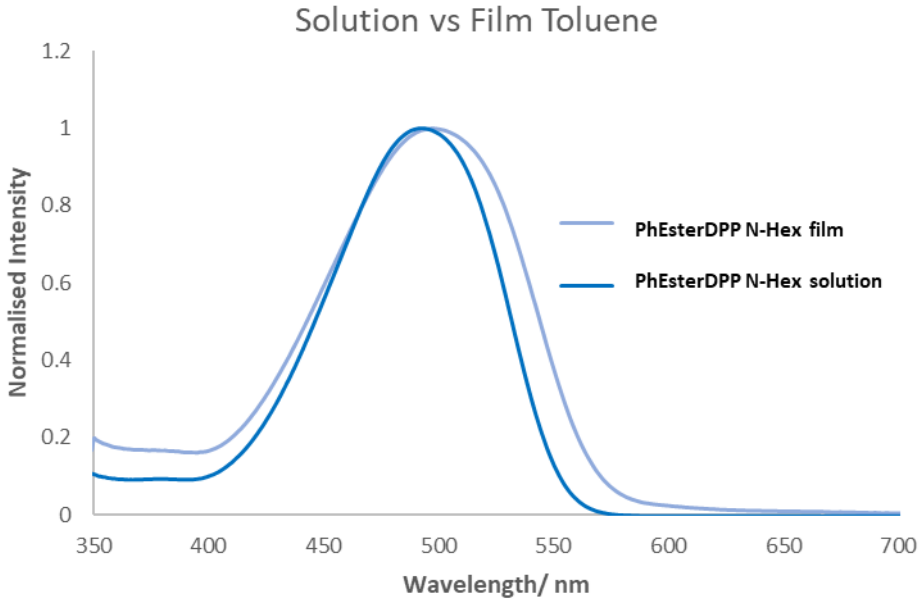

ESI 1.14. Solid and solution absorption of **PhEsterDPP N-Hex** in toluene

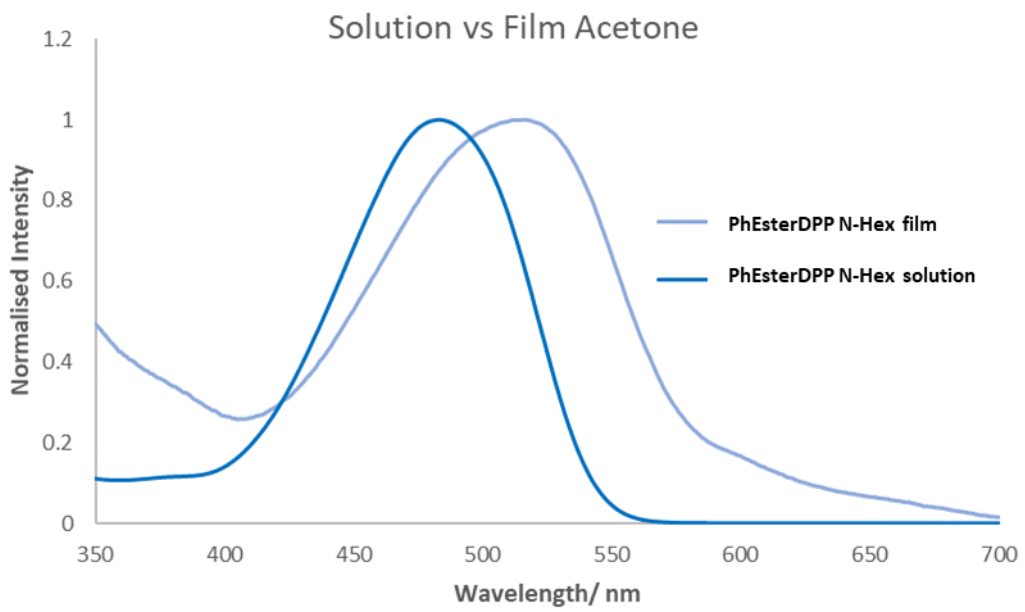

ESI 1.15 Solid and solution absorption of **PhEsterDPP N-Hex** in acetone

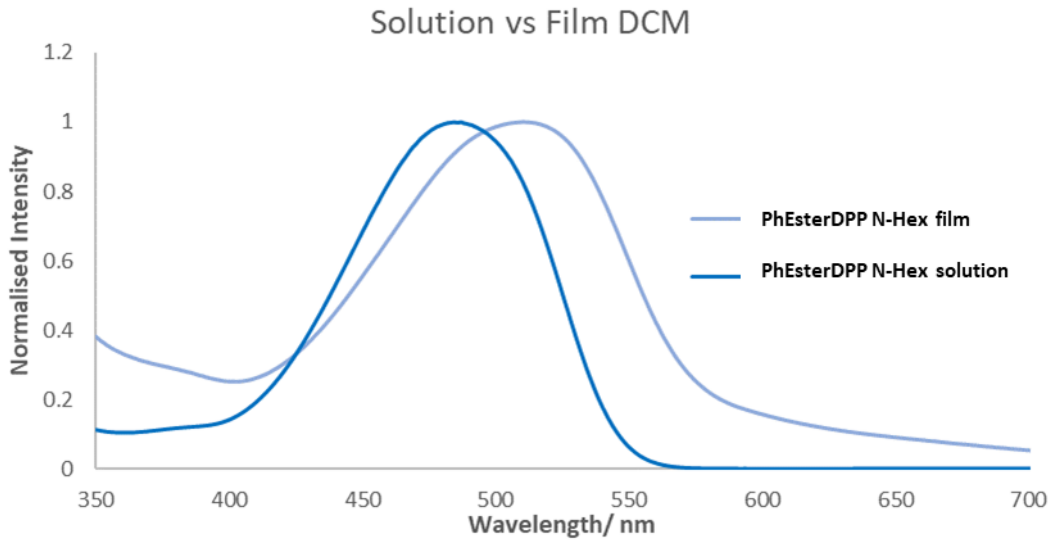

ESI 1.16 Solid and solution absorption of **PhEsterDPP N-Hex** in DCM

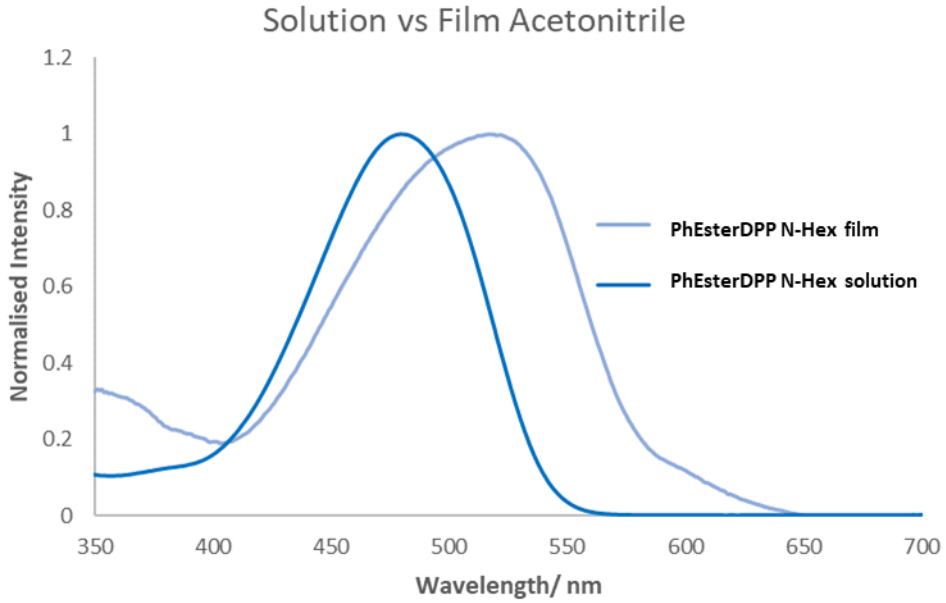

ESI 1.17 Solid and solution absorption of **PhEsterDPP N-Hex** in acetonitrile

ESI 1.18 Table of solution and solid state UV/Vis absorption properties of **PhEsterDPP NH** and **PhEsterDPP N-Hex**

Compound	Solvent	Absorption λ_{max} solution [nm]	Absorption λ_{max} film [nm]	Absorption edge onset film [nm]	Optical E_g film [eV]
PhEsterDPP NH	THF	529	555	613	2.03
PhEsterDPP N-Hex	Toluene	493	497	572	2.17
	THF	488	504	577	2.15
	DCM	485	510	582	2.13
	Acetone	483	517	584	2.13
	Acetonitrile	480	517	593	2.09

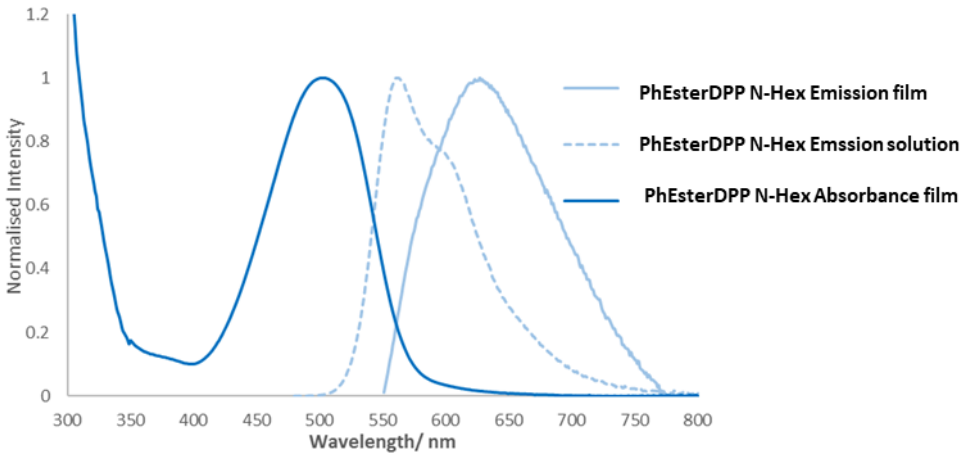

ESI 1.19 Thin film UV/Vis absorption and solution and thin film emission spectra of **PhEsterDPP N-Hex** in THF.

ESI 1.20 Table of Solution and solid state photophysical properties of **PhEsterDPP N-Hex**

Compound	Absorption λ_{max} solution [nm]	Emission λ_{max} solution [nm]	Absorption λ_{max} film [nm]	Emission λ_{max} film [nm]	Stokes shift solution [nm]	Stokes shift film [nm]
PhEsterDPP N-Hex	488	563	504[a]	627[a]	75	123[a]

. [a]Thin films were formed on glass slides by drop casting of a concentrated THF solution (0.5 mg ml^{-1})

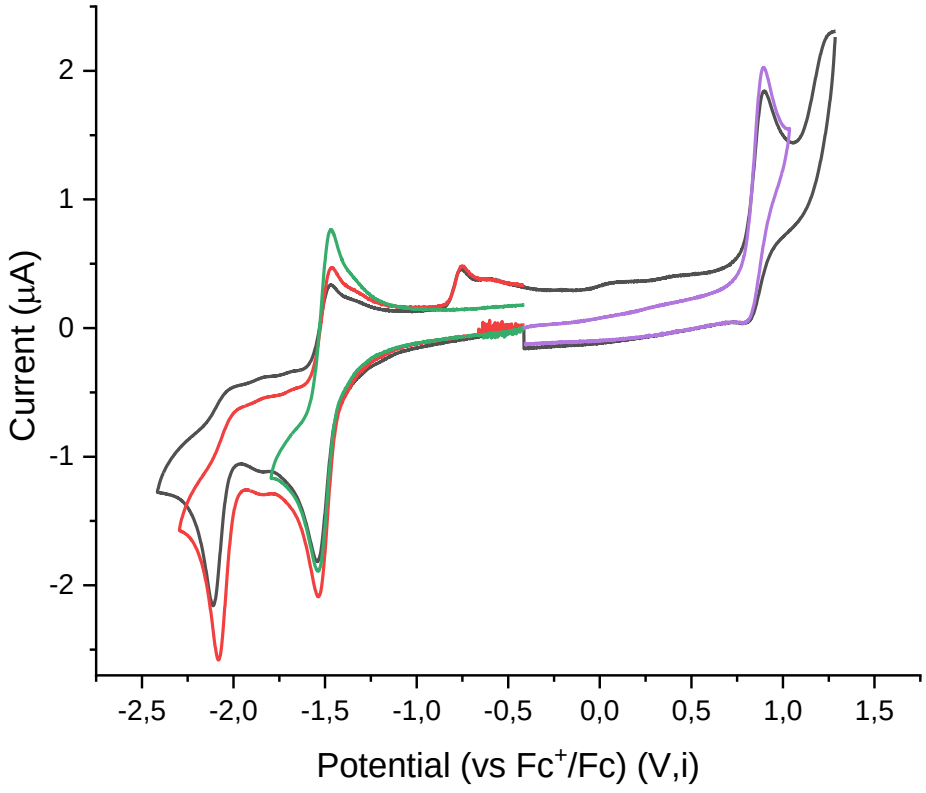

ESI 1.21 Cyclic voltammogram obtained for **PhAcetDPP N-EA**, at a scan rate of 100 mVs^{-1}, under an argon atmosphere (Black line), cyclic voltammogram obtained for the first and second reduction processes, at a scan rate of 100 mVs^{-1} (Green red lines). Cyclic voltammogram obtained for the oxidation process, at a scan rate of 100 mVs^{-1}. Voltammograms were obtained in acetonitrile containing [*n*-Bu_4N][PF_6] (0.2 M). Potentials are plotted against the Fc^+/Fc couple employed as an internal standard.

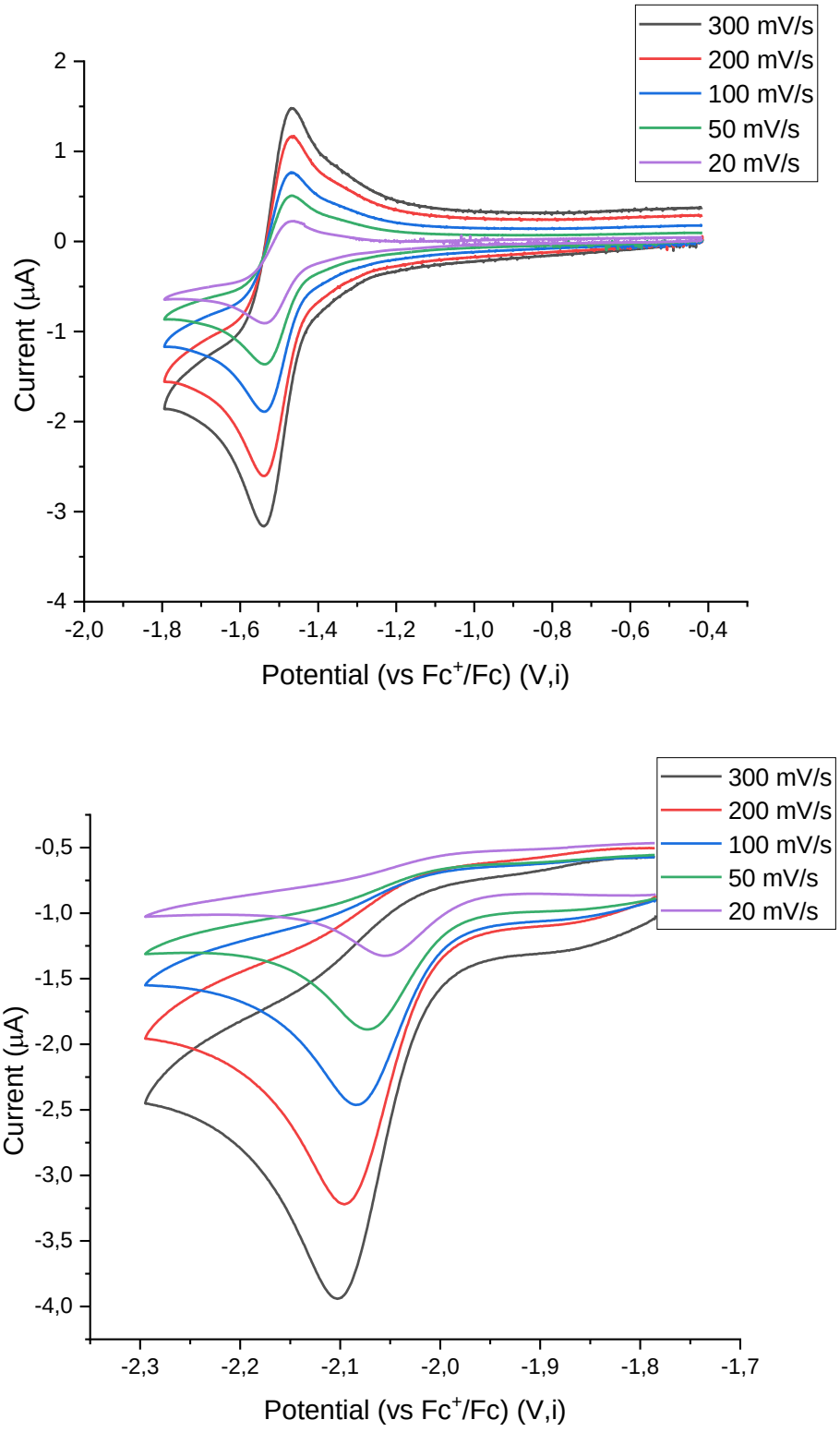

ESI 1.22 Scan rate dependence of the reduction process for **PhAcetDPP N-EA** portraying reduction of neutral molecule to radical anion (Top) to dianion (Bottom), determined through cyclic voltammetry (referenced against potential of Fc^{+}/Fc).

ESI 1.23 Table of Peak potentials of first and second reduction process **PhAcetDPP N-EA** (referenced against potential of Fc^+/Fc), and E_p^a-E_p^c for Fc^+/Fc for comparison.

Scan rate [mV s^{-1}]	E_{pc} (1st) [V]	E_{pa} (1st) [V]	E_{pa} - E_{pc} (1st) [V]	$E_{1/2}$ Red (1st) [V]	E_{pc} (2nd) [V]	E_{pa} (2nd) [V]	E_{pa} - E_{pc} (2nd) [V]	$E_{1/2}$Red (2nd) [V]	E_{pa} - E_{pc} Fc^+/Fc [V]
300	-1.53	-1.46	0.07	-1.50	-2.10	N.A.	N.A.	N.A.	0.06
200	-1.53	-1.46	0.07	-1.50	-2.09	N.A.	N.A.	N.A.	0.06
100	-1.53	-1.46	0.07	-1.50	-2.08	N.A.	N.A.	N.A.	0.06
50	-1.53	-1.46	0.07	-1.50	-2.07	N.A.	N.A.	N.A.	0.06
20	-1.53	-1.46	0.07	-1.50	-2.05	N.A.	N.A.	N.A.	0.06

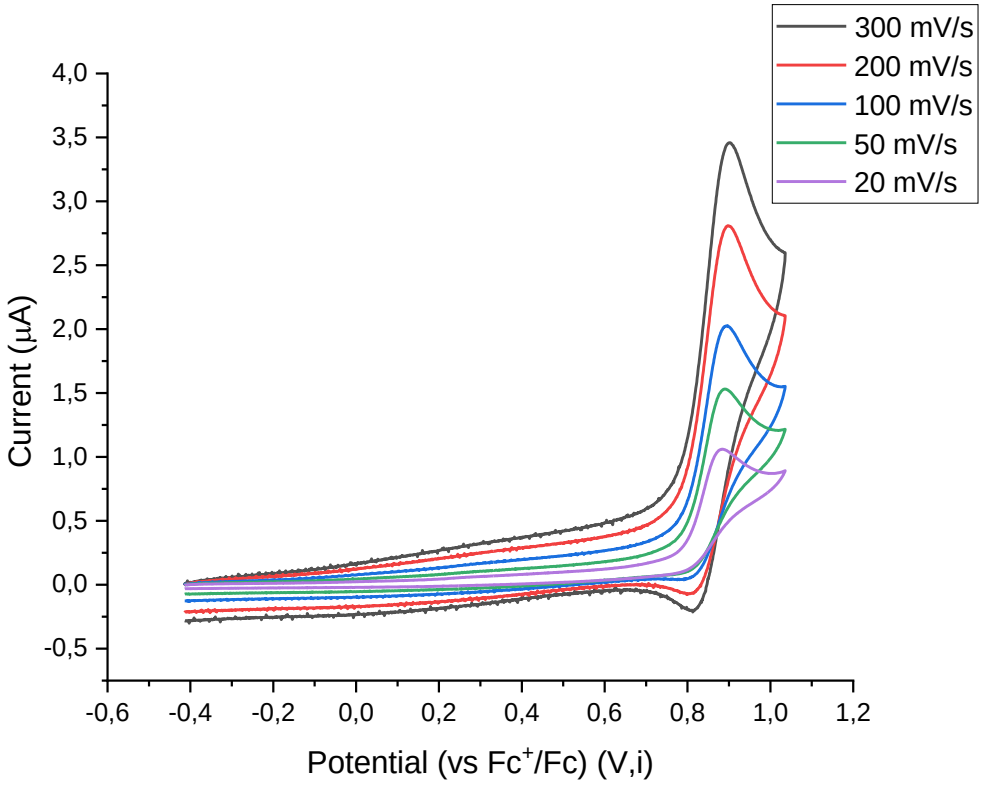

ESI 1.24 Scan rate dependence of the Oxidation processes of the **PhAcetDPP N-EA** portraying oxidation of neutral molecule to radical cation, determined through cyclic voltammetry at 100 mV/s scan rate (referenced against potential of Fc^+/Fc).

ESI 1.25 Table of Peak potentials of oxidation process for **PhAcetDPP N-EA** (referenced against potential of Fc^{+}/Fc).

Scan rate [mV s^{-1}]	E_{pc} [V]	E_{pa} [V]	E_{pa} - E_{pc} [V]	$E_{1/2}$ Ox [V]
300	0.90	0.81	0.09	0.86
200	0.90	0.81	0.08	0.85
100	0.89	0.81	0.08	0.85
50	0.89	N.A.	N.A.	N.A.
20	0.88	N.A.	N.A.	N.A.

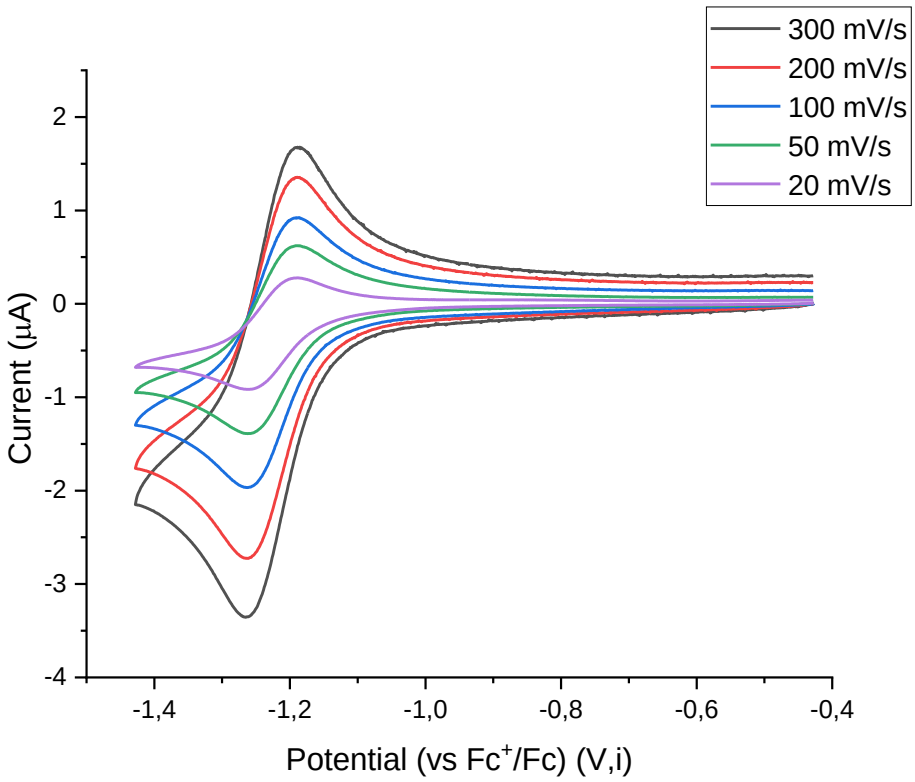

ESI 1.26 Scan rate dependence of the 1st reduction process for **PhAldDPP N-EA** portraying reduction processes, determined through cyclic voltammetry (referenced against potential of Fc^{+}/Fc).

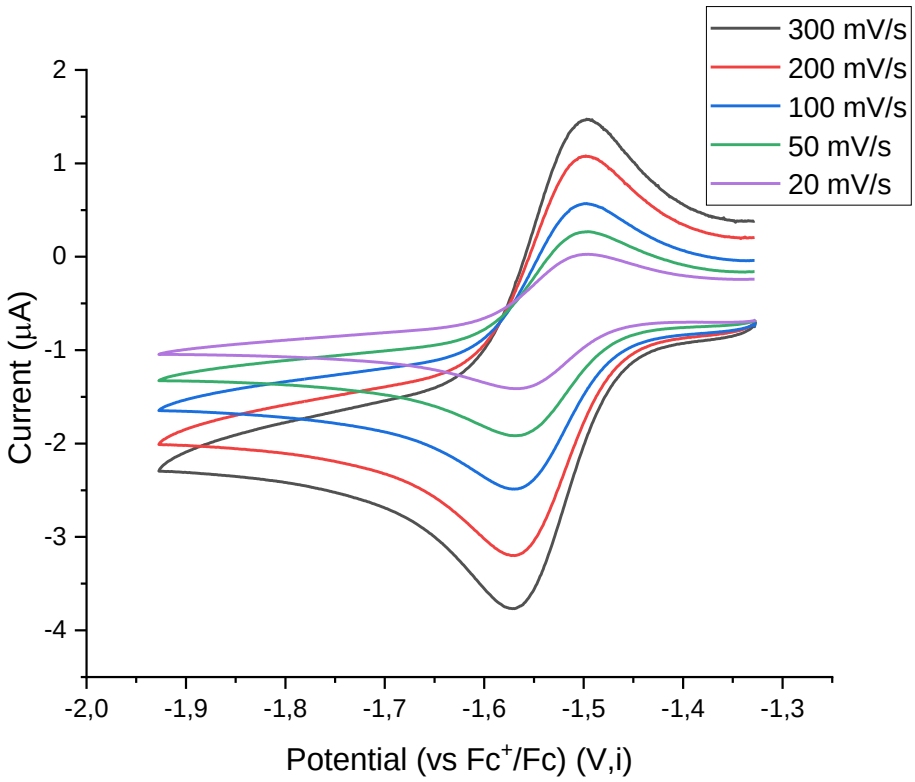

ESI 1.27 Scan rate dependence of the 2nd reduction process for **PhAldDPP N-EA** portraying reduction processes, determined through cyclic voltammetry (referenced against potential of Fc^{+}/Fc).

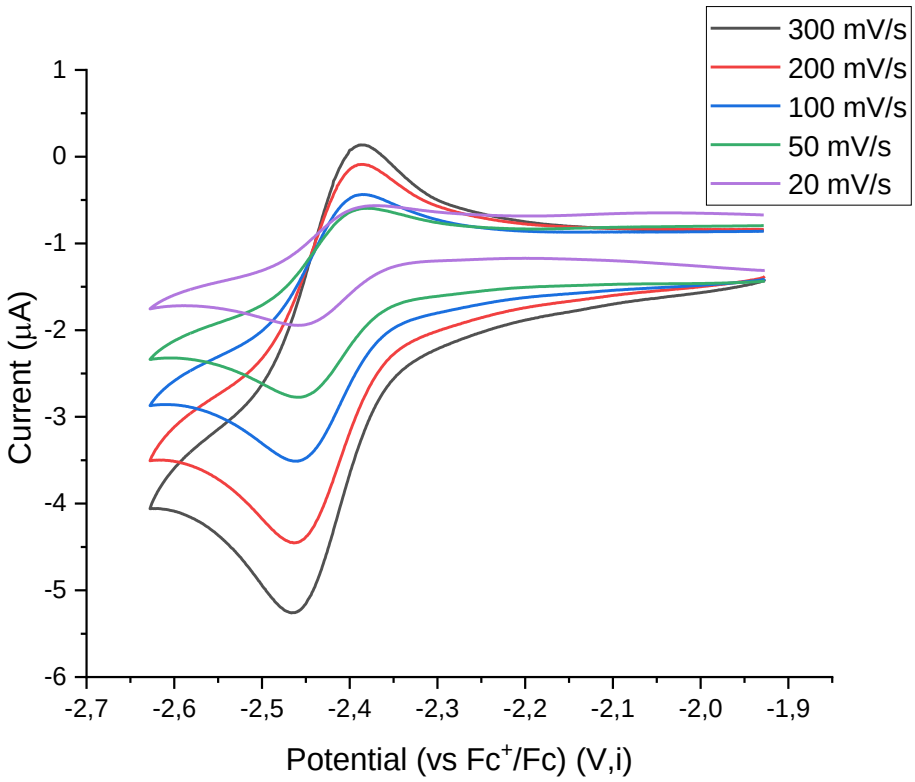

ESI 1.28 Scan rate dependence of the 3rd reduction process for **PhAldDPP N-EA** portraying reduction processes, determined through cyclic voltammetry (referenced against potential of Fc^+/Fc).

ESI 1.29 Table of Peak potentials of the reduction processes for **PhAldDPP N-EA** (referenced against potential of Fc^+/Fc), and E_p^a-E_p^c for Fc^+/Fc for comparison.

Scan rate [mV s^{-1}]	**E_{pc} (1st) [V]**	**E_{pa} (1st) [V]**	**E_{pa} - E_{pc} (1st) [V]**	**$E_{1/2}$Red (1st) [V]**	**E_{pc} (2nd) [V]**	**E_{pa} (2nd) [V]**	**E_{pa} - E_{pc} (2nd) [V]**	**$E_{1/2}$ Red (2nd) [V]**	**E_{pc} (3rd) [V]**	**E_{pa} (3rd) [V]**	**E_{pa} - E_{pc} (3rd) [V]**	**$E_{1/2}$Red (3rd) [V]**	**E_{pa} - E_{pc} Fc^+/Fc [V]**
300	-1.26	-1.19	0.08	-1.23	-1.57	-1.49	0.08	-1.53	-2.46	-2.38	0.08	-2.42	0.06
200	-1.26	-1.18	0.08	-1.22	-1.56	-1.49	0.07	-1.525	-2.46	-2.38	0.08	-2.42	0.06
100	-1.26	-1.18	0.08	-1.22	-1.56	-1.50	0.06	-1.53	-2.46	-2.38	0.08	-2.42	0.06
50	-1.26	-1.18	0.08	-1.22	-1.56	-1.50	0.06	-1.53	-2.45	-2.38	0.08	-2.42	0.06
20	-1.26	-1.18	0.07	-1.22	-1.56	-1.50	0.06	-1.53	-2.45	-2.38	0.08	-2.42	0.06

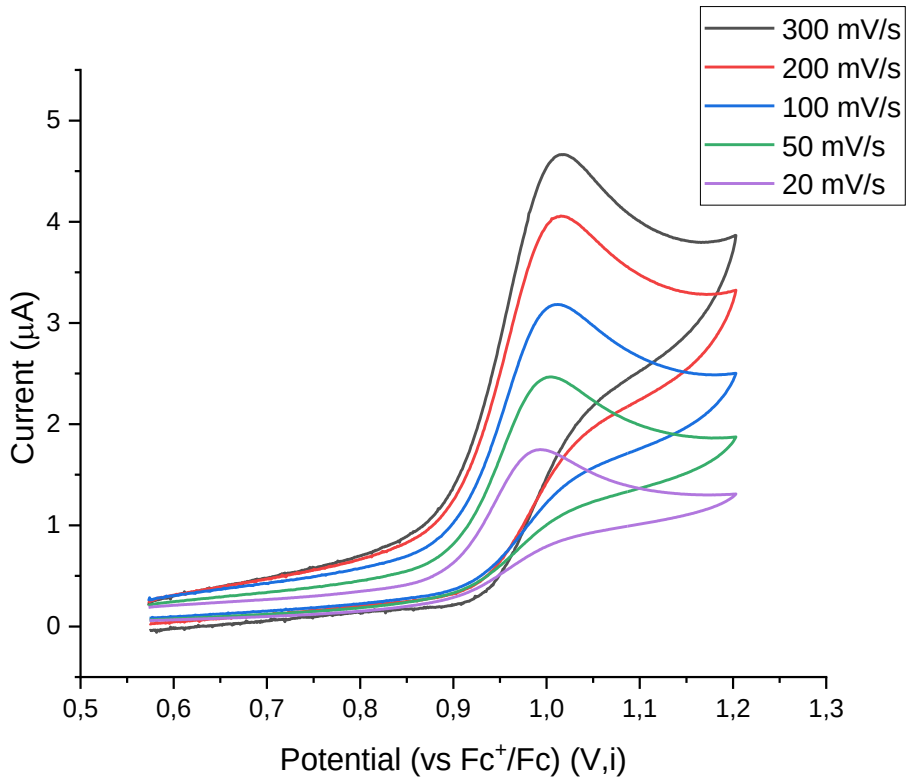

ESI 1.30 Scan rate dependence of oxidation processes of the **PhAldDPP N-EA** derivatives portraying oxidation of neutral molecule to radical cation, determined through cyclic voltammetry at variable scan rate (referenced against potential of Fc^+/Fc).

ESI 1.31 Table of peak potentials of oxidation process for **PhAldDPP N-EA** (referenced against potential of Fc^+/Fc).

Scan rate [mV s^{-1}]	E_{pc} [V]	E_{pa} [V]	E_{pa} - E_{pc} [V]	$E_{1/2}$ Ox [V]
300	0.90	N.A.	N.A.	N.A.
200	0.90	N.A.	N.A.	N.A.
100	0.89	N.A.	N.A.	N.A.
50	0.89	N.A.	N.A.	N.A.
20	0.88	N.A.	N.A.	N.A.

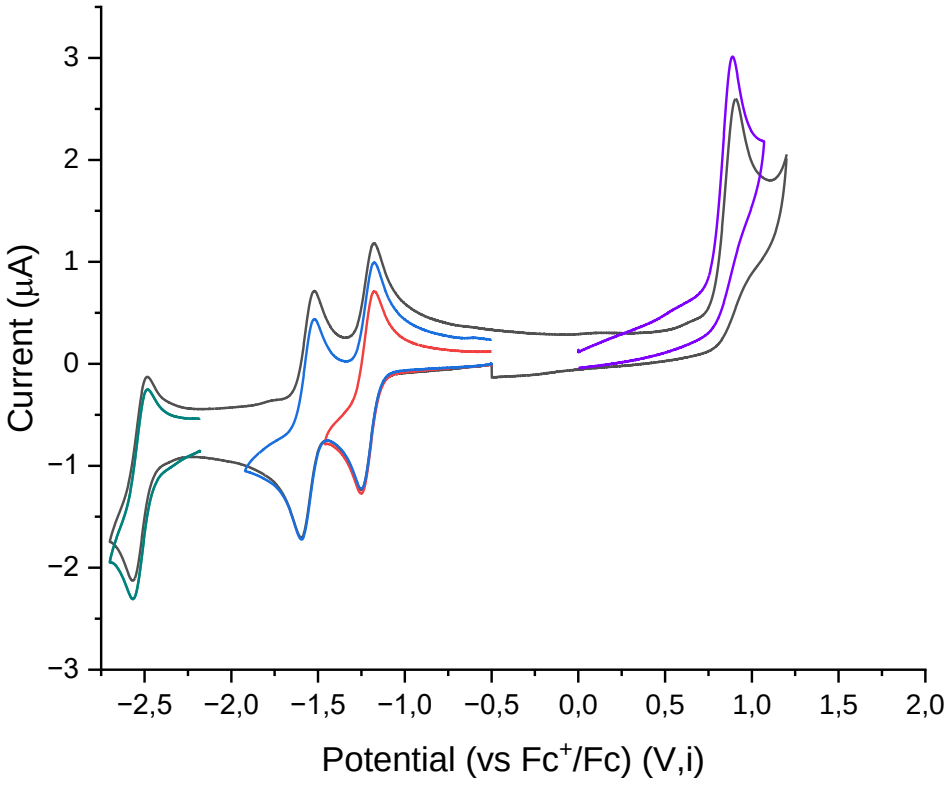

ESI 1.32 Cyclic voltammogram obtained for **PhAldDPP N-EA**, at a scan rate of 100 mVs-1, under an argon atmosphere (black line), cyclic voltammogram obtained for the first, second and third reduction processes, at a scan rate of 100 mVs-1 (red, blue and green lines). Cyclic voltammogram obtained for the oxidation process (Purple line), at a scan rate of 100 mVs-1. Voltammograms were obtained in DMF containing [n-Bu_4N][PF_6] (0.2 M). Potentials are plotted against the Fc^+/Fc couple employed as an internal standard.

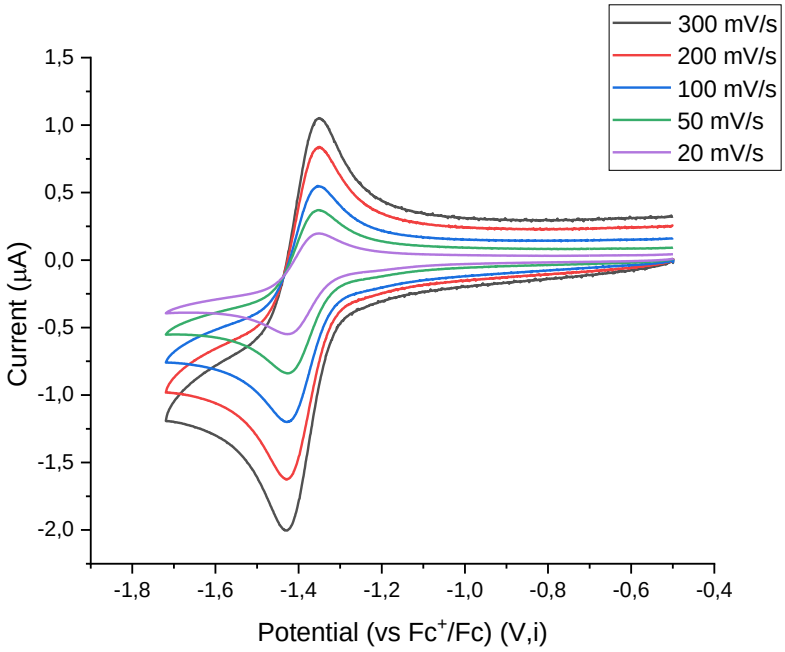

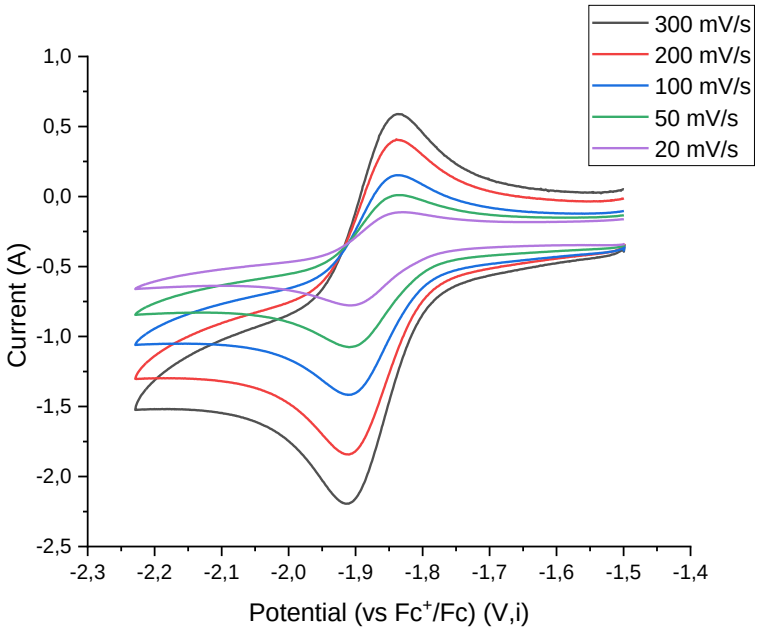

ESI 1.33 Scan rate dependence of first and second reduction process of **PhEsterDPP NH** portraying reduction of neutral molecule to radical anion to dianion, determined through cyclic voltammetry (referenced against potential of Fc^{+}/Fc).

ESI 1.34 Table of peak potentials of first reduction process **PhEsterDPP NH** (referenced against potential of Fc/Fc^{+}), and E_p^a-E_p^c for Fc^{+}/Fc for comparison.

Scan rate [mV s^{-1}]	E_{pa} (1st) [V]	E_{pc} (1st) [V]	E_{pa} - E_{pc} (1st) [V]	$E_{1/2}$ Red (1st) [V]	E_{pa} (2nd) [V]	E_{pc} (2nd) [V]	E_{pa} - E_{pc} (2nd) [V]	$E_{1/2}$Red(2nd) [V]	E_{pa} - E_{pc} Fc^{+}/Fc [V]
300	-1.38	-1.31	0.07	-1.36	-1.92	-1.84	0.08	-1.88	0.06
200	-1.38	-1.31	0.07	-1. 36	-1.92	-1.84	0.08	-1.88	0.06
100	-1.38	-1.31	0.07	-1. 36	-1.92	-1.84	0.08	-1.88	0.06
50	-1.38	-1.31	0.07	-1. 36	-1.91	-1.84	0.08	-1.88	0.06
20	-1.38	-1.31	0.07	-1. 36	-1.91	-1.84	0.08	-1.88	0.06

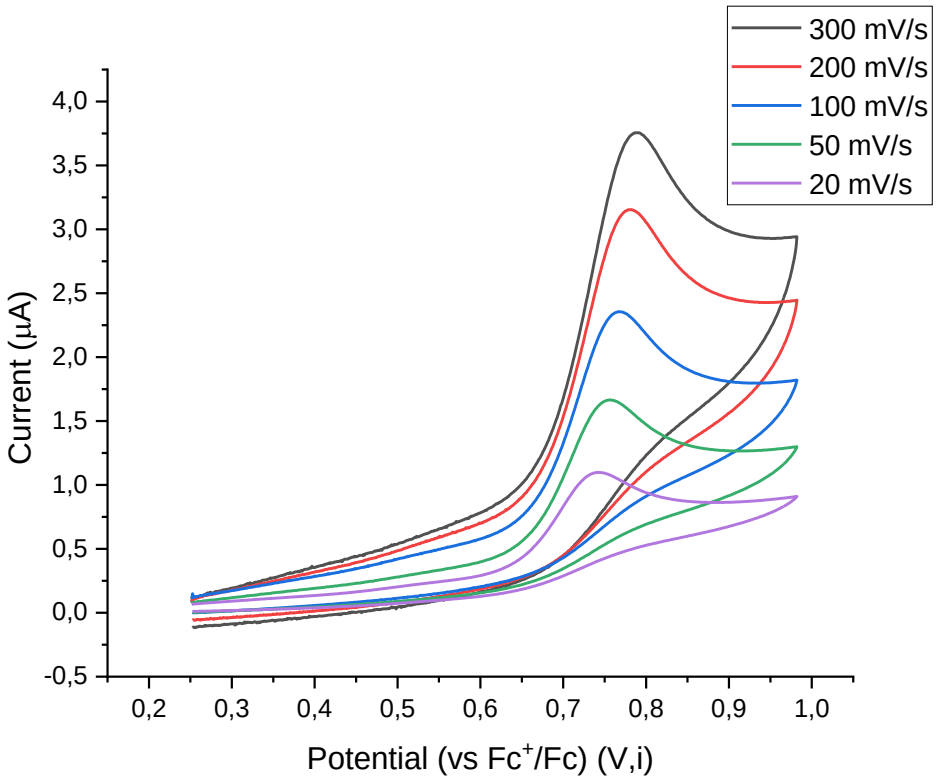

ESI 1.35 Scan rate dependence oxidation processes of the **PhEsterDPP *N*H** derivatives portraying oxidation of neutral molecule to radical cation, determined through cyclic voltammetry at 100 mV/s scan rate (referenced against potential of Fc^{+}/Fc).

ESI 1.36 Table of peak potentials of oxidation process **PhEsterDPP *N*H** (referenced against potential of Fc^+/Fc).

Scan rate [mV s]	E_{pc} [V]	E_{pa} [V]	E_{pa} - E_{pc} [V]	$E_{1/2}$ Ox [V]
300	0.64	N.A.	N.A.	N.A.
200	0.63	N.A.	N.A.	N.A.
100	0.61	N.A.	N.A.	N.A.
50	0.60	N.A.	N.A.	N.A.
20	0.59	N.A.	N.A.	N.A.

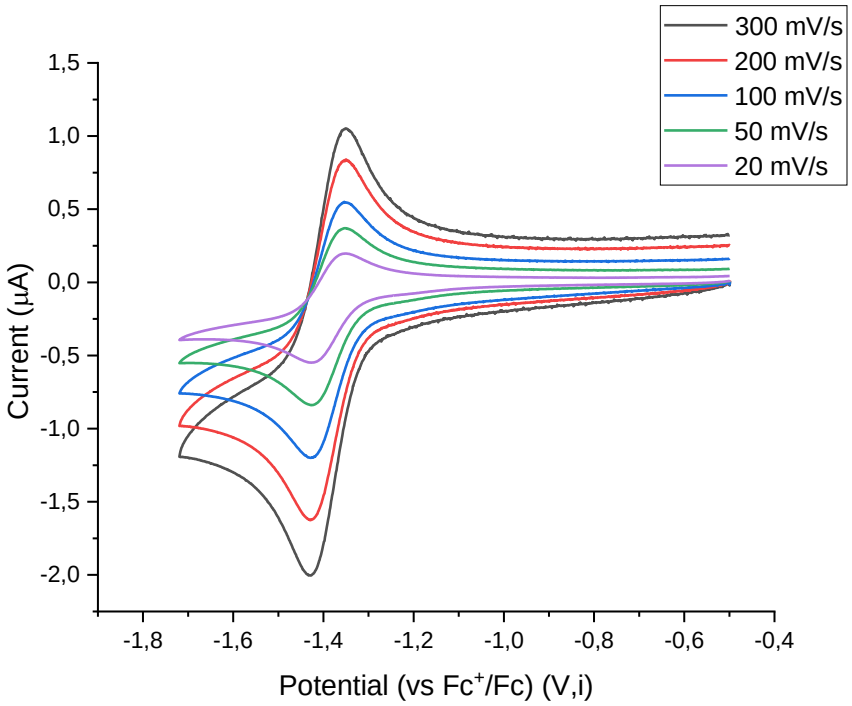

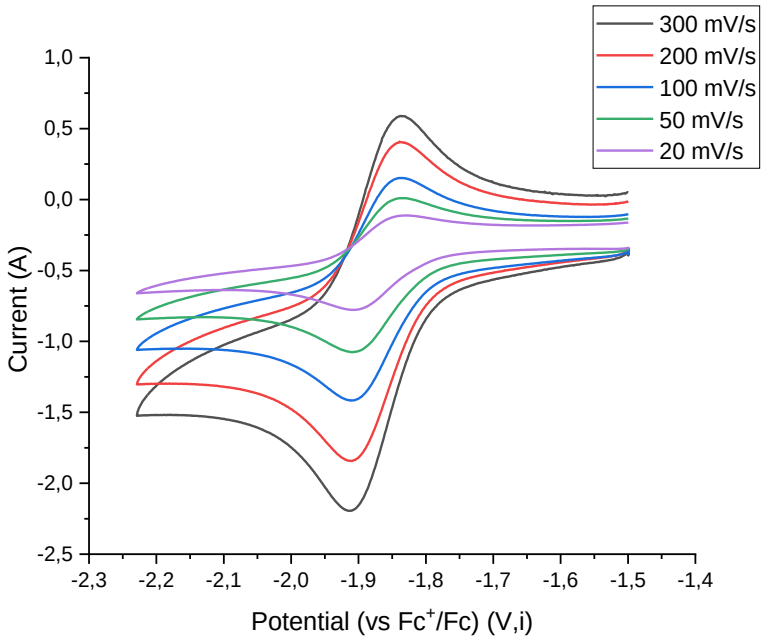

ESI 1.37 Scan rate dependence of first and second reduction process of **PhEsterDPP N-Hex** portraying reduction of neutral molecule to radical anion to dianion, determined through cyclic voltammetry (referenced against potential of Fc^{+}/Fc). on a glassy carbon electrode in DMF solution with [n-Bu_4N][PF_6] (0.2 M) as supporting electrolyte.

ESI 1.38 Table of peak potentials of first reduction process **PhEsterDPP N-Hex** (referenced against potential of Fc^+/Fc), and E_p^a-E_p^c for Fc^+/Fc for comparison.

Scan rate [mV s^{-1}]	E_{pa} (1st) [V]	E_{pc} (1st) [V]	E_{pa} - E_{pc} (1st) [V]	$E_{1/2}$ Red (1st) [V]	E_{pa} (2nd) [V]	E_{pc} (2nd) [V]	E_{pa} - E_{pc} (2nd) [V]	$E_{1/2}$Red (2nd) [V]	E_{pa} - E_{pc} Fc^+/Fc [V]
300	-1.38	-1.31	0.07	-1.36	-1.92	-1.84	0.08	-1.88	0.06
200	-1.38	-1.31	0.07	-1. 36	-1.92	-1.84	0.08	-1.88	0.06
100	-1.38	-1.31	0.07	-1. 36	-1.92	-1.84	0.08	-1.88	0.06
50	-1.38	-1.31	0.07	-1. 36	-1.91	-1.84	0.08	-1.88	0.06
20	-1.38	-1.31	0.07	-1. 36	-1.91	-1.84	0.08	-1.88	0.06

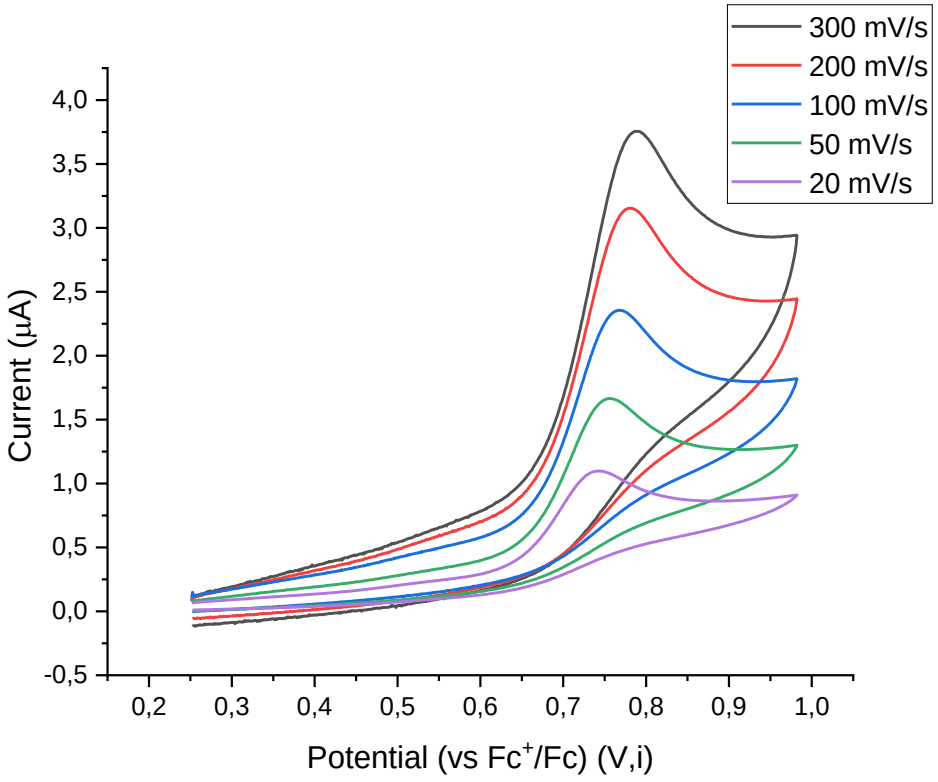

ESI 1.39 Scan rate dependence of oxidation processes of the **PhEsterDPP N-Hex** derivatives portraying oxidation of neutral molecule to radical cation, determined through cyclic voltammetry at 100 mV/s scan rate (referenced against potential of Fc^+/Fc). on a glassy carbon electrode in DMF solution with [*n*-Bu_4N][PF_6] (0.2 M) as supporting electrolyte.

ESI 1.40 Table of peak potentials of oxidation process **PhEsterDPP N-TBA** (referenced against potential of Fc^{+}/Fc).

Scan rate [mV s]	E_{pc} [V]	E_{pa} [V]	E_{pa} - E_{pc} [V]	$E_{1/2}$ Ox [V]
300	0.64	N.A.	N.A.	N.A.
200	0.63	N.A.	N.A.	N.A.
100	0.61	N.A.	N.A.	N.A.
50	0.60	N.A.	N.A.	N.A.
20	0.59	N.A.	N.A.	N.A.

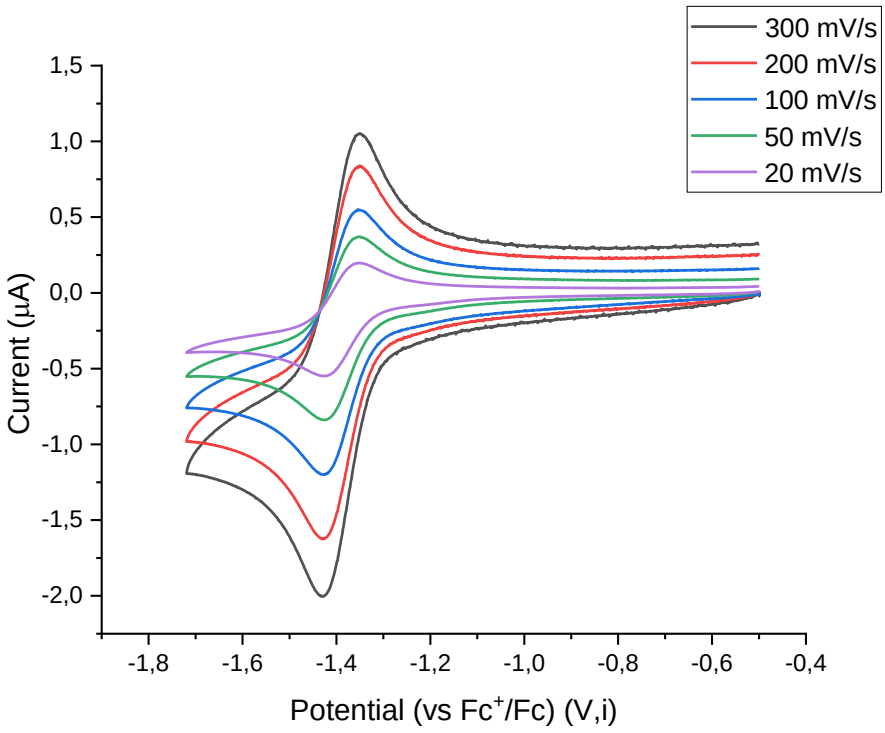

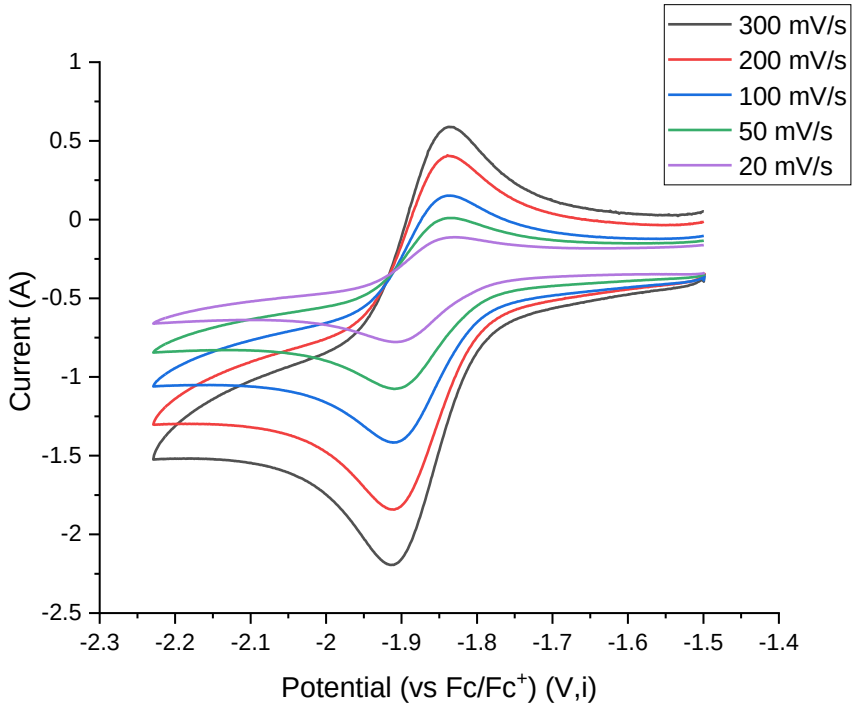

ESI 1.41 Scan rate dependence of first and second reduction process of **PhEsterDPP N-TBA** portraying reduction of neutral molecule to radical anion to dianion, determined through cyclic voltammetry (referenced against potential of Fc^{+}/Fc). on a glassy carbon electrode in DMF solution with [*n*-Bu_4N][PF_6] (0.2 M) as supporting electrolyte.

ESI 1.42 Table of peak potentials of first reduction process **PhEsterDPP N-TBA** (referenced against potential of Fc^+/Fc), and E_p^a-E_p^c for Fc^+/Fc for comparison.

Scan rate [mV s^{-1}]	E_{pa} (1st) [V]	E_{pc} (1st) [V]	E_{pa} - E_{pc} (1st) [V]	$E_{1/2}$ Red (1st) [V]	E_{pa} (2nd) [V]	E_{pc} (2nd) [V]	E_{pa} - E_{pc} (2nd) [V]	$E_{1/2}$Red (2nd) [V]	E_{pa} - E_{pc} Fc^+/Fc [V]
300	-1.38	-1.31	0.07	-1.36	-1.92	-1.84	0.08	-1.88	0.06
200	-1.38	-1.31	0.07	-1. 36	-1.92	-1.84	0.08	-1.88	0.06
100	-1.38	-1.31	0.07	-1. 36	-1.92	-1.84	0.08	-1.88	0.06
50	-1.38	-1.31	0.07	-1. 36	-1.91	-1.84	0.08	-1.88	0.06
20	-1.38	-1.31	0.07	-1. 36	-1.91	-1.84	0.08	-1.88	0.06

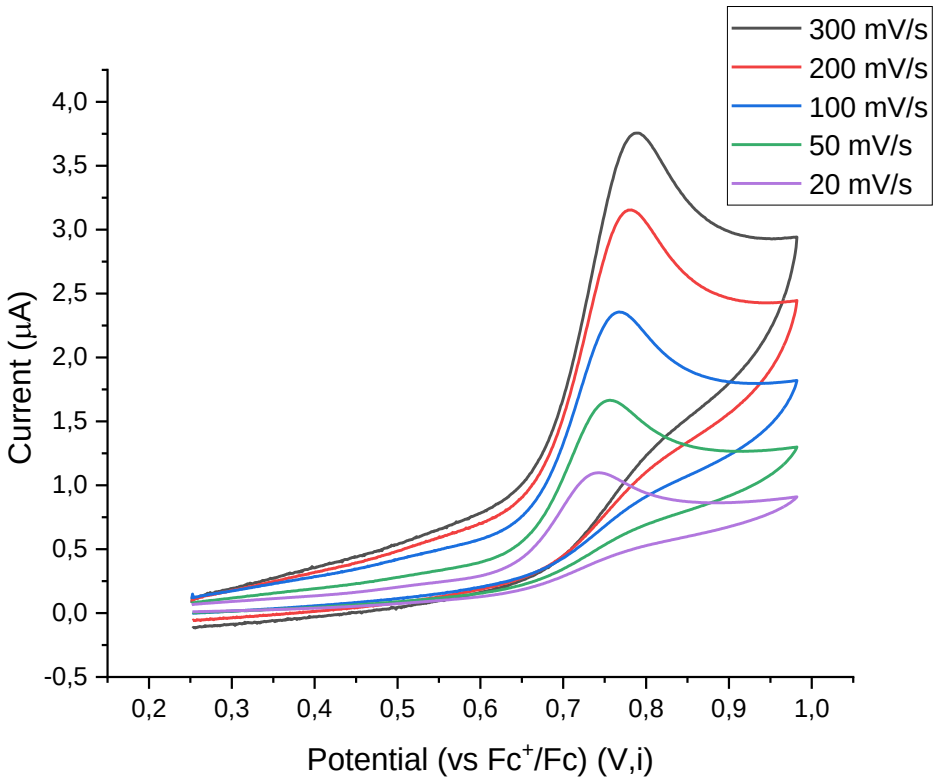

ESI 1.43 Scan rate dependence of oxidation processes of the **PhEsterDPP N-TBA** derivatives portraying oxidation of neutral molecule to radical cation, determined through cyclic voltammetry at 100 mV/s scan rate (referenced against potential of Fc^+/Fc). on a glassy carbon electrode in DMF solution with [*n*-Bu_4N][PF_6] (0.2 M) as supporting electrolyte.

ESI 1.44 Table of peak potentials of oxidation process **PhEsterDPP N-TBA** (referenced against potential of Fc^{+}/Fc).

Scan rate [mV s]	E_{pc} [V]	E_{pa} [V]	E_{pa} - E_{pc} [V]	$E_{1/2}$ Ox [V]
300	0.64	N.A.	N.A.	N.A.
200	0.63	N.A.	N.A.	N.A.
100	0.61	N.A.	N.A.	N.A.
50	0.60	N.A.	N.A.	N.A.
20	0.59	N.A.	N.A.	N.A.

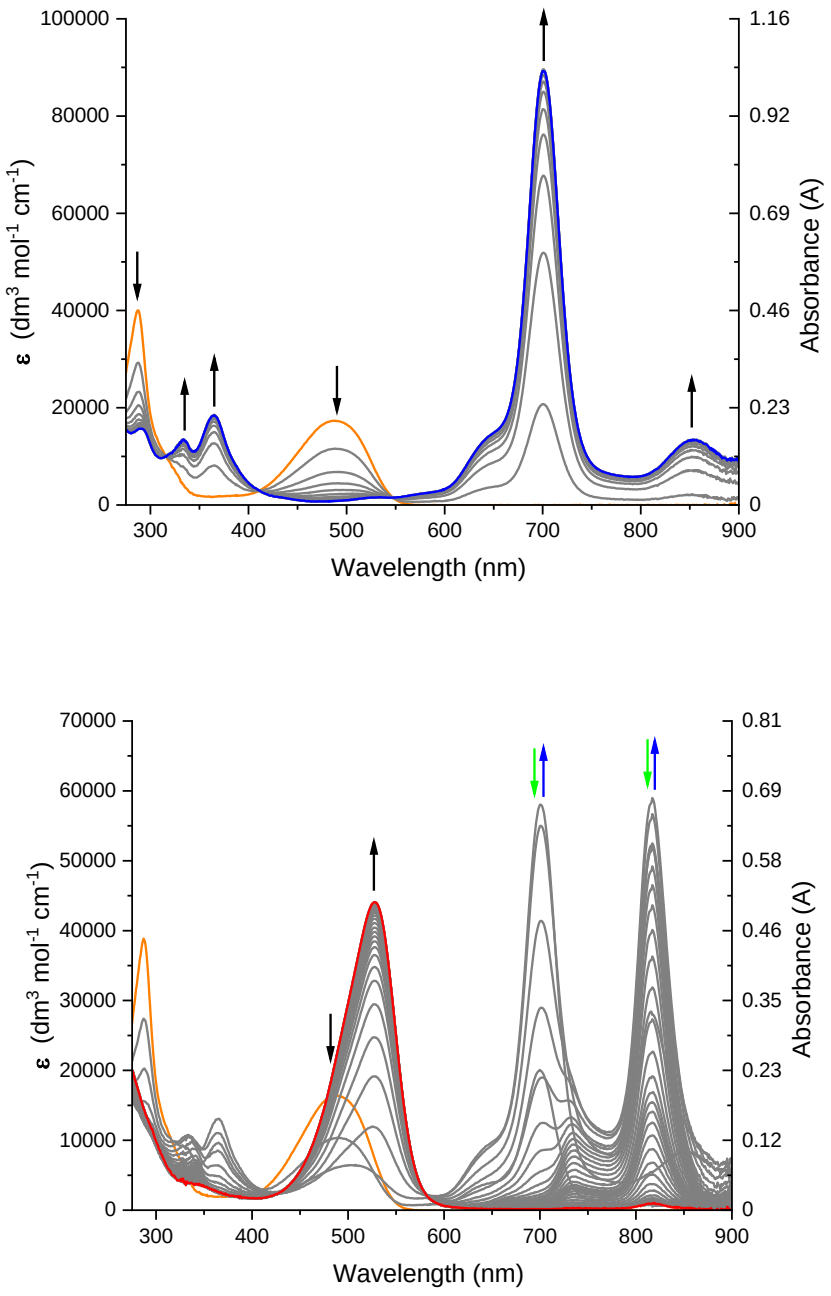

ESI 1.45 UV-visible absorption monitoring of the first reduction process (top) and second reduction process (bottom) of **PhEsterDPP N-Hex.** In orange line represents the neutral species, the blue line represents the first reduced species, and the red line represents the second reduced species. Spectra were recorded in DMF containing [*n*-Bu_4N][PF_6] (0.2M) as the supporting electrolyte at 273K. Blue arrow indicate the first part of the evolution of the spectra, green arrow indicate the second part of the evolution of the spectra.

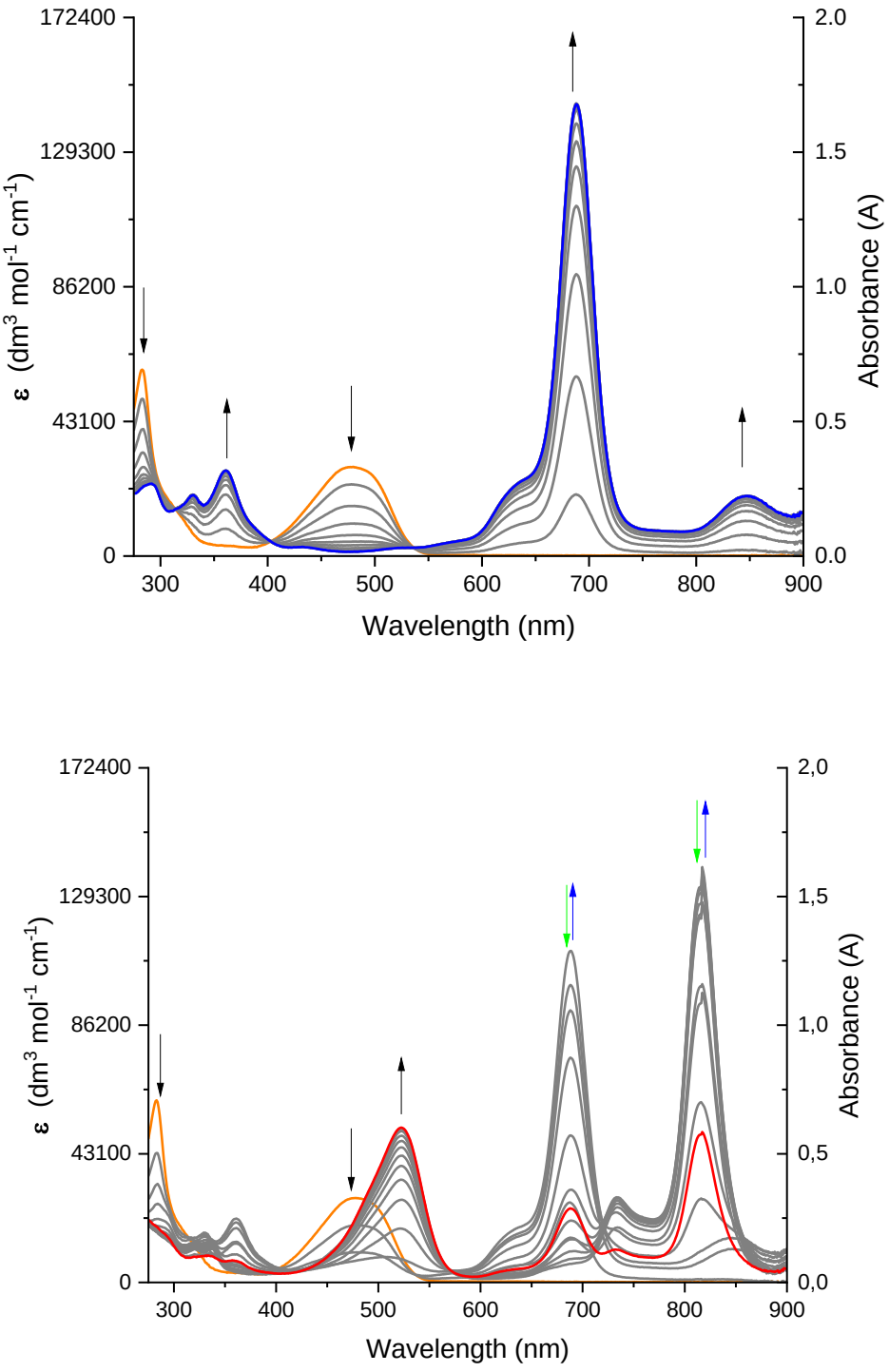

ESI 1.46 UV-visible absorption monitoring of the first reduction process (top) and second reduction process (bottom) of **PhEsterDPP *N*-TBA.** In orange line represents the neutral species, the blue line represents the first reduced species, and the red line represents the second reduced species. Spectra were recorded in DMF containing [*n*-Bu_4N][PF_6] (0.2M as the supporting electrolyte at 273K). Blue arrow indicate the first part of the evolution of the spectra, green arrow indicate the second part of the evolution of the spectra.

ESI 1.47 Table of isobestic points for radical anion formation

Compound	**Isosbestic point / nm**
PhEsterDPP NH	565
PhEsterDPP N-TBA	403, 563
PhEsterDPP N-Hex	411, 547
PhAldDPP N-EA	418,553

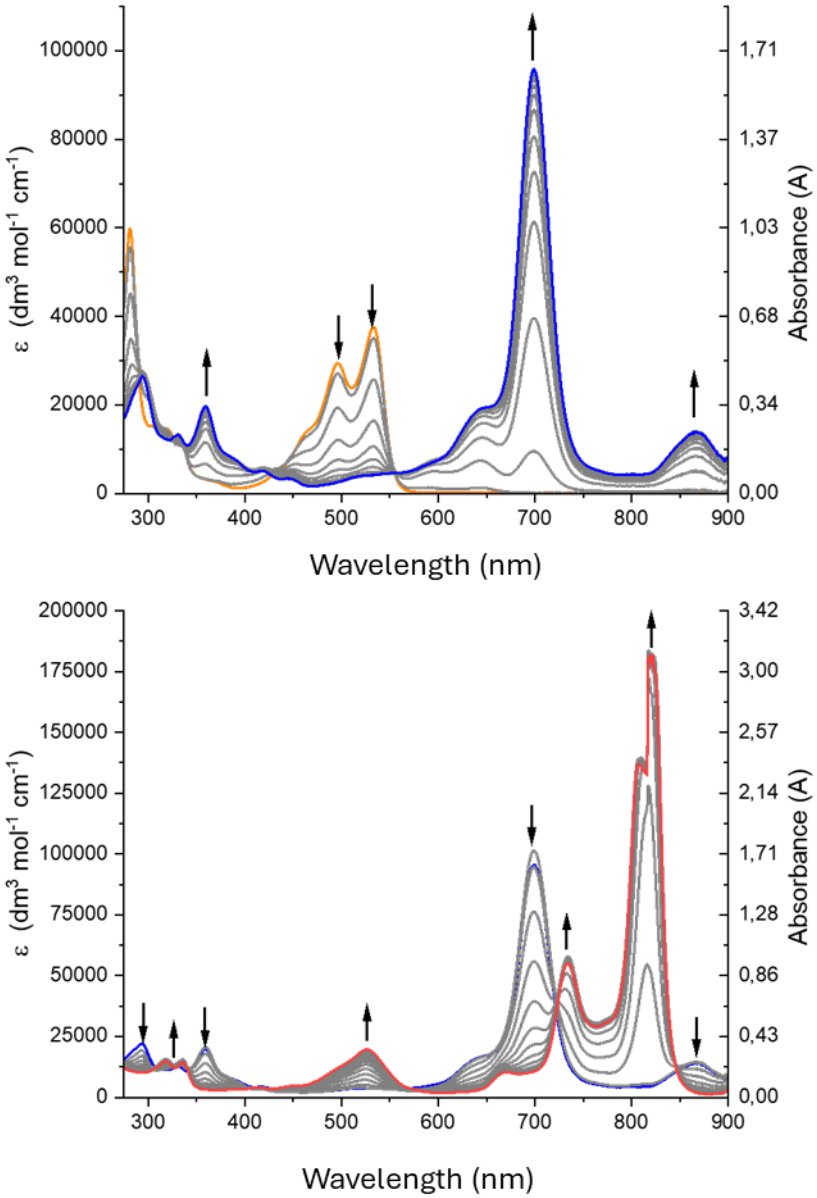

ESI 1.48 UV-visible absorption monitoring of the first reduction process (left) and second reduction process (right) of **PhEsterDPP NH.** In orange line represents the neutral species, the blue line represents the first reduced species, and the red line represents the second reduced species. Spectra were recorded in DMF containing [*n*-Bu_4N][PF_6] (0.2M) as the supporting electrolyte at 273K.

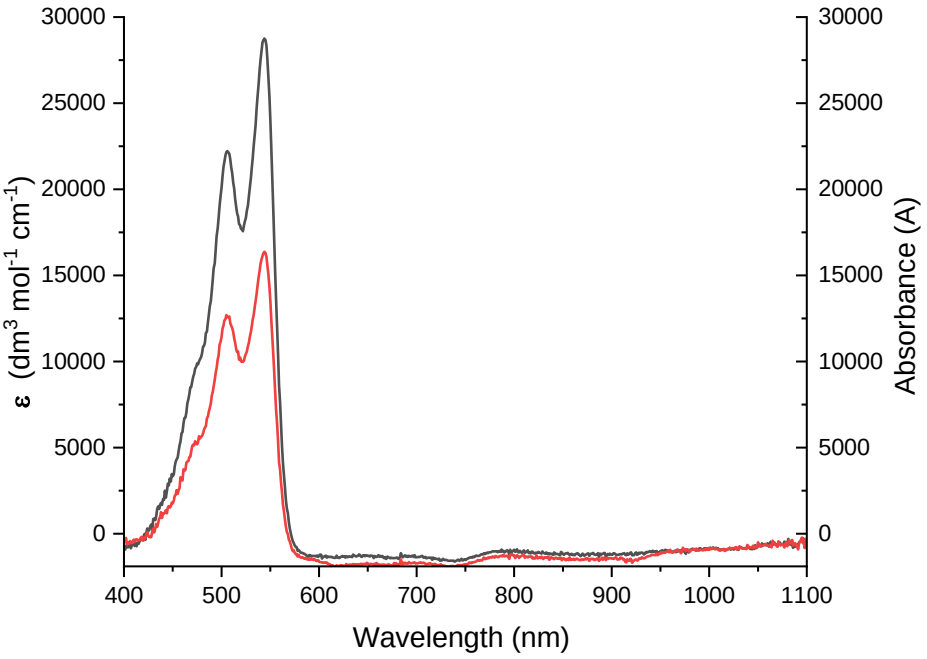

ESI 1.49 UV-visible absorption spectra of **PhEsterDPP NH** (prior to reduction: black line) and after first reduction-reoxidation cycle (red line). Spectra were recorded in DMF containing [*n*-Bu_4N][PF_6] (0.2 M) as the supporting electrolyte at 273 K.

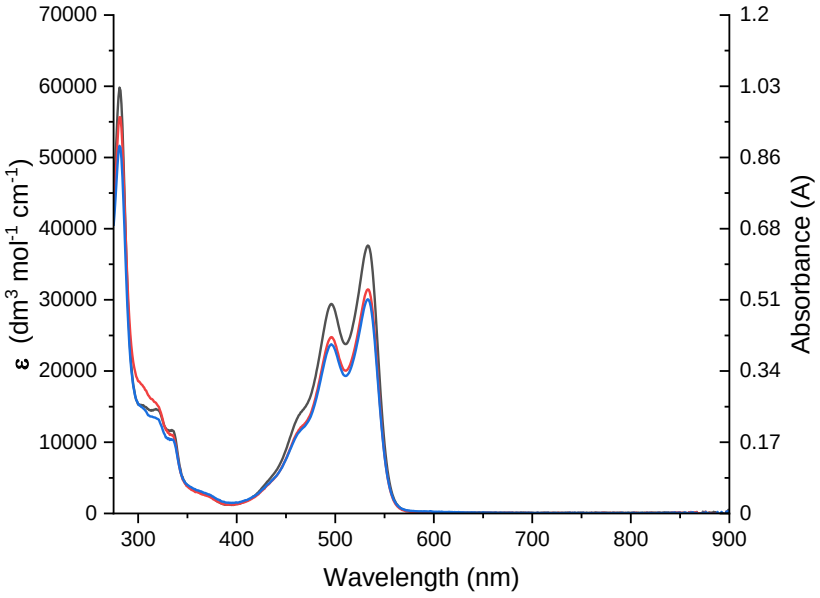

ESI 1.50 UV-visible absorption spectra of **PhEsterDPP NH** (first scan: black line), after the first reduction-reoxidation cycle (red line) and after the second reduction-reoxidation cycle (blue line). Spectra were recorded in DMF containing [*n*-Bu_4N][PF_6] (0.2 M) as the supporting electrolyte at 273 K.

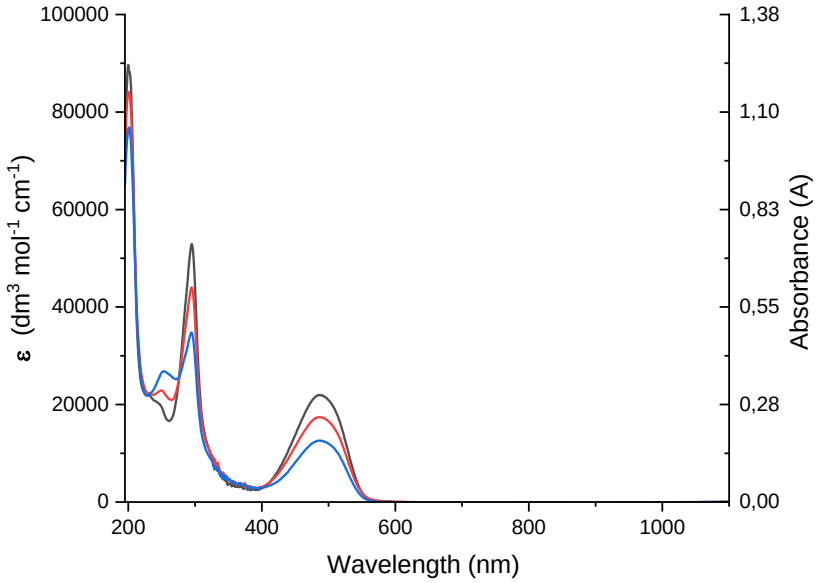

ESI 1.51 UV-visible absorption spectra of **PhAldDPP N-EA** (prior to reduction: black line), after first reduction-reoxidation cycle (red line) and after second reduction-reoxidation cycle (blue line). Spectra were recorded in DMF containing [*n*-Bu_4N][PF_6] (0.2 M) as the supporting electrolyte at 273 K.

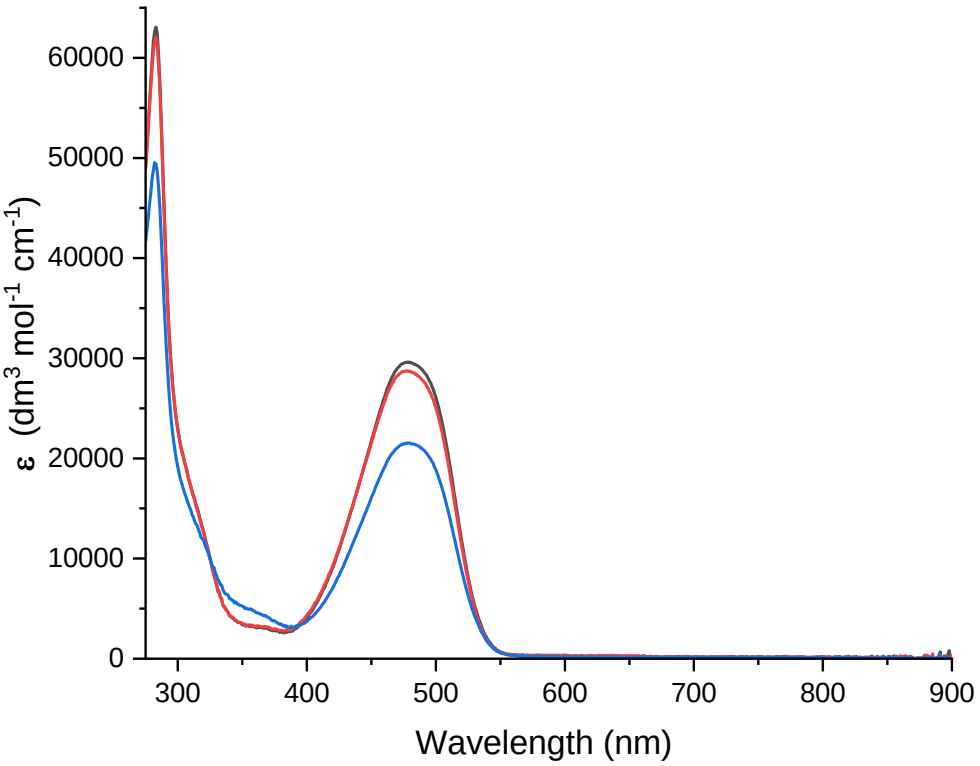

ESI 1.52 UV-visible absorption spectra of **PhEsterDPP N-Hex** (prior to reduction: black line), after first reduction-reoxidation cycle (red line) and after second reduction-reoxidation cycle (blue line). Spectra were recorded in DMF containing [*n*-Bu_4N][PF_6] (0.2 M) as the supporting electrolyte at 273 K.

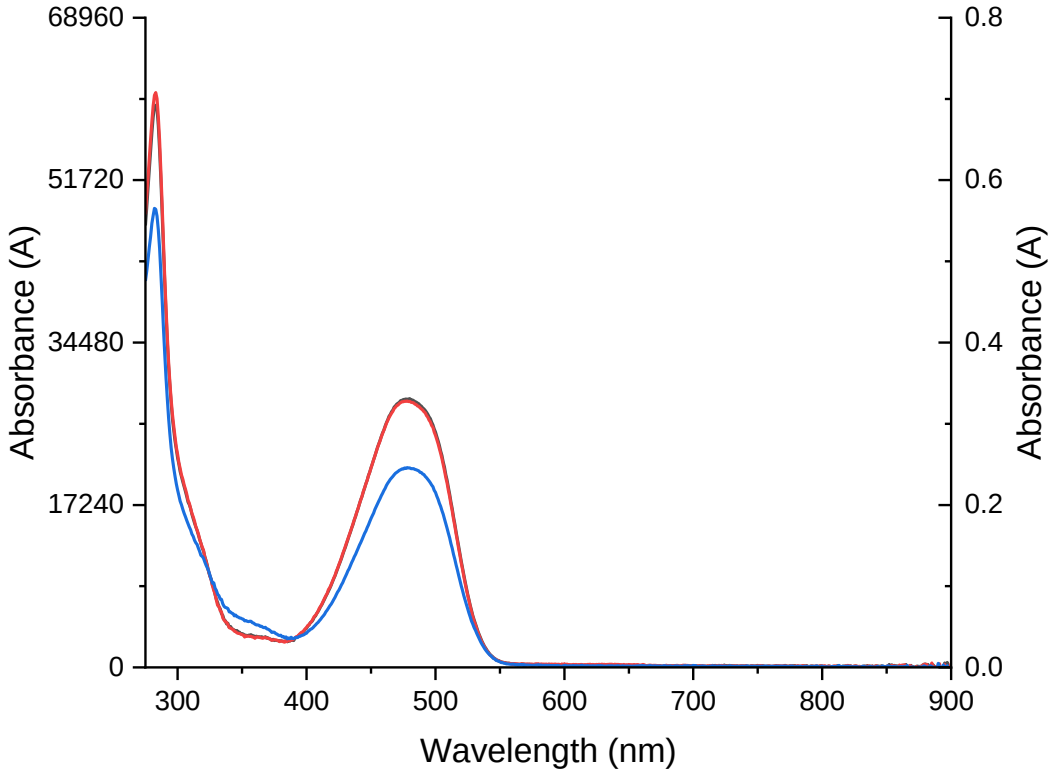

ESI 1.53 UV-visible absorption spectra of **PhEsterDPP N-TBE** (prior to reduction: black line), after first reduction-reoxidation cycle (red line) and after second reduction-reoxidation cycle (blue line). Spectra were recorded in DMF containing [*n*-Bu_4N][PF_6] (0.2 M) as the supporting electrolyte at 273 K.

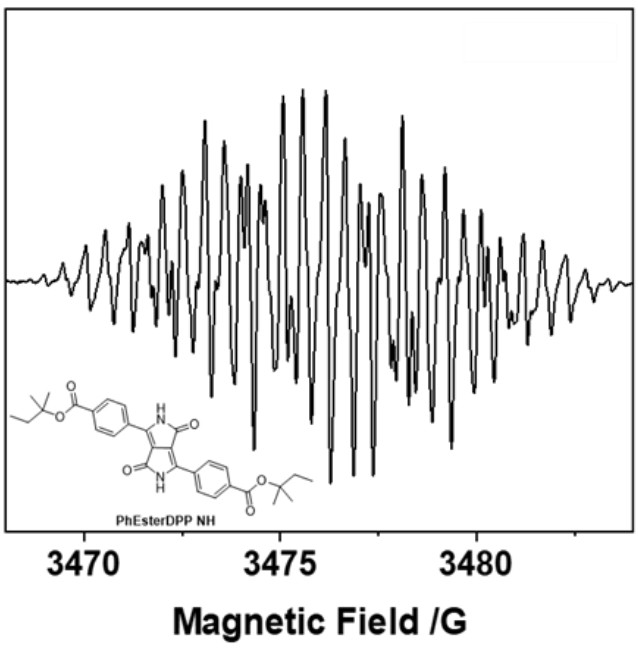

ESI 1.54 EPR of singly reduced **PhEsterDPP NH**

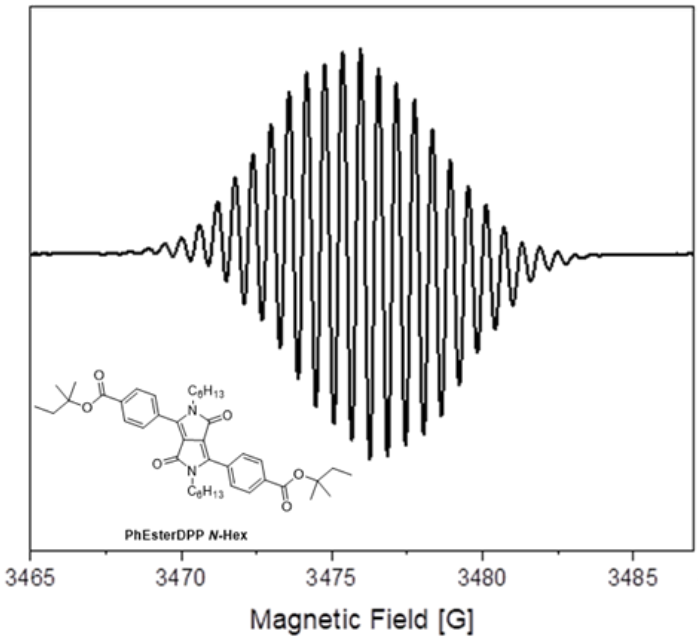

ESI 1.55 EPR of singly reduced **PhEsterDPP N-Hex**

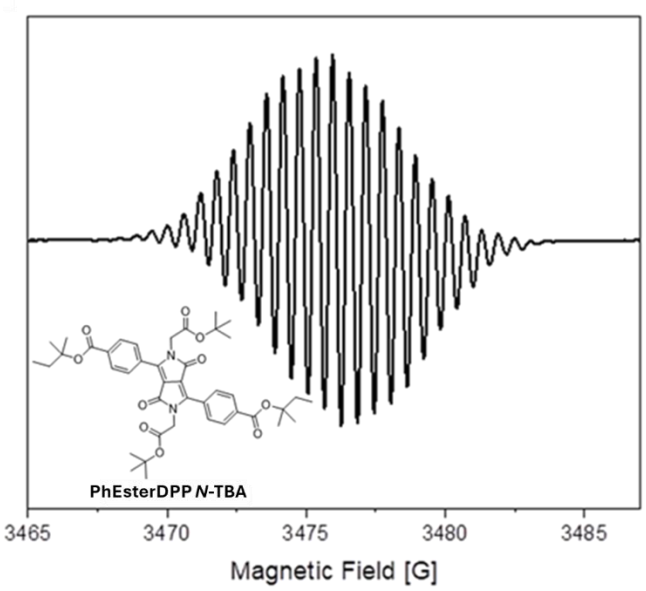

ESI 1.56 EPR of singly reduced **PhEsterDPP N-TBA**

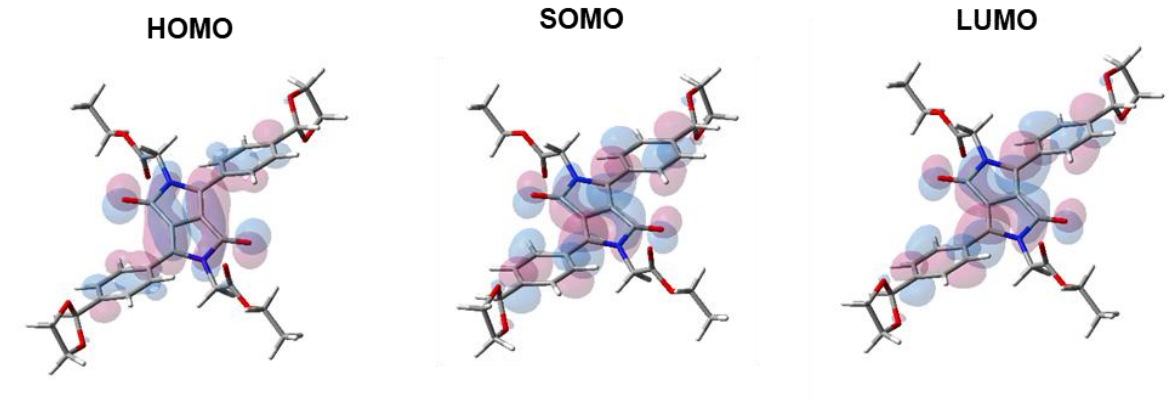

ESI 1.57 Calculated electron density distributions by DFT for **PhAcetDPP N-EA**

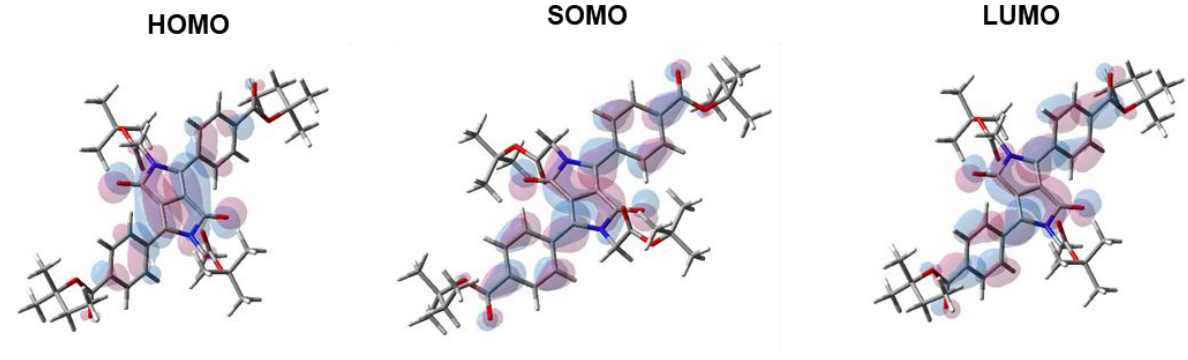

ESI 1.58 Calculated electron density distributions by DFT for **PhEsterDPP N-EA**

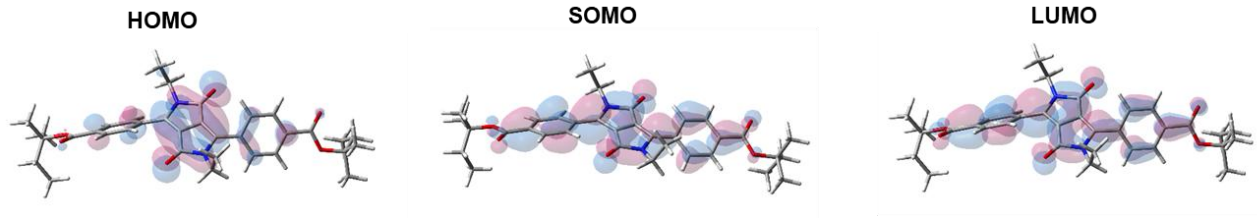

ESI 1.59 Calculated electron density distributions by DFT for **PhEsterDPP N-Hex**

ESI 1.60 Table of Crystallisation conditions and structural data for **PhEsterDPP NH, PhEsterDPP N-TBA, PhEsterDPP N-Hex, PhAldDPP N-EA** and **PhAcetDPP N-EA**

Compound	Crystallisation conditions	Space group	*Z*
PhEsterDPP NH	Slow evaporation THF	P-1	2
PhEsterDPP N-Hex	Slow evaporation CH_2Cl_2	P 2_1/c	4
PhAldDPP N-EA	Slow evaporation Acetone	P2_1	1
PhAcetDPP N-EA	Slow evaporation Acetone	P 2_1/c	2
PhEsterDPP N-TBA	Slow evaporation CH_2Cl_2	P-1	2

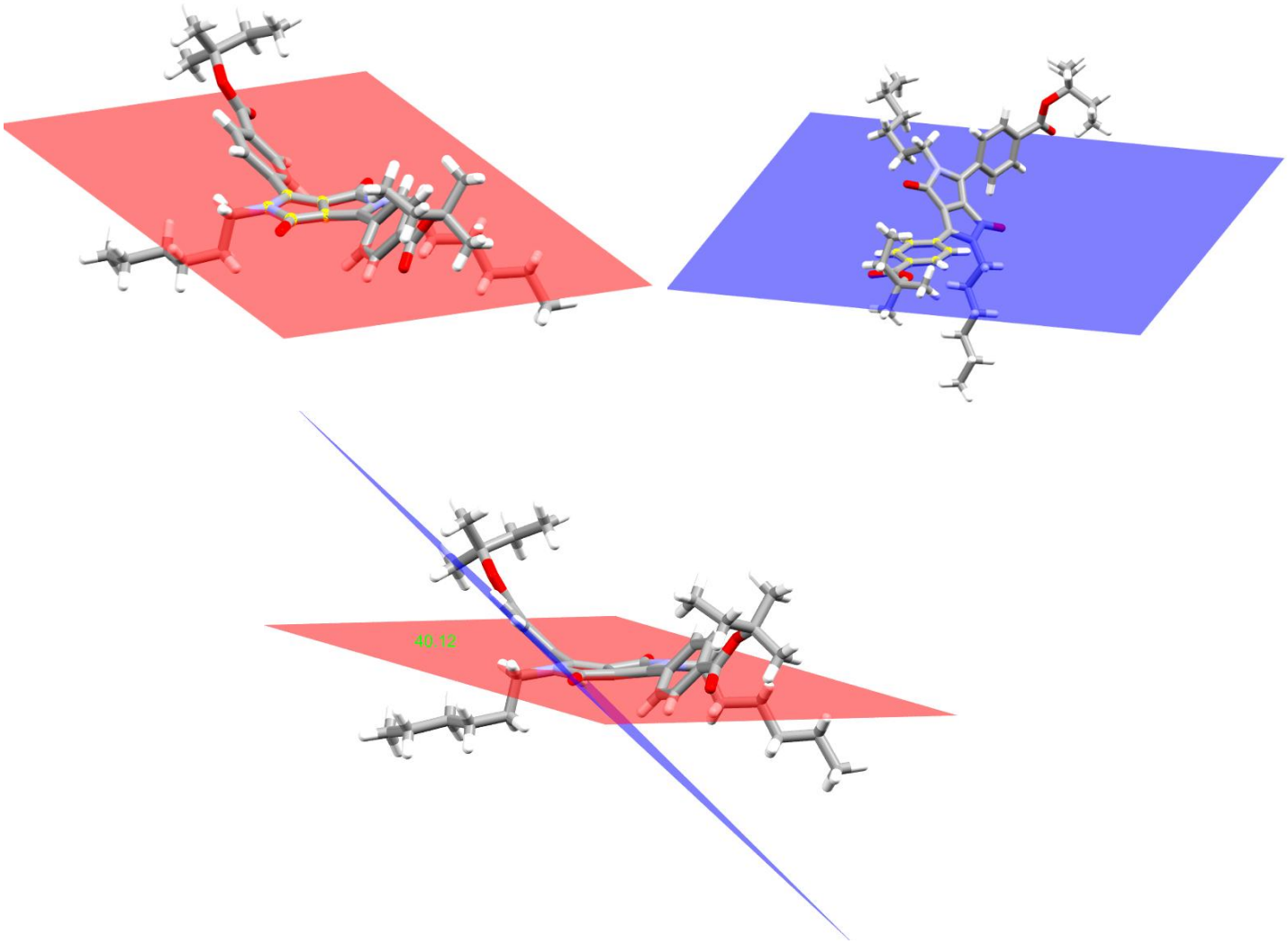

ESI 1.61 Example of DPP-aryl angle calculation with a plane on the aryl ring and a plane on the connected lactam.

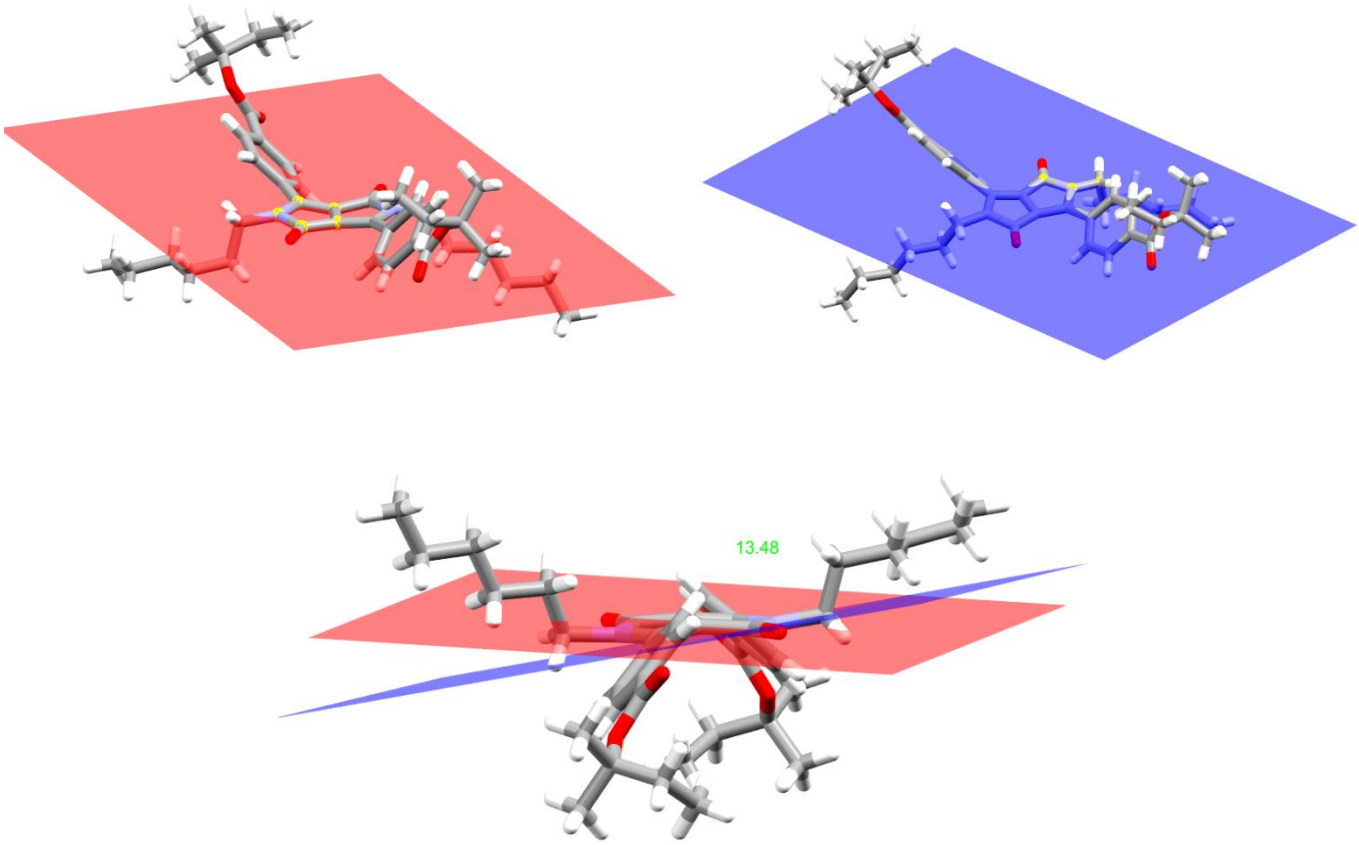

ESI 1.62 Example of DPP-Alkyl angle calculation with a plane on the lactam and a plane on [Clactam – N – C(R)].

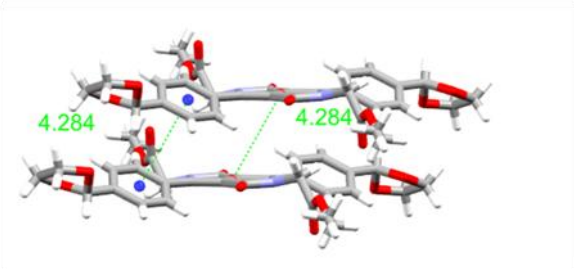

PhAcetDPP *N*-EA
(Slipped stack Lac-Lac Ph-Ph)

ESI 1.63 Main π system interactions of of **PhAcetDPP N-EA**

ESI 1.64 Table of solid state interactions, packing and calculated mobility values for **PhAcetDPP N-EA** obtained from single crystal structure

Compound	**DPP aryl-lactam dihedral (°)l**	**DPP aryl-alkyl dihedral (°)l**	**π -π stacking interaction (Å)**	**H bonding (Å)**	**Bulk packing**	**Mobility (cm^2/V s)**
PhAcetDPP *N*-EA	32.7	14.0	4.28 (Lac-Lac slip stack) 4.28 (Ph-Ph slip stack)	n/a	Herringbone	4.20×10^{-3}

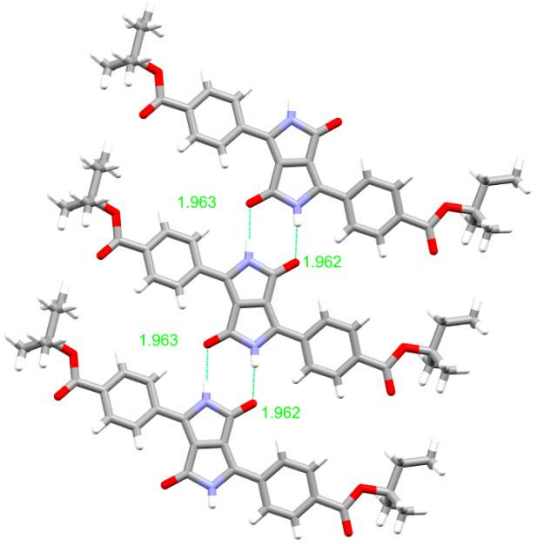

ESI 1.65 Hydrogen bonding interactions between neighbouring chromophores for **PhEsterDPP NH**.

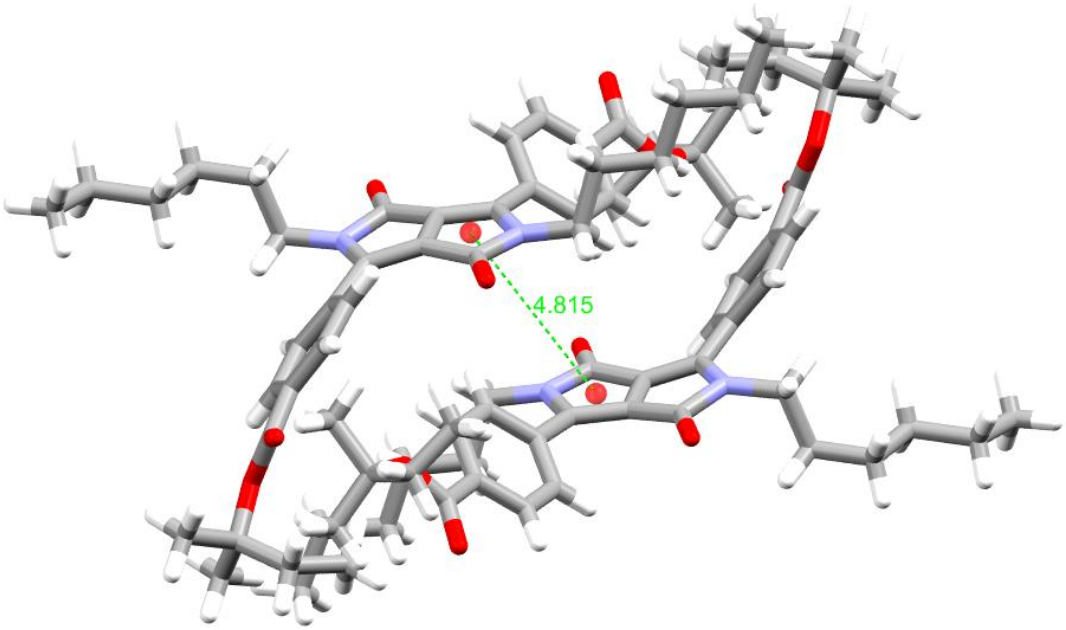

ESI 1.66 Slipped weak π–π interaction of **PhEsterDPP N-Hex**.

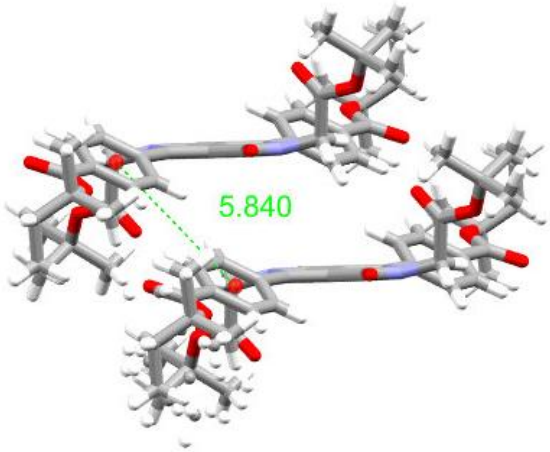

ESI 1.67 Slipped stack interaction **PhEsterDPP N-TBA**.

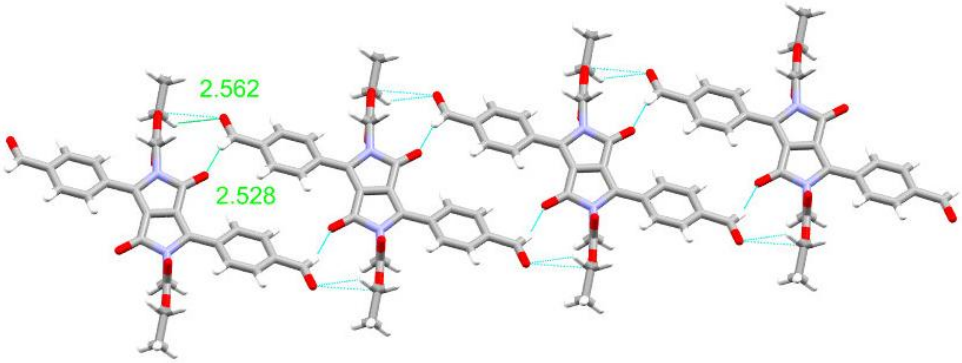

ESI 1.68 Hydrogen bond interactions of **PhAldDPP N-EA**.

ESI 1.69. Table of short range interactions of **PhEsterDPP NH**.

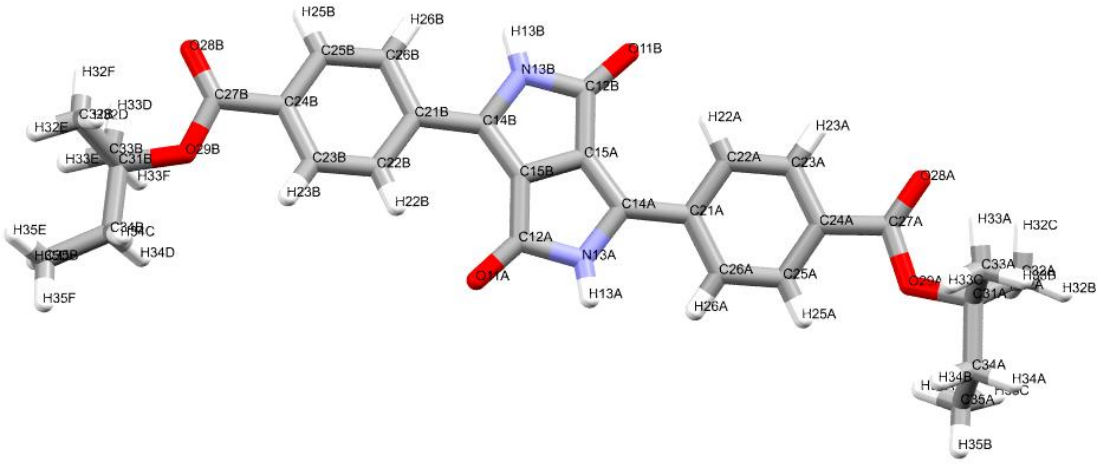

Number	Atom1	Atom2	Length
1	O28A	H35B	2.586
2	O11B	N13A	2.812
3	O11B	H13A	1.963
4	O11B	H26A	2.517
5	C12B	H13A	2.774
6	N13B	O11A	2.819
7	H13B	O11A	1.962
8	H13B	C12A	2.823
9	H26B	O11A	2.430
10	C12B	C24B	3.326
11	C14B	C26B	3.350
12	C21A	C12B	3.341
13	H32A	O28B	2.693
14	H33A	H33A	2.359
15	C25A	H32D	2.807
16	C35A	C23B	3.305

ESI 1.70 Table of short range interactions of **PhEsterDPP N-Hex**.

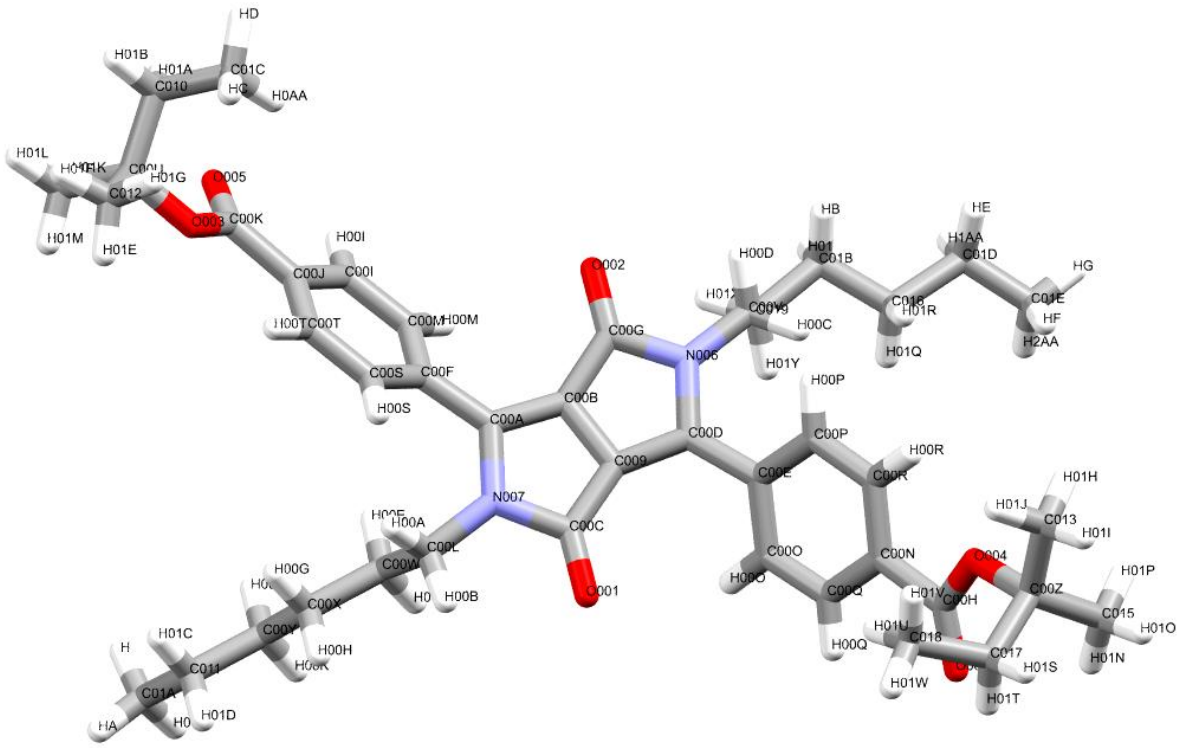

Number	Atom1	Atom2	Length
1	O002	H00H	2.429
2	HB	O001	2.308
3	HE	H00O	2.351
4	O005	H01I	2.494
5	H01K	H01I	2.386
6	H01	H01N	2.234
7	HA	H01Q	2.398
8	O002	C00P	3.206
9	O002	H00P	2.470
10	O005	H01H	2.647
11	H01A	H01P	2.381
12	O001	H00A	2.679
13	O001	H00S	2.436
14	O008	H01E	2.613
15	C00C	C00L	3.337
16	H01M	H01T	2.267
17	C009	H01F	2.871
18	C00C	H01F	2.733
19	H00F	C012	2.869

ESI 1.71 Table of short range interactions of **PhAldDPP N-EA**.

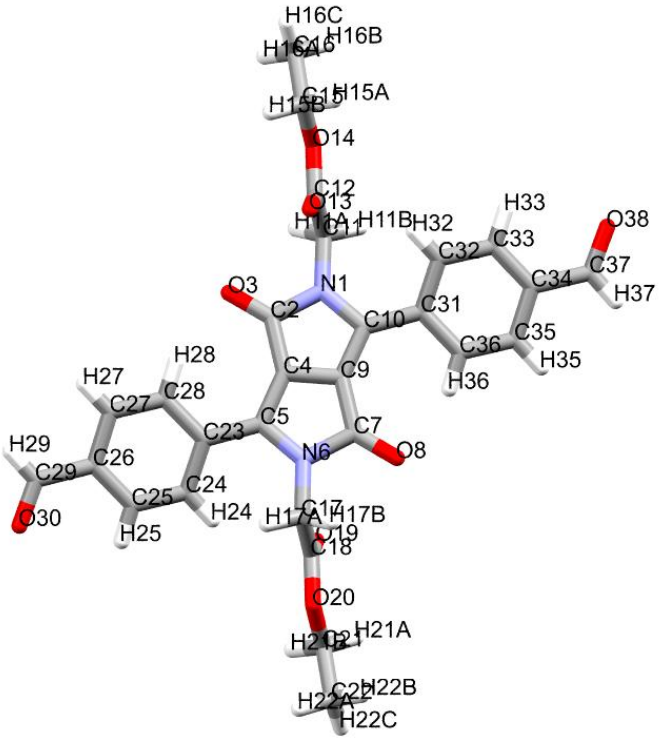

Number	Atom1	Atom2	Length
1	C2	C27	3.388
2	C2	C28	3.134
3	C4	C28	3.301
4	H11B	O13	2.469
5	H16B	H15B	2.396
6	O19	H17A	2.442
7	C35	C7	3.376
8	C36	C7	3.141
9	C36	C9	3.302
10	O8	H29	2.579
11	C21	O30	3.174
12	H21A	O30	2.581
13	H37	O3	2.528
14	O38	C15	3.167
15	O38	H15B	2.562
16	O38	H21B	2.661

ESI 1.72 Table of short range interactions of **PhEsterDPP N-TBA**.

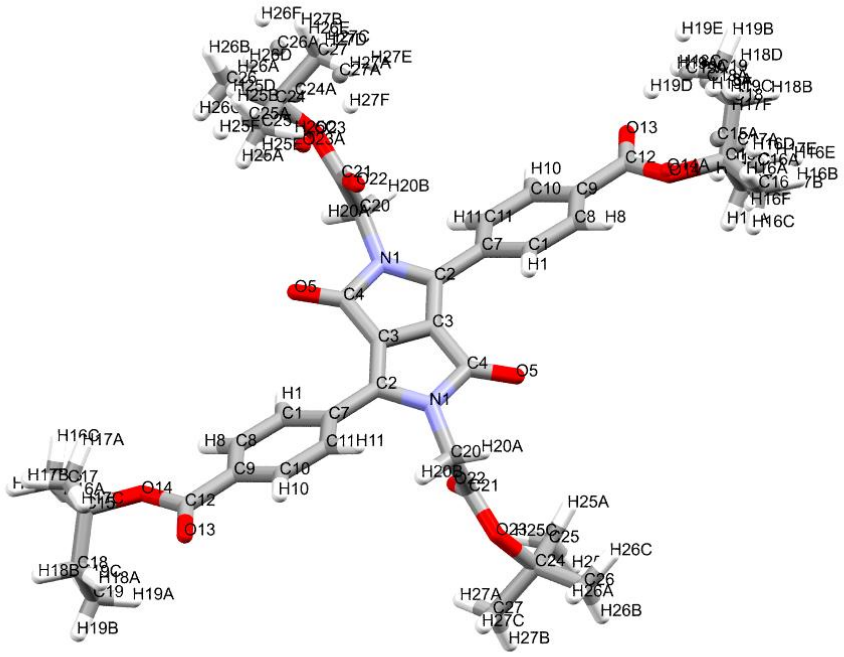

Number	Atom1	Atom2	Length
1	O18	H9	2.71
2	C1	C9	3.301
3	C1	H9	2.678
4	C9	C3	3.356
5	C13	O002	3.086
6	H13A	O18	2.639
7	H13B	O002	2.346
8	O002	H15B	2.625
9	C11	O18	3.114
10	C12	O18	3.053
11	H13A	H12B	2.388

Number	Atom1	Atom2	Length
1	C17	H17A	2.716
2	H17A	H17A	2.066
3	O13	H26A	2.668
4	H25A	H18B	2.315
5	O5	H17B	2.565
6	C8	H16C	2.796
7	H8	H17C	2.339
8	O22	H11	2.539

9	C10	H27B	2.816

ESI 1.73 Table of short range interactions of **PhAcetDPP N-EA**.

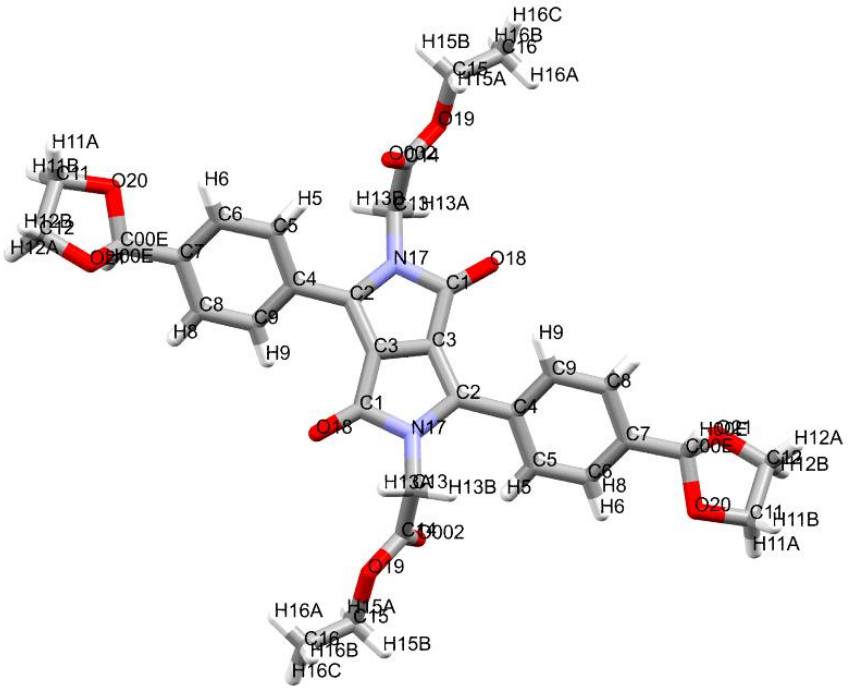

Number	Atom1	Atom2	Length
1	O18	H9	2.71
2	C1	C9	3.301
3	C1	H9	2.678
4	C9	C3	3.356
5	C13	O002	3.086
6	H13A	O18	2.639
7	H13B	O002	2.346
8	O002	H15B	2.625
9	C11	O18	3.114
10	C12	O18	3.053
11	H13A	H12B	2.388

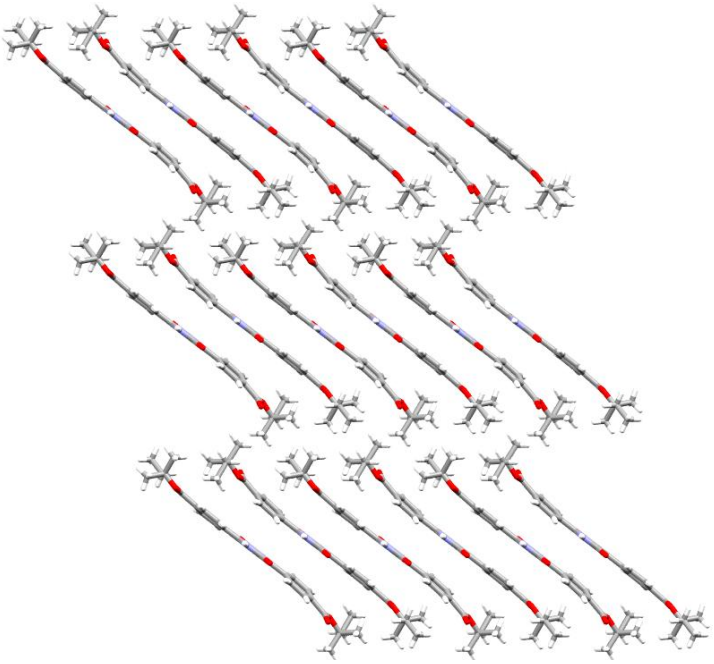

ESI 1.74. Infinite stack for **PhEsterDPP NH** (Lamellar). Hydrogen atoms omitted for clarity. Viewed along a axis.

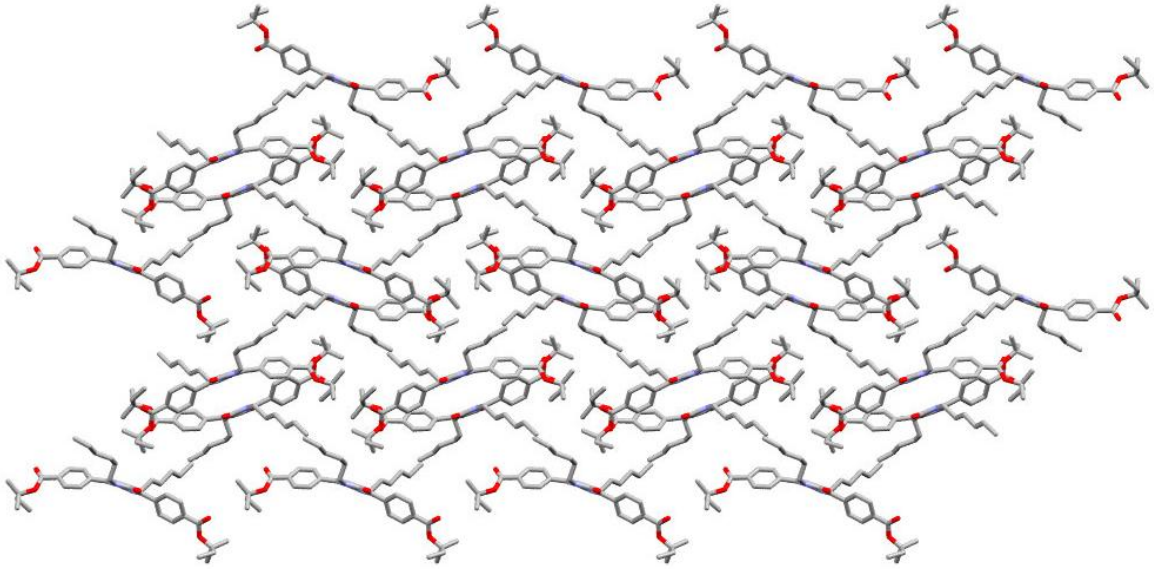

ESI 1.75 Infinite stack for **PhEsterDPP N-Hex** (herringbone). Hydrogen atoms omitted for clarity. Viewed along *a* axis.

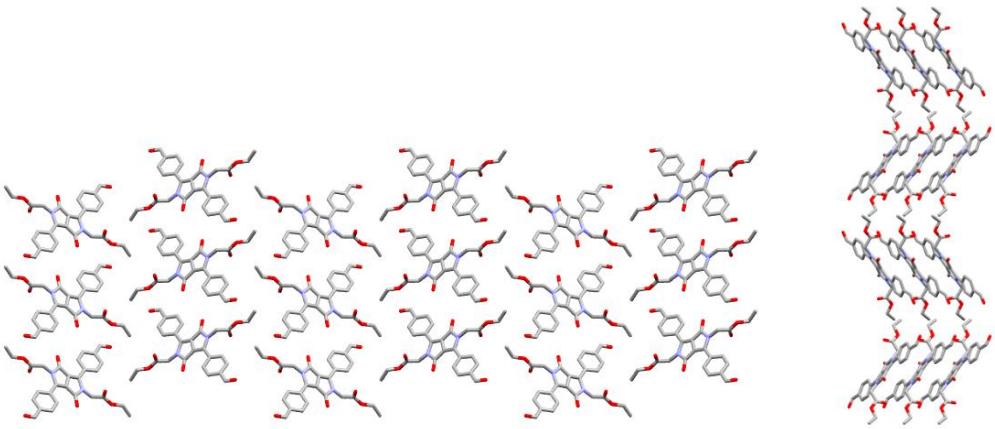

ESI 1.76 Infinite stacks of **PhAldDPP N-EA** viewed along *a* and *b* directions respectively herringbone packing.

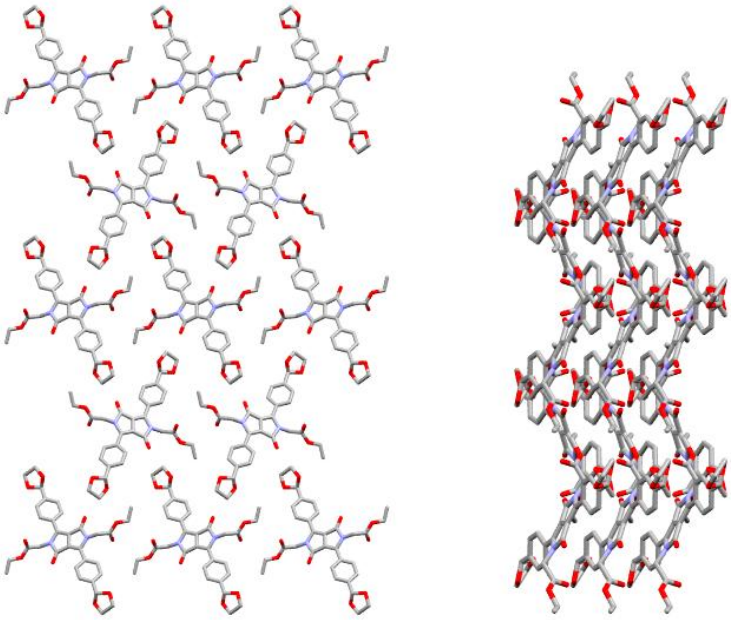

ESI 1.77 Infinite stacks of **PhAcetDPP N-EA** viewed along *a* and *c* directions, respectively, showing herringbone packing.

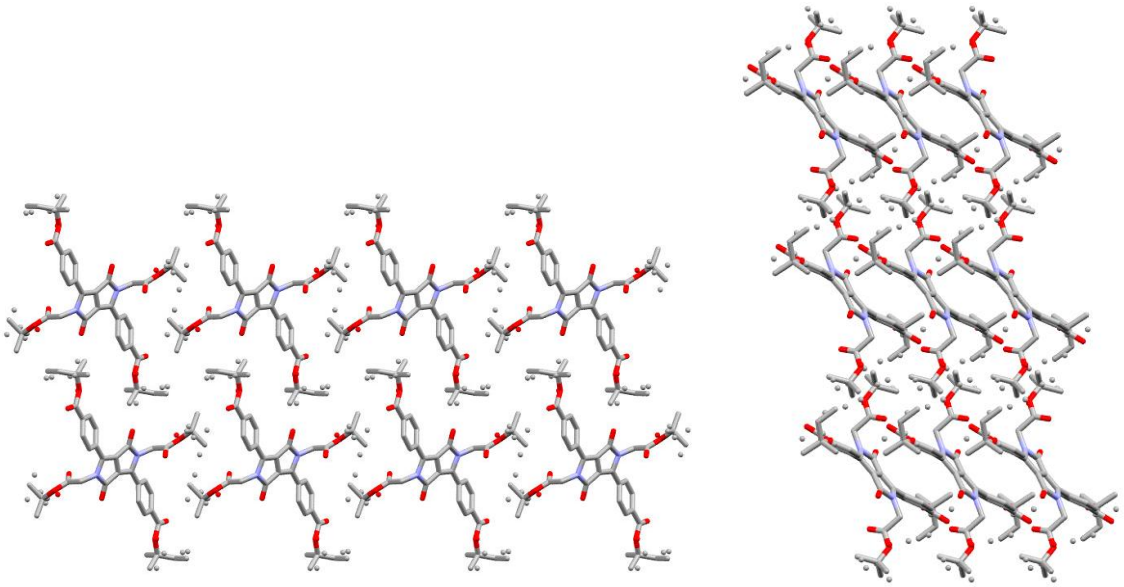

ESI 1.78 Infinite stacks of **PhEsterDPP N-TBA** viewed along *a* and *c* directions, respectively, showing lamellar packing.

.

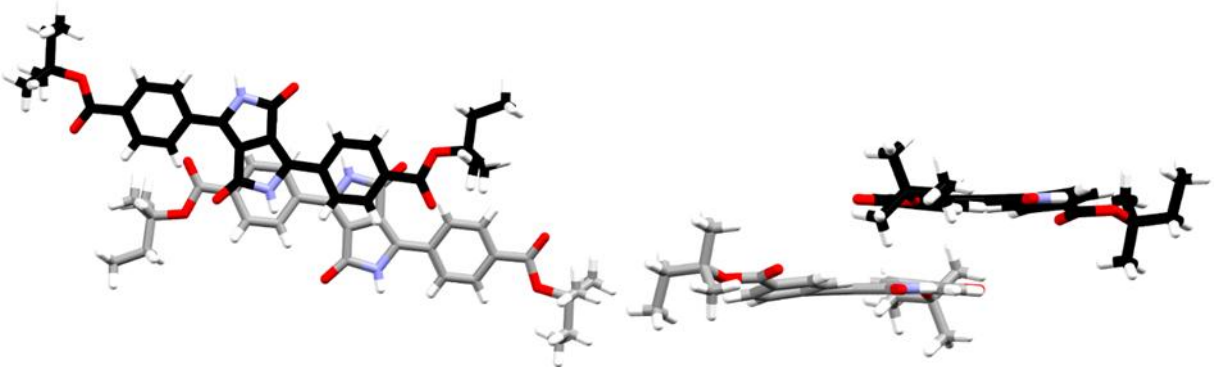

ESI 1.79 Nearest neighbours for **PhEsterDPP NH** allowing appreciation of **t**he longitudinal, lateral and vertical displacement.

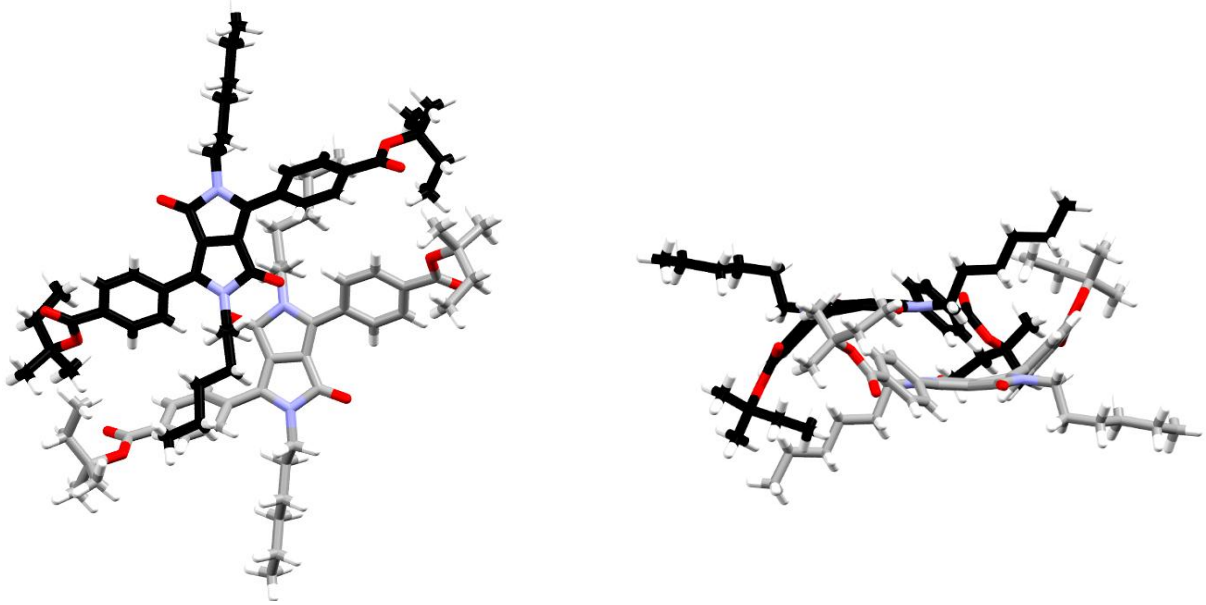

ESI 1.80 Nearest neighbours for **PhEsterDPP N-Hex** allowing appreciation of **t**he longitudinal, lateral and vertical displacement.

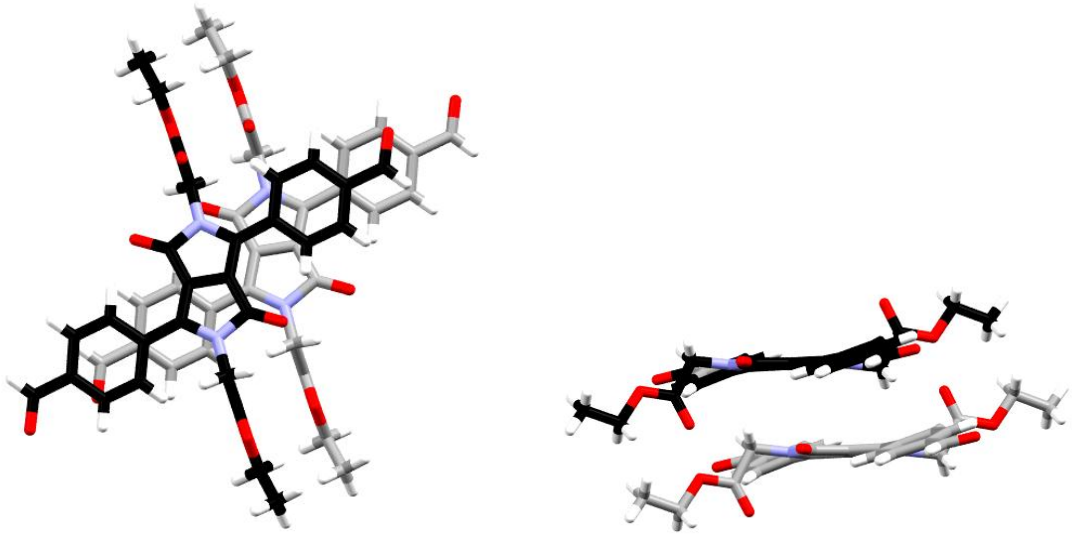

ESI 1.81 Nearest neighbours for **PhAldDPP N-EA** allowing appreciation of **t**he longitudinal, lateral and vertical displacement.

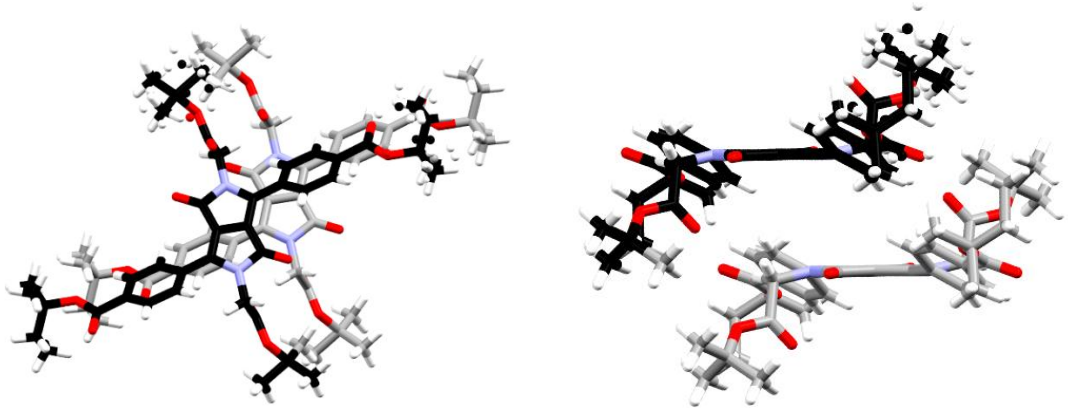

ESI 1.82 Nearest neighbours for **PhEsterDPP N-TBA** allowing appreciation of **t**he longitudinal, lateral and vertical displacement.

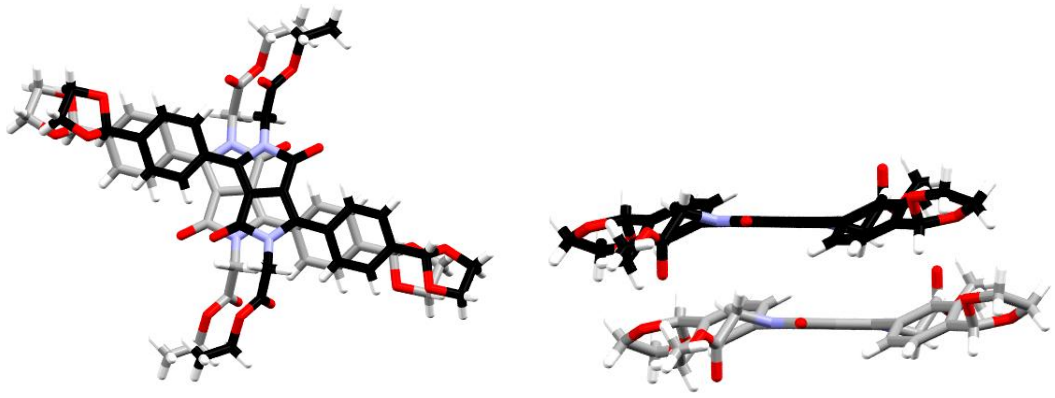

ESI 1.83 Nearest neighbours for **PhAcetDPP N-EA** allowing appreciation of **t**he longitudinal, lateral and vertical displacement.

ESI 1.84 Table of the longitudinal, lateral and vertical displacement of **PhEsterDPP NH, PhEsterDPP N-TBA, PhEsterDPP N-Hex, PhAldDPP N-EA** and **PhAcetDPP N-EA.**

Compound	Vertical displacement (Å)	Longitudinal displacement (Å)	Lateral displacement (Å)	Overall displacement (Å)
PhEsterDPP *N*H	3.32	5.75	2.49	6.27
PhEsterDPP *N*-Hex	3.49	0.31	4.88	4.89
PhAldDPP *N*-EA	3.18	0.60	3.46	3.51
PhEsterDPP *N*-TBA	4.79	2.22	2.49	3.34
PhAcetDPP *N*-EA	2.10	0.68	3.67	3.73

ESI 1.85 Table of separation distances and electronic coupling for unique neighbouring molecules of **PhEsterDPP NH** ***DFT details:*** CAM-B3LYP/6-31+G(d,p), Gaussian 16 defaults.

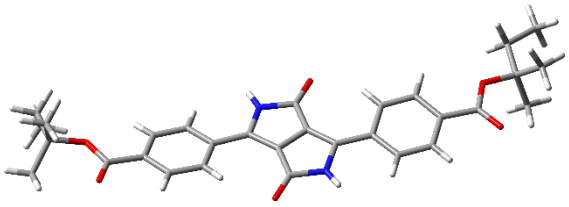

Reorganisation energy =0.5 eV

Hole Mobility = 0.047 cm^2/s

Electronic Coupling (meV)	Centroid-Centroid Distance (Å)
76	4.7
2	7.8
35	7.3

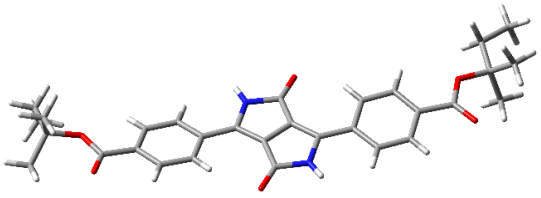

Reorganisation energy = 0.37 eV

Electron Mobility = 0.082 cm^2/s

Electronic Coupling (meV)	Centroid-Centroid Distance (Å)
42	4.7
17	7.8
22	7.3

ESI 1.86 Table of separation distances and electronic coupling for unique neighbouring molecules of **PhEsterDPP N-Hex *DFT details:*** CAM-B3LYP/6-31+G(d,p), Gaussian 16 defaults.

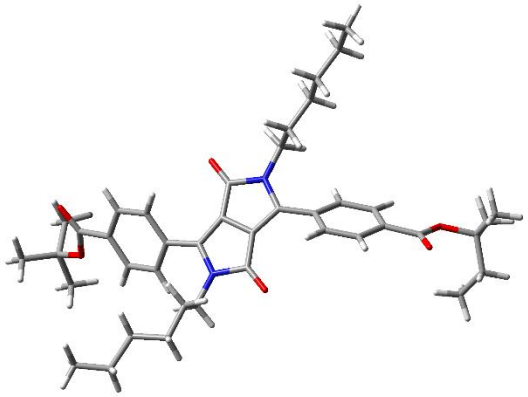

Electronic Coupling (meV)	Centroid-Centroid Distance (Å)
20	6.25
29	6.1

Reorganisation energy = 0.6 eV

Hole Mobility = 0.004 cm^2/s

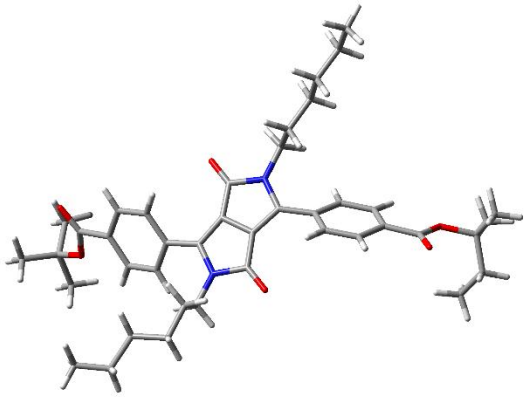

Electronic Coupling (meV)	Centroid-Centroid Distance (Å)
12	6.25
12	6.1

Reorganisation energy = 0.6 eV

Electron Mobility = 0.0009 cm^2/s

ESI 1.87 Table of separation distances and electronic coupling for unique neighbouring molecules of **PhAldDPP N-EA** ***DFT details:*** CAM-B3LYP/6-31+G(d,p), Gaussian 16 defaults.

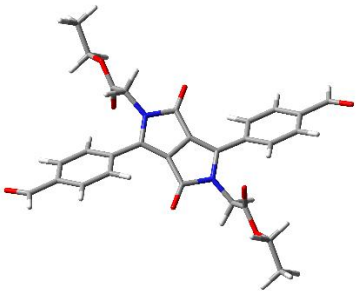

Electronic Coupling (meV)	Centroid-Centroid Distance (Å)
139	4.7
4	10.9

Reorganisation energy = 0.61 eV

Hole Mobility = 0.0325 cm^2/s

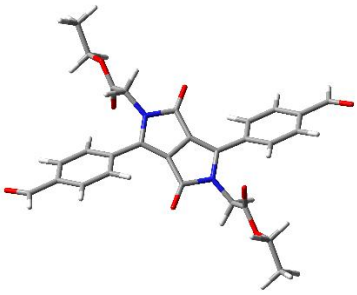

Electronic Coupling (meV)	Centroid-Centroid Distance (Å)
43	4.7
9	10.9

Reorganisation energy = 0.61 eV

Electron Mobility = 0.0038 cm^2/s

ESI 1.88 Table of separation distances and electronic coupling for unique neighbouring molecules of **PhAcetDPP N-EA** ***DFT details:*** CAM-B3LYP/6-31+G(d,p), Gaussian 16 defaults.

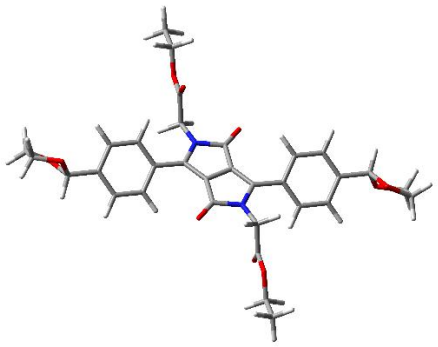

Electronic Coupling (meV)	Centroid-Centroid Distance (Å)
91	4.3
3	15.0

Reorganisation energy = 0.71 eV

Hole Mobility = 0.0042 cm^2/s

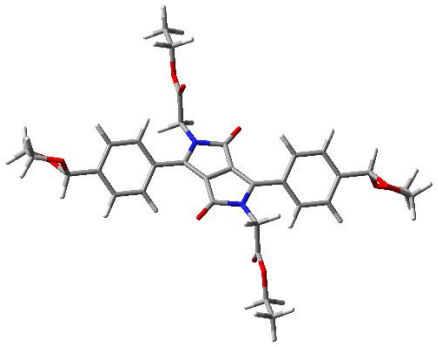

Electronic Coupling (meV)	Centroid-Centroid Distance (Å)
94	4.3
2	15.0

Reorganisation energy = 0.53 eV

Electron Mobility = 0.029 cm^2/s

ESI 1.89 Table of separation distances and electronic coupling for unique neighbouring molecules of **PhEsterDPP N-TBA** ***DFT details:*** CAM-B3LYP/6-31+G(d,p), Gaussian 16 defaults.

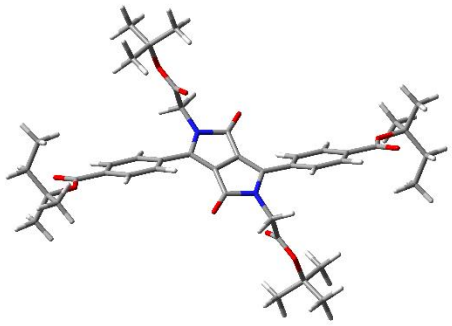

Electronic Coupling (meV)	Centroid-Centroid Distance (Å)
16	5.8
0.1	15.1

Reorganisation energy = 0.63 eV

Hole Mobility = 0.00053 cm^2/s

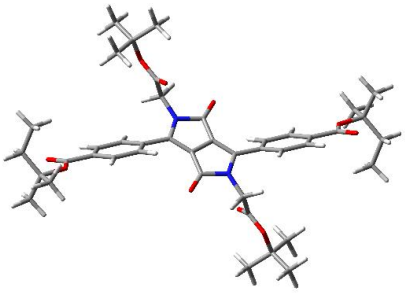

Electronic Coupling (meV)	Centroid-Centroid Distance (Å)
65	5.8
3	15.1

Reorganisation energy = 0.66 eV

Electron Mobility = 0.0065 cm^2/s

5. Crystallographic tables

	PhEsterDPP-NH	**PhEsterDPP-N-Hex**	**PhEsterDPP-N-TBE**	**PhAcetDPP-N-EA**	**PhAldDPP-N-EA**
Chemical formula	$C_{30}H_{32}N_2O_6$	$C_{42}H_{56}N_2O_6$	$C_{42}H_{52}N_2O_{10}$	$C_{32}H_{32}N_2O_{10}$	$C_{28}H_{24}N_2O_8$
M_r	516.57	684.88	744.85	604.59	516.49
Crystal system, space group	Triclinic, *P*-1	Monoclinic, $P2_1/c$	Triclinic, *P*-1	Monoclinic, $P2_1/c$	Monoclinic, $P2_1$
Temperature (K)	120	120	100	100	120
a, *b*, *c* (Å)	7.2531 (18), 11.037 (3), 17.617 (3)	10.2495 (14), 19.920 (2), 19.0550 (19)	5.8396 (8), 12.9726 (16), 13.3022 (9)	4.2839 (8), 13.7577 (10), 24.820 (2)	4.7334 (1), 27.8912 (5), 9.0268 (2)
a, b, g (Å)	71.884 (18), 84.07 (2), 77.28 (2)	90, 90.267 (11), 90	82.093 (8), 84.147 (9), 80.352 (11)	90, 93.298 (12), 90	90, 99.357 (2), 90
V (Å^3)	1306.5 (5)	3890.5 (8)	980.8 (2)	1460.4 (3)	1175.86 (4)
Z	2	4	1	2	2
Radiation type	Cu *K*a	Synchrotron, l = 0.6889 Å	Synchrotron, l = 0.6889 Å	Synchrotron, l = 0.6889 Å	Cu *K*a
m (mm^{-1})	0.75	0.07	0.08	0.09	0.90
Crystal size (mm)	0.11 × 0.07 × 0.04	0.08 × 0.05 × 0.04	0.08 × 0.01 × 0.002	0.08 × 0.02 × 0.003	0.13 × 0.04 × 0.01
Diffractometer	SuperNova, Atlas S2	DLS EH1 Rigaku Saturn724+	DLS EH1 Fluid Film Devices, Dectris PILATUS 2M	DLS EH1 Fluid Film Devices, Dectris PILATUS 2M	Rigaku XtalLAB PRO *MM007*, PILATUS3 R 200K
T_{min}, T_{max}	0.920, 1.000	0.623, 1.000	0.341, 1.000	0.989, 1.0	0.881, 1.000
No. of measured, independent and observed [$I > 2\sigma(I)$] reflections	6741, 2739, 1195	16925, 2078, 1432	8339, 2770, 1721	5581, 1298, 816	15203, 4693, 4193
R_{int}	0.192	0.160	0.129	0.087	0.052
q_{max} (°)	50.4	16.0	22.5	19.1	75.4

$(\sin q/l)_{max}$ ($Å^{-1}$)	0.500	0.400	0.555	0.476	0.628
$R[F^2 > 2s(F^2)]$, $wR(F^2)$, S	0.094, 0.233, 0.96	0.069, 0.205, 1.09	0.104, 0.308, 1.01	0.115, 0.307, 1.13	0.054, 0.151, 1.04
No. reflections; parameters; restraints	2739, 355, 370	2078, 506, 684	2770, 333, 429	1298, 200, 297	4693, 345, 1
Dr_{max}, Dr_{min} (e $Å^{-3}$)	0.32, -0.30	0.17, -0.16	0.35, -0.27	0.42, -0.29	0.42, -0.25
Absolute structure parameter (Flack)	–	–	–	–	0.49 (12)
CCDC	2079927	2079928	2579064	2579065	2579066

References

1 Brouwer AM, Standards for photoluminescence quantum yield measurements in solution (IUPAC Technical Report). Pure Appl Chem. 2011; 83: 2213–28. http://dx.doi.org/10.1351/PAC-REP-10-09-31

2 Gagne RR, Koval CA, Lisensky GC. Ferrocene as an internal standard for electrochemical measurements. Inorg Chem. 1980; 19: 2854–2855. https://doi.org/10.1021/ic50211a080

3 Riaño A, Mayorga Burrezo P, Mancheño MJ, Timalsina A, Smith J, Facchetti A, Marks TJ, López Navarrete JT, Segura JL, Casado J, Ponce Ortiz R. The unusual electronic structure of ambipolar dicyanovinyl-substituted diketopyrrolopyrrole derivatives. J Mater Chem C Mater. 2014; 2: 6376–86. https://doi.org/10.1039/C4TC00714J

4 Cosier J, Glazer AM, A nitrogen-gas-stream cryostat for general X-ray diffraction studies. J Appl Crystallogr. 1986; 19: 105–107. https://doi.org/10.1107/S0021889886089835

5 Rigaku Oxford Diffraction, (2018), CrysAlisPro Software system, version 1.171.40.45a, Rigaku Corporation, Oxford, UK.

6 Dolomanov OV, Bourhis LJ, Gildea RJ, J. Howard AK, Puschmann H. OLEX2: a complete structure solution, refinement and analysis program. J Appl Cryst. 2009; 42: 339–41. https://doi.org/10.1107/S0021889808042726

7 Sheldrick GM. SHELXT – Integrated space-group and crystal-structure determination. Acta Crystallogr A. 2015; 71: 3–8. https://doi.org/10.1107/S2053273314026370

8 Sheldrick GM, Crystal structure refinement with SHELXL. Acta Crystallogr C Struct Chem. 2015; 71: 3–8. https://doi.org/10.1107/S2053229614024218

9 Allan D, Nowell H, Barnett S, Warren M, Wilcox A, Christensen J, Saunders L, Peach A, Hooper M, Zaja L, Patel S, Cahill L, Marshall R, Trimnell S, Foster A, Bates T, Lay S, Williams M, Hathaway P, Winter G, Gerstel M, Wooley R. A Novel Dual Air-Bearing Fixed-χ Diffractometer for Small-Molecule Single-Crystal X-ray Diffraction on Beamline I19 at Diamond Light Source. Crystals. 2017; 7: 336. https://doi.org/10.3390/cryst7110336 “

10 CheckCIF,” can be found under http://checkcif.iucr.org

11 Gaussian 16, Revision B.01, Frisch, M.J., Trucks, G.W., Schlegel, H.B., Scuseria, G.E., Robb, M.A., Cheeseman, J.R.; Scalmani, G.; Barone, V.; Petersson, G.A.; Nakatsuji, H.; Li, X.; Caricato, M.; Marenich, A.V.; Bloino, J., Janesko, B.G., Gomperts, R., Mennucci, B., Hratchian, H.P., Ortiz, J.V., Izmaylov, A.F., Sonnenberg, J.L., Williams-Young, D., Ding, F., Lipparini, F., Egidi, F., Goings, J., Peng, B., Petrone, A., Henderson, T., Ranasinghe, D., Zakrzewski, V.G., Gao, J., Rega, N., Zheng, G., Liang, W., Hada, M., Ehara, M., Toyota, K., Fukuda, R., Hasegawa, J., Ishida, M., Nakajima, T., Honda, Y., Kitao, O., Nakai, H., Vreven, T., Throssell, K., Montgomery Jr., J.A., Peralta, J.E., Ogliaro, F., Bearpark, M.J., Heyd, J.J., Brothers, E.N., Kudin, K.N., Staroverov, V.N., Keith, T.A., Kobayashi, R., Normand, J., Raghavachari, K., Rendell, A.P., Burant, J.C., Iyengar, S.S., Tomasi, J., Cossi, M., Millam, J.M., Klene, M., Adamo, C., Cammi, R., Ochterski, J.W., Martin, R.L., Morokuma, K., Farkas, O., Foresman, J.B., Fox, D.J. Gaussian, Inc., Wallingford CT (2016) GaussView 5.0. Wallingford, E.U.A.

12 Baumeier B, Kirkpatrick J, Andrienko D. Density-functional based determination of intermolecular charge transfer properties for large-scale morphologies. Phys Chem Chem Phys. 2010; 12: 11103–13. https://doi.org/10.1039/C002337J

13 Valeev EF, Coropceanu V, da Silva Filho DA, Salman S, Brédas JL. Effect of Electronic Polarization on Charge-Transport Parameters in Molecular Organic Semiconductors. J Am Chem Soc. 2006; 128: 9882–9886. https://doi.org/10.1021/ja061827h

14 Liu T, Troisi A. Absolute Rate of Charge Separation and Recombination in a Molecular Model of the P3HT/PCBM Interface. J Phys Chem C. 2011; 115: 2406–2415. https://doi.org/10.1021/jp109130y

15 Sokolov AN, Atahan-Evrenk S, Mondal R, Akkerman HB, Sánchez-Carrera RS, Granados-Focil S, Schrier J, Mannsfeld SCB, Zoombelt AP, Bao Z, Aspuru-Guzik A. From computational discovery to experimental

characterization of a high hole mobility organic crystal. Nat Commun. 2011; 2:437: 1-8. https://doi.org/10.1038/ncomms1451

16 Becke AD. Density-functional exchange-energy approximation with correct asymptotic behavior. Phys Rev A. 1988; 38: 3098–3100. https://doi.org/10.1103/PhysRevA.38.3098

17 Becke AD. Density-functional thermochemistry. III. The role of exact exchange. J Chem Phys. 1993; 98: 5648–52. https://doi.org/10.1063/1.464913

18 Lee C, Yang W, Parr RG. Development of the Colle-Salvetti correlation-energy formula into a functional of the electron density. Phys Rev B. 1988; 37: 785–89. https://doi.org/10.1103/PhysRevB.37.785

19 Qiao Z, Xu YB, Lina SM, Peng JB, Cao D. Synthesis and characterization of red-emitting diketopyrrolopyrrole-alt-phenylenevinylene polymers. Synth Metals 2010; 160: 1544-1550. https://doi.org/10.1016/j.synthmet.2010.05.019

20 Pop F, Humphreys J, Schwarz J, Brown L, Van Den Berg A, Amabilino DB. Towards more sustainable synthesis of diketopyrrolopyrroles. New J Chem. 2019; 43: 5783–90.https://doi.org/10.1039/C9NJ01074B